UNIVERSIDADE DA BEIRA INTERIOR
Engenharia

Design Optimization for AM of MECSE CubeSat's Mechanical System

Miguel Costa Gonçalves Esteves

Dissertação para obtenção do Grau de Mestre em
Engenharia Aeronáutica
(Ciclo de Estudos Integrado)

Orientador: Professor Doutor Pedro Vieira Gamboa
Co-orientador: Mestre Miguel Sousa Machado

Covilhã, outubro de 2018

Dedication

This work is dedicated to my parents and girlfriend

"*It would not be much of a universe if it wasn't home to the people you love*"

Stephen Hawking

Acknowledgments

In the first place I would like to express my profound gratitude to professor Pedro Gamboa for his guidance throughout this work. His motivation and believe were crucial to the completion of this masters degree.

Secondly, to the Ocean, Space and Aeronautics team at CEiiA who are a true example of hard work, preservence and passion, the major cores which drive to the sucess. Working alongside them helped me becoming not only a better professional but also a better person, enduring heavy work loads perseverantly, maintaining focus and rigour. I would like to thank particularly to Miguel Machado , Ana Azevedo and Bruno Albuquerque who dedicated their precious time and knowledge to my work, leading me in the rigth path. I wish them all the best.

Likewise, my profound gratitude to CEiiA's Academy team for giving me the chance to come to CEiiA, in the first place for the Summer Intership, invinting me afterwards for this Master Internship, in which the present work was developed. To Rui Dias, head of the Academy's team, whom from day one was an example of leadership and motivation, to Inês Martins, whom had always a kind word in the most difficult moments, and to Madalena Pinheiro, whose hard work and dedication are core for the Academy's projects, a huge thank you for this enriching experience.

To André Santos, Oleh Tkachuk, Alexandre Dionísio, Rafael Coelho, Luis Oliveira and Paulo Ferreira my thanks for the countless hours of companionship.

Last but not least, to my family and girlfriend whom support and encouragment were determinant to accomplish this work, without their encouragement this work would not even have started.

Resumo

Magnetohydrodynamics/Electrohydronamics CubeSat Experiment (MECSE) é um CubeSat em desenvolvimento na Universidade da Beira Interior, resultante da colaboração do C-MAST (Centro de Ciências e Tecnologia Mecânica e Aeroespacial) e o CEiiA (Centro de Engenharia e Desenvolvimento de Produto). A missão do MECSE é validar a teoria de que um campo eletromagnético permite diminuir a espessura da camada de plasma, permitindo a realização de comunicações durante a reentrada de veículos na atmosfera terrestre, evitando a fase de blackout.

O MECSE apresenta atualmente uma estrutura clássica, constituída por um painel superior e inferior, conectados por duas armações laterais, conectadas entre si por seis frisos. Todos os componentes estruturais são feitos de alumínio 7075. Esta dissertação de mestrado tem por objetivo o desenvolvimento de uma nova estrutura com recurso a otimização topológica para ser produzida através de Fabricação Aditiva, garantindo a integridade estrutural do CubeSat e de todos os sistemas no seu interior, vitais para a realização da missão proposta.

A abordagem adotada para a obtenção desta nova estrutura começou pela criação de uma casca de alumínio com as dimensões do MECSE. Pontos de massa foram colocados no Centro de Gravidade (CG) de cada sistema e fixos à estrutura através de ligações rígidas. Foram aplicados os constrangimentos e as cargas à estrutura de acordo com as normas definidas pelo fabricante do lançador do MECSE bem como os objetivos para otimização topológica e corridas as análises. As estruturas otimizadas resultantes das análises realizadas foram posteriormente analisadas estaticamente de modo a validar o processo de otimização.

Com este trabalho, foi obtida uma estrutura mais leve com uma redução de massa de 115g. As fixações dos componentes dentro da estrutura foram desenhados bem como uma metodologia para a montagem e desmontagem do CubeSat. A estrutura final otimizada foi reanalisada e foi concluído que uma nova metodologia de montagem deverá ser reestudada, uma vez que esta reduziu a frequência natural para um valor abaixo do imposto pelas normas.

Palavras-chave

CubeSat, MECSE, Fabricação Aditiva, Otimização Topológica

Abstract

Magnetohydrodynamics/Electrohydronamics CubeSat Experiment (MECSE) is an under development CubeSat at University of Beira Interior (UBI), in a collaboration effort between C-MAST (Center for Mechanical and Aerospace Science and Technologies) and CEiiA (Centre of Engineering and Product Development). MECSE's mission is to validate the theory that an electromagnetic field can re-shape the layer of plasma allowing communication during atmosferic re-entry of vehicles, avoiding out the Radio Frequency (RF) blackout.

Currently MECSE presents a classic structure composed by one top and one end plate, connected by to side frames, connected itself by six ribs. All this structural elements are made of aluminium 7075. The goal of this masters dissertation is to develop a new structure by means of topology optimization with the goal of being produced by additive manufacturing, ensuring the structural integrity of the CubeSat and all of its components in its interior, vital to the sucess of the mission.

The adopted approach to reach this new stucture started by the creation of an aluminium shell structure with the dimensions of the MECSE. Mass points were applied in the Center of Gravity (CG) of which systems an attached to the structure with rigid connectors. Constraints and loads were applied according to the requirements defined by the MECSE's launch provider as well as the topology optimization's objectives. The optimized structures obtained were then analyzed in order to validate the optimization process and the new structure.

A ligther structure was achieved, with a mass saving of 115g. Attachements for all the components inside were defined as weel as an methodology for the assembly of the CubeSat. This final optimized geometry was reanalyzed and was concluded that a new assembly methodology must be developed since the proposed fragilize the stucture by reducing its first natural frequency for less than the requirements.

Keywords

CubeSat, MECSE, Additive Manufacturing, Topology Optimization

Contents

List of Figures

List of Tables

Abbreviated Terms

1D	One-dimensional
2D	Two-dimensional
3D	Three-dimensional
AM	Additive Manufacturing
ASTM	American Society for Testing Materials
BJ	Binder Jetting
C-MAST	Center for Mechanical and Aerospace Science and Technologies
CAD	Computer Aided Design
CAE	Computer Aided Engineering
Cal Poly	California Polytechnic State University
CDS	CubeSat Design Specifications
DAR	Deviation Waiver Approval Request
DED	Direct Energy Deposition
DOF	Degree of Freedom
FAA	Federal Aviation Administration
FC	Furnace Cooling
FEA	Finite Element Analysis
FEM	Finite Element Method
GPS	Global Positioning System
GSC	Guiana Space Centre
HIP	Hot Isostatic Press
IR	Infrared
ISS	International Space Station
LC	Load Case
LEO	Low Earth Orbit
LS	Load Step
LV	Launch Vehicle
ME	Material Extrusion
MECSE	Magnetohydrodynamics/Electrohydrodynamics CubeSat Experiment
MJ	Material Jetting
MS	Margin of Safety
P-POD	Poly Picosatellite Orbital Deployer
PBF	Powder Bed Fusion
PDE	Partial Differential Equations
QSL	Quasi-Static Loads
RF	Radio Frequency
SIMP	Solid Isotropic Material with Penalization
SL	Sheet Lamination
SLS	Selective Laser Sintering
SPL	Single Pico-Satellite Launcher
SRS	Shock Response Spectra
T-POD	Tokyo Pico-satellite Orbital Deployer
TPU	Tomsk Polytechnic University
UBI	Universidade da Beira Interior
UN	United Nations

UV	Ultraviolet
VP	Vat Photopolymerization
X-POD	eXperimental Push Out Deployer

Nomenclature

C	Constitutive matrix
E	Modulus of elasticity
F	Load vector
f	Natural frequency
G	Shear Modulus
K	Stiffness matrix
k	Constant of the spring
l	Original element length
M	Mass matrix
MAXDIM	Maximum member size
MINDIM	Minimum member size
u	Displacement vector
$\ddot{u}$	Acceleration
U_x	Displacement in the x direction
U_y	Displacement in the y direction
U_z	Displacement in the z direction
x	Displacement vector

Greek

α	Thermal expansion coefficient
δ	Elongation
ε	Strain
θ_x	Rotation about the x axis
θ_y	Rotation about the y axis
θ_z	Rotation about the z axis
ν	Poisson's Ratio
ρ	Density
σ	Stress
ϕ	Eigenvector
ω	Circular natural frequency

Chapter 1

Introduction

In this chapter the author's Motivation will be presented along with a brief summary of Additive Manufacturing and Topology Optimization. Also, taking into account that the MECSE Satellite will be the subject of this thesis it is important to present some aspects of the project.

1.1 Motivation

The access to space used to be nearly impossible due to launch costs. This trend changed with the development of the CubeSat program. The program aimes to drive down launch costs providing a standard set of dimensions for a satellite's external physical structure and intends to be fully built by students in a short period of time (1-2 year) allowing them to get real, first-hand experience of the problems and issues involved [1].

The Magnetohydrodynamics/Electrohydrodynamics CubeSat Experiment (MECSE) is an under development Small Satellite with both educational and scientific purposes which mission is the validation of the theory that a magnetic field can reduce the plasma density surrounding the spacecraft during atmospheric re-entry allowing communications during the Radio Frequency (RF) blackout [2]. Due to the consequences that this phenomena has during this critical phase of the flight its mitigation must be a top priority in space research.

As a result of traditional manufacturing technology restrictions on a product, which the designer may have originally envisioned as having a certain aesthetic and functionality, may need to be compromised so that it can be cost-effectively made. A designers' original design vision has to be compromised to the extent that the product can be made. With Additive Manufacturing (AM), complexity and geometry no longer affect manufacturability. Almost anything the designer imagines can be made precisely as the designer conceived [3]. The main benefits of the AM process come in design flexibility, low material waste, low CAD-to-part time and cost of producing parts from hard materials that are otherwise difficult to machine [4]. The complexity of the part does not affect whether it can be produced, or even its cost [3].

Due to the design freedom available with AM, it is a perfect application for topology optimization [4]. Topology optimization is used for obtaining the best layout of structural components to achieve predetermined performance goals [5]. The topology optimization has great impact on the performance of structures [6]. Using the right material for a specific application can give great pay-off such as lower weight, higher stiffness or strength or improvement of thermal or dynamic response [7]. Combining this two processes a strong structure is obtained with a reduction in it's mass and production costs.

This work aims to optimize the MECSE's Mechanical Subsystem regarding AM production and to manufacture the first prototype of the structure.

1.2 State-of-the-Art

> "We have either not used or only begun to use most of the major characteristics of space, so changes in future space exploration should be far larger than what has occurred to date. To take practical advantage of these characteristics, we must greatly reduce the costs of exploring and exploiting space [1]."

The Cold War kicked the human race to space. The knowledge about ballistic missiles acquired by the United States and the Soviet Union after the end of the Second World War led both countries to fear a thermonuclear war which could cause the destruction of their territories. The fear and suspicion was so intense that real time monitoring and communications was front burner. The Soviet Union managed to come first with the launch of the Sputnik I, the first ever satellite to be put in orbit, launched on October 1957 [8].

Portugal entered the space exploration in 1993 with the PoSAT-1. This 50 kg satellite was mainly used for the Portuguese army as a communication system during United Nations (UN) peace missions, but also by universities for scientific purposes. It has stopped transmitting in 2006 and its re-entry and consequent destruction is expected to be in 2043 [9].

The purpose of all space missions is to fulfil the needs of the stakeholders as effectively, as quickly and as low cost as possible. Hence, there is a wide range of missions. Some examples of missions are summed in Table 1.1.

Table 1.1: Space missions applications [1].

	Communications and Navigation	Applications	Science	Education and Training	Exploration	Resource Utilization	Military	Other
Applications	Telephone	Weather	Earth monitoring	CubeSats	Moon	Materials processing	Surveillance	Space tourism
	TV (commercial)	Earth resources	Telescopes (visible, UV, IR, X-Ray, gamma ray, Radio)	Training missions	Planets and Satellites	Solar power satellites	Reconnaissance	Burial in space
	TV (direct broadcast)	Fire detection	Particle detection	Educational satellites Student viewing and tracking	Asteroids	Asteroid mining	Tactical	Space Colonies
	Satellite Radio	Oceanography	Magnetic fields		Comets	Atmosphere mining	Comm.	Lunar colonization
	Store and Forward	Disaster monitoring	Planetary		Beyond the Solar System Human and unmanned fly-bys, orbiters,	Lunar resource utilization	Space surveillance	Mars colonies
	Space-to-Space	Search and Rescue	SETI			Mars in-situ propellants	Missile warning	Space Stations
	Relay Satellites	Crop monitoring	Solar		Surface Rovers	He^3 from Lunar Regolith	Nuclear detection	Technology demonstration
	Military Comm	Global warming	Biological		Lunar/Mars sample return		ELINT	Technology tests
	Navigation (air, ships, cars, people)	Warning of space hazards	Materials research				SIGINT	Spacecraft repair, refurbishment,
	Amateur Radio	Commercial cargo/vehicle tracking					IMINT	Tugs, OTVs
		Ice flows					SDI	Tethers
		Orbital debris monitoring					Space-based laser	Prayer Wheel
							ASATs	Interstellar Travel
							Wind measurements	
Examples	IntelSat	LandSat	Hubble	StarShine	Apollo	Industrial Space Facilty	DSP	Sputnik
	Direct TV	SPOT	Chandra	EDUSAT	Galilio	SPS	FLTSATCOM	Celestis
	OrbComm	SeaSat	COBE	AAUSat	Cassini		MILSTAR	ISS
	Iridium	NPOES	IRAS	OUFTI-1	Voyager		GPS	MIR
	GlobalStar	GOES	JWST	PLUME	Mariner		BSTS	SkyLab

This wide range of missions implies that all the satellites differ from each other, not only in

physical structure but also in software and hardware. Consequently, satellites have different sizes and shapes, and can also be distinguished for their mass Table 1.2.

Table 1.2: Categorization of satellites in accordance with their mass [10].

Satellite Category	Net Weight
Large	> 1000 kg
Medium	500 - 1000 kg
Mini	100 – 500 kg
Micro (Cubesat)	**10 -100 kg**
Nano (Cubesat)	**1 – 10 kg**
Pico (Tubesat)	**0.1 – 1 kg**

Small satellites are defined as satellites weighting less than 500 kg. They have been flying since the beginning of the space program due to limitations in size and capability of Launch Vehicles (LV). Nowadays the microminiaturization of electronics allowed satellites to perform similar tasks as its predecessors with a reduction in size and budget. This brings a new approach to space because it is feasible to launch several satellites together, reducing the launch cost per vehicle, and offering a less expensive mean of exploring space [1].

With the establishment of Small Satellites, a variety of new terms came into use: minisatellite (500-100 kg), microsatellite (100-10 kg), nanosatellite (10-1 kg), picosatellite (1-0.1 kg) [1] and more recently, even femtosatellite (100-10 g), attosatellite (10-1 g) and zeptosatellite (1-0.1 g) [11]. A downward leader to illustrate this terms and reduction in scale is shown in Figure 1.1.

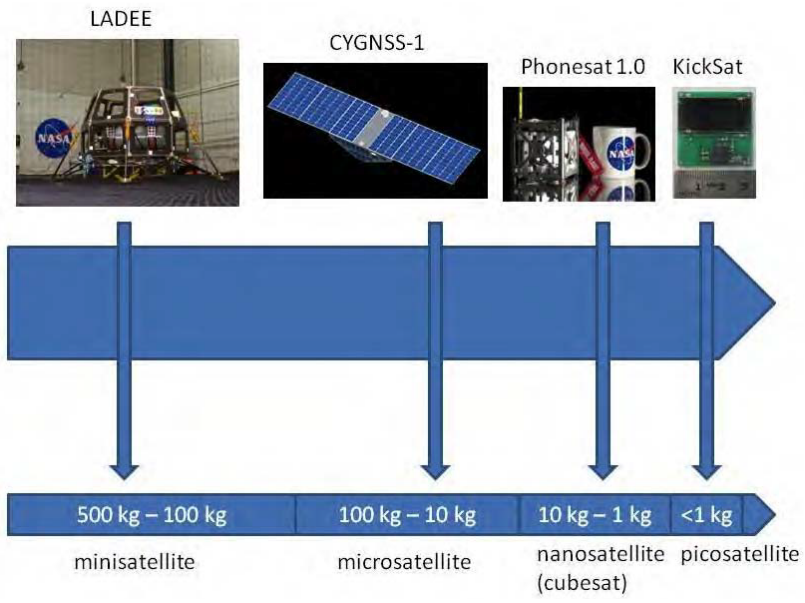

Figure 1.1: Overview of the variety of spacecraft that fall into the small spacecraft category [12].

1.2.1 CubeSat

"A CubeSat is a 10 cm cube with a mass of up to 1.33 kg" [13]. They are measured in units (U) and are designed in **1U, 1.5U, 2U, 3U, 6U** or **12U** configuration [14] as depicted in Figure 1.2. Bigger sizes have been developed but not standardized yet [15].

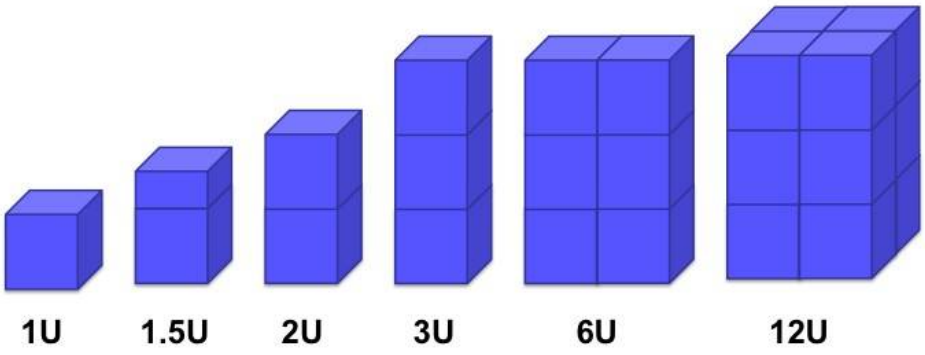

Figure 1.2: CubeSat form factor [16].

The CubeSat project began in 1999 as a collaborative effort between Prof. Jordi Puig-Suari at California Polytechnic State University (Cal Poly) and Prof. Bob Twiggs at Stanford University [13]. The primary goal of their development was to provide a standard set of dimensions for the picosatellite's structure [1]. With their standardization, projects' costs and development time are reduced, allowing launches to be more frequent, increasing accessibility to space [13].

The first CubeSat was launched in 2003 [1] and in 2012 the launch of the hundredth CubeSat was celebrated [17]. At the end of 2013, the count was up to 155 CubeSats launched and in 2015, Planet Labs [18] announced the launch of 100 CubeSats [19]. According to SpaceWorks Forecast [20], over 300 Small Satellites were launched in 2017, an increase of 205% when compared to 2016 (Figure 1.3). For 2018, they predict the launch of 263 Small Satellites, slightly lower than the previous year. For the next 5 years a total of 2600 launches are predicted.

Launches have been increasing year after year. This trend is expected to increase even more as LV dedicated to CubeSats come onto the market [14]. When this happens, the launch service becomes cheaper, expanding the market, allowing universities, researchers or even particular enthusiasts to launch their projects [12].

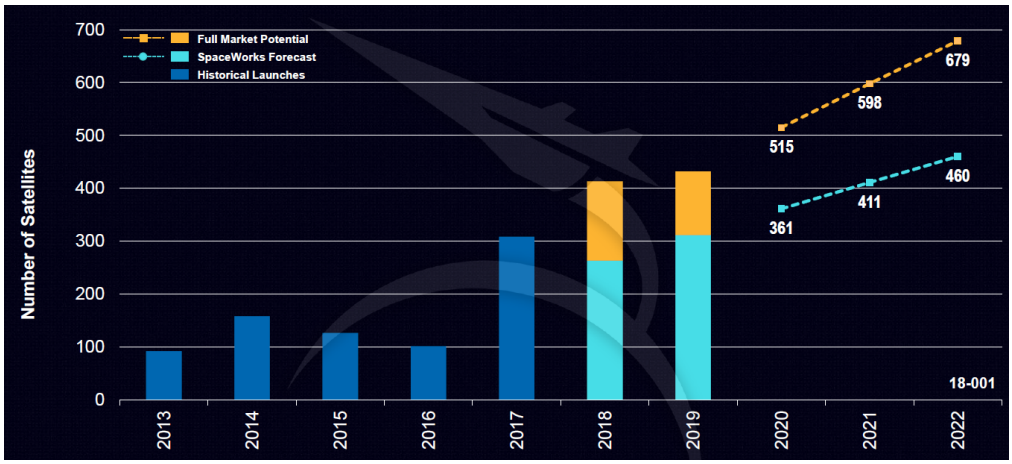

Figure 1.3: 2018 small satellite launch history & market forecast [20].

According to [21], more than half of the CubeSat missions had educational objectives. These missions main purpose is to teach students in all phases of the development of a satellite, giving them direct control over the progress of the program [22], the CubeSat program is ideal to

achieve this purpose as it provides a low-cost platform to access space [23].

The shift towards the CubeSat program brought up two trends: a reduction in the number of "real-world" missions (e.g. communications or technology development) and an increase in the failure rates (due to a failure rate among CubeSats of 40%) [22]. It should be noted, however, that educational missions tend to launch a lot of new systems and which increases the risk and the failure rates [17]. Failure is this type of missions has a certain degree of acceptance because without trying new things, ideas, processes, and techniques, pushing the boundaries of knowledge, inovation would not occur [1].

In order to define the design requirements of a CubeSat, a container must be selected in order to have realistic constraints. The Poly Picosatellite Orbital Deployer (P-POD) was selected as the MECSE's container [15]. There are other deployers that have been developed such as the X-POD, the T-POD and the SPL. The X-POD (eXperimental Push Out Deployer) was developed by the University of Toronto Institute for Aerospace Studies/Space Fligth Laboratory with the intent of being custom built for each sattelite as well as tailored to satellites of different sizes ranging from a single CubeSat to larger nanosatellites. The T-POD (Tokyo Pico-satellite Orbital Deployer) was developed by Tokyo Institute of Technology and originally deployed only a single 1U CubeSat, being later expand to a 2U configuration. The SPL (Single Pico-satellite Launcher) was manufactured by Astrofein in Germany in a 1U configuration. Their innovation is the customization of the separation velocity by the customer [1].

1.2.1.1 P-POD

While the miniaturization and standardization brought by the CubeSat received much of the attention, the true innovation of the program is the P-POD [17] (Figure 1.4). The P-POD has been used to deploy over 90% of all CubeSats and 100% of them since 2007 [1]. The P-POD's task is to open the door and push CubeSats out [24]. In order to do that, a non-explosive release mechanism controls the deployment minimizing shock to the LV and CubeSats [25].

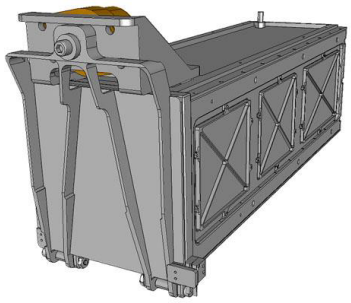

Figure 1.4: P-POD [13].

P-POD has a tubular design and can support deployable hardware up to 340.5mm x 100mm x 100mm [26], the equivalent of three 1U CubeSats or one 3U CubeSat [13]. The P-POD has a mass of 3kg and is manufactured from Aluminium T-7075 [1], due to the material's high strength, ease of manufacture and low cost [23, 27]. The surface is treated with an Alodine finish which not only prevents the surface from oxidizing but also a non-uniform charging of the structure in the plasma associated with Low Earth Orbit (LEO) [1]. P-PODs have an operational temperature between -45°C and +65°C [24].

The tubular design of the P-POD creates a low spin trajectory upon deployment [1] and a 4kg CubeSat have an exit velocity from the P-POD of approximately 2.0m/s [26]. Its structure is design to sustain 15G [27] (with a maximum deflection of less than 1mm in order to prevent loading of the CubeSats [23]) as well as to provide a Faraday cage to protect the payload from electromagnetic interference [27].

1.2.1.2 CubeSat Design Requirements

In order to ensure a safe deployment of all satellites within the LV, the requirements issued by Cal Poly in CubeSat Design Specifications (CDS) [13] must be met by all the participants and that the requirements issued by the launch provider must super seed all the others since the launch environment establishes critical conditions. This are detailed in Appendix A.

This document also states that any CubeSat that violates any of their requirements must fill out the *Deviation Waiver Approval Request* (DAR) (see Appendix B). This is entended to facilitate the communication and explicit documentation between CubeSat developers, P-POD integrators, range safety personel, and LV providers in a quick and easy way by helping to better identify and address any issues that may arise prior to integration and launch. The process flow in depicted in Figure 1.5.

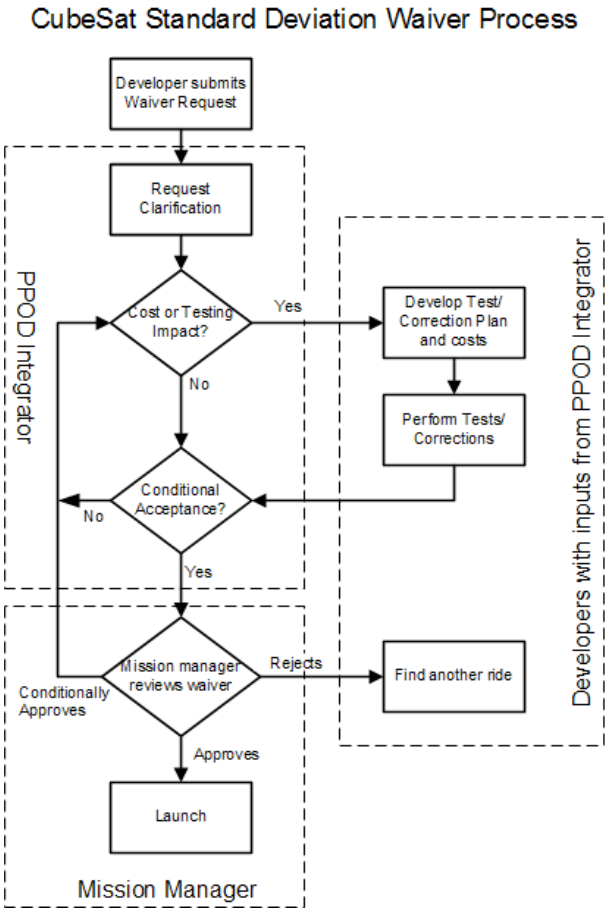

Figure 1.5: CubeSat Standard Deviation Wavier Process Flow Diagram [13].

Upon completion of the DAR, the P-POD integrator will review the request, resolve any questions, and determine if there are any additional tests, analyses or costs to support the waiver

submission. If so, the developers in accordance to the P-POD integrators will define the test plan and perform them before the waiver is conditionally accepted by the P-POP integrator. Waivers can only be accepted conditionally accepted by the P-POD integrators after a lauch has been identified for the CubeSat. Once the launch has been identified, the waiver becomes mission specific and passes to the LV Mission Manager for review, who has the final say on acceptance of the waiver and may require more corrections and/or testing to be performed before approving the waiver [13].

1.2.2 Additive Manufacturing

In the space industry, weight saving and component performance under extreme conditions and launch, material machinability and production quantities are critical factors since the components not only have to be light but also extremely stiff. Supported by the recent developments of design optimization tools and manufacturing capabilities, components and parts produced using AM are emerging in the space industry [28].

Satellites are getting smaller and smaller and AM is responsable for part of that [29]. The smallest satellite to be placed in orbit weighted 64g and was developed in Tamil Nadu, India, with the purpose of seeing how 3D printed Carbon fiber performs in outer space [29]. The first CubeSat with a full three-dimensional (3D) printed structure was the Tomsk-TPU-120, developed by a group of students from Tomsk Polytechnic University (TPU) in Siberia and was launched from the International Space Station (ISS) on March 2016 [30, 31].

Additive Manufacturing (AM) is defined by the American Society for Testing and Materials (ASTM) [32] as "a process of joining materials to make objects from 3D model data, usually layer upon layer, as opposed to subtractive manufacturing methodologies" [33]. Initially, AM was exclusively used to create visualization models of the products as they were in development but as the technology developed, available materials and accuracy were improved allowing the overall quality of the output to be improved. Now, fully functional parts can be made in a variety of materials (such as plastics, resins, metals, wax or ceramics) without wasting as much raw material, further extending the application range [34, 35, 36].

AM has mainly been used in order to accelerate product development [35] but its impact continues to grow [37]. The technology has been applied to fields as varied as medicine, architecture, and forensics [38]. In Figure 1.6 the growth in metal AM system sales is depicted.

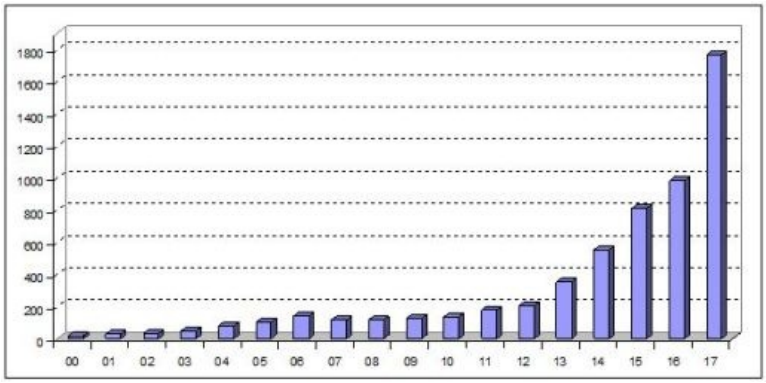

Figure 1.6: Rise in metal AM system sales [38].

In 2016, 983 sales were estimated, but in 2017 that number grew up almost 80% with a prediction of 1768 sales [38]. For 2018, the expenses with AM are expected to raise 55% [35]. This exponential rising is due to the focus on the reliability and output material quality [39]. Particularly for aerospace applications, where the material quality is an all-dominant factor, the incresing reliability is starting to pay off, with this sector representing already 4% of the AM total market (Figure 1.7).

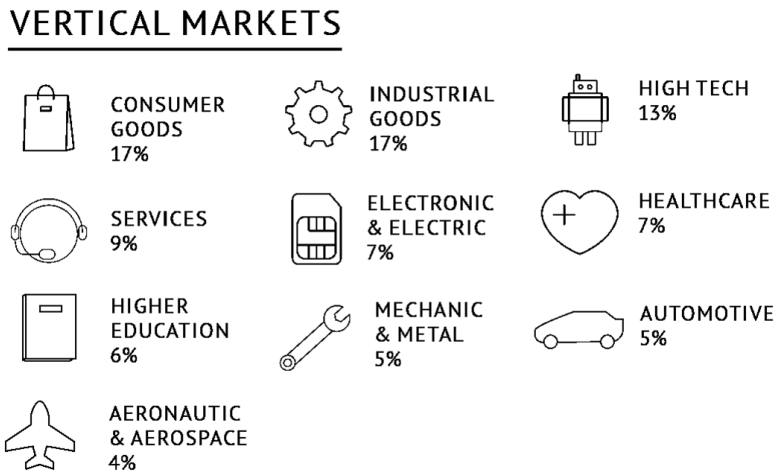

Figure 1.7: AM Vertical Markets [35].

1.2.2.1 Development of Modern AM Techniques

AM has roots in photosculpture (1.8(a)) and topography (1.8(b)) which date back to 1860 and 1890, respectively. Both technologies used manual layer deposition in order to obtain topographical maps and exact three-dimensional (3D) replicas of any object (including human forms) [37]. AM can even be dated back to the construction of the pyramids in Egypt and in South America, has they were built layer upon layer, adding material as they went [34]

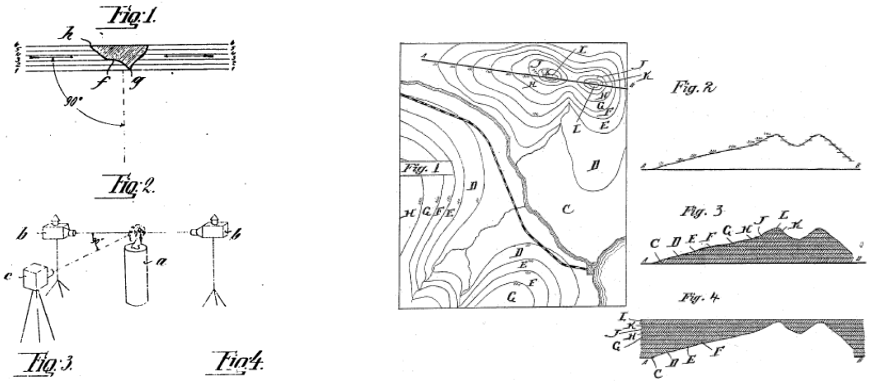

(a) Photosculpture method [37]

(b) Topography method [40]

Figure 1.8: AM roots

In 1951, Munz [41] proposed a system that has features of current stereolithography (SL) techniques. In Munz's system (Figure 1.9), he disclosed a system for selectively exposing a transparent photo emulsion in a layer wise fashion and hardened according to the cross-section of a

scanned object using a piston mechanism. Subsequently this object can be manually carved or photochemically etched out to create a three-dimensional object [37, 42].

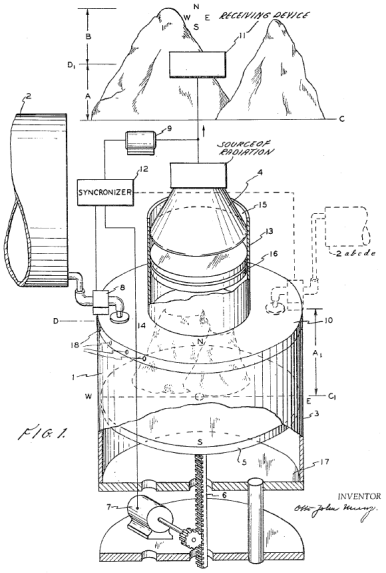

Figure 1.9: Munz's photopolymer technique [41].

In 1968, Swainson [43] proposed a process to directly fabricate a plastic pattern by selective, 3D polymerization of a photosensitive polymer at the intersection of two laser beams (Figure 1.10). Although laboratory hardware was constructed, a commercially viable process was not achieved [37, 42].

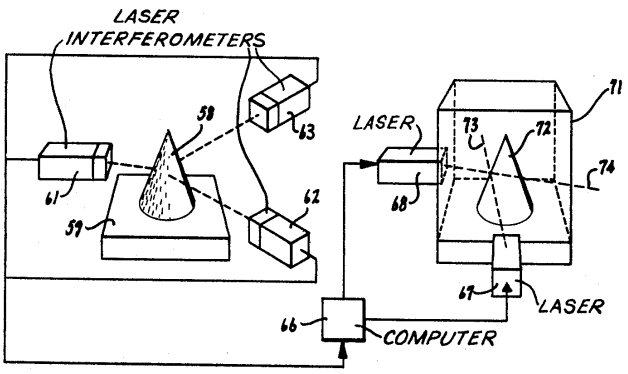

Figure 1.10: Swainson's photochemical system [43].

Ciraud was the first to introduce, in 1971, a powder deposition method using an energy beam that has all the features of modern direct deposition AM techniques (Figure 1.11). To produce an object, small particles are applied to a matrix by gravity, magnetostatics, electrostatics, or positioned by a nozzle located near the matrix. A laser, electron beam, or plasma beam then heats the particles locally and as a consequence of this heating, the particles adhere to each other to form a continuous layer [37, 42].

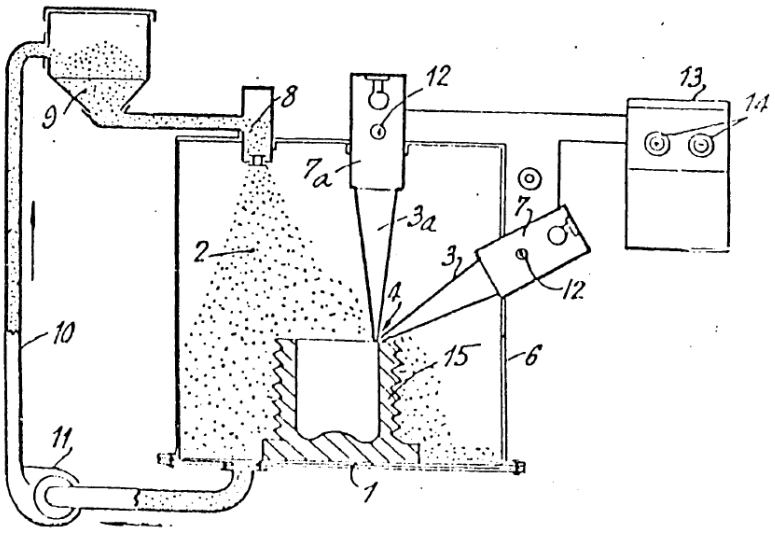

Figure 1.11: Ciraud's powder deposition method [37].

In 1979, Housholder [44] presented the earliest description of a Selective Laser Sintering (SLS) process without having it commercialized (Figure 1.12). The solidification can be achieved by using heat and a selected mask or by using a controlled heat scanning process [37, 42].

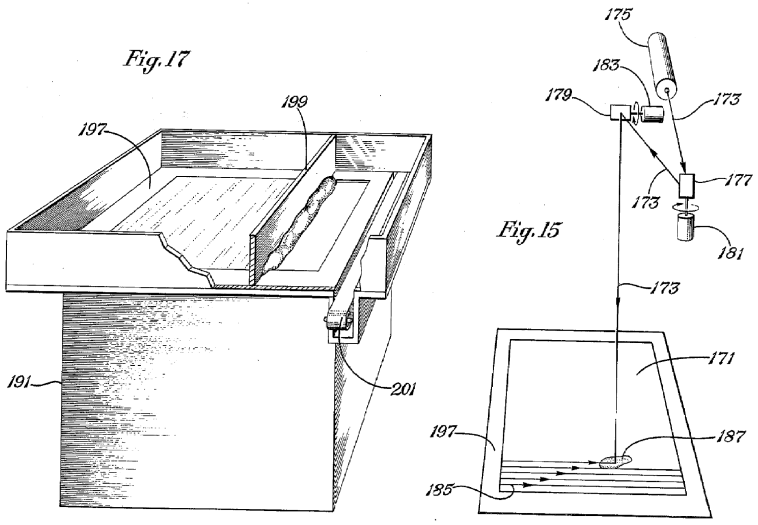

Figure 1.12: Housholder's powder process [44].

Kodama [45] was the first to publish the first rapid prototyping system of a functional photopolymer rapid prototyping system using photopolymer materials [37, 42]. In his method, a solid model is fabricated by building up a part in layers where exposed areas correspond to a cross-section in the model. He studied three different methods for achieving this (Figure 1.13): (a) Using a mask to control exposure of Ultraviolet (UV) source and immersing the model downward into a liquid photopolymer vat to create new layers; (b) Using a mask as in (a), but the mask and exposure is positioned on the bottom of the vat and the model is drawn upward to create a new layer; (c) Immersing the model, as in (a), but using an x-y plotter and an optical fibre to expose the new layer.

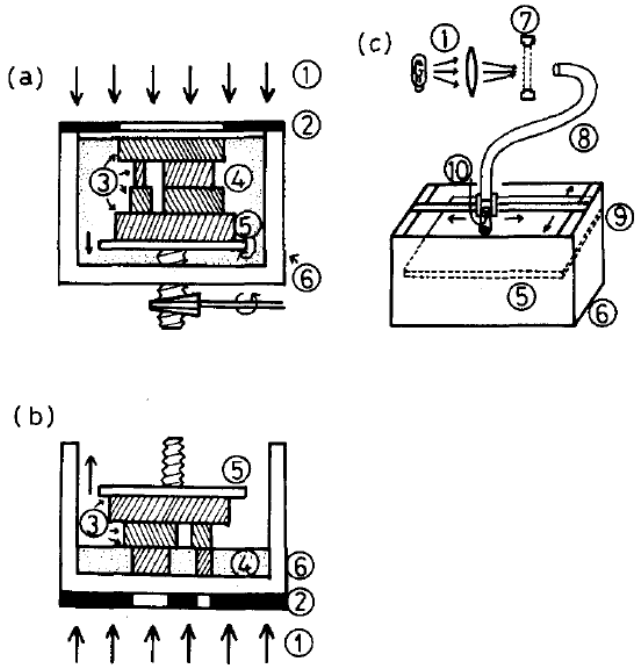

Figure 1.13: Kodama's process. In the Figure, 1.ultraviolet rays, 2.mask, 3.solidified layers, 4.liquid photo-hardening, 5.movable plate, 6.receptacle, 7.shutter, 8.optical fiber, 9.XY plotter and 10.optical lens [45].

Herbert's [46] system used a computer to direct a UV laser beam to a photopolymer layer with a mirror system on an X-Y plotter. An liquid photopolymer was then added to create a new layer (Figure 1.14) [37, 42].

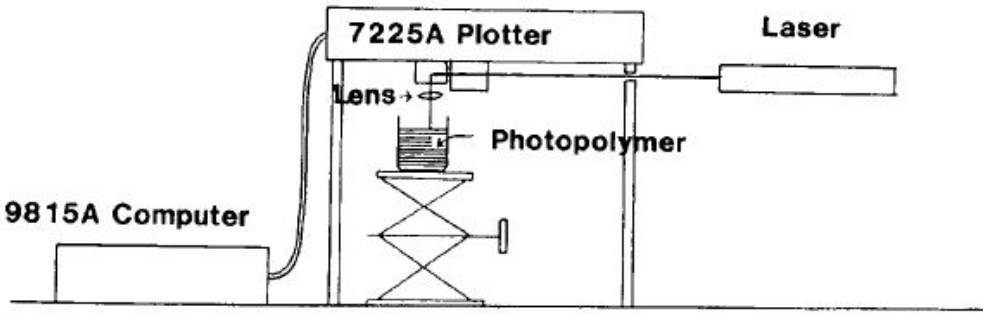

Figure 1.14: Herbert's process [37].

In the late 1980s and early 1990s a huge amount of AM processes appeared leading to the foundation of a vast number of companies dedicated in exclusive to AM [37]. A sum up of the historical development of AM technologies in done in Figure 1.15.

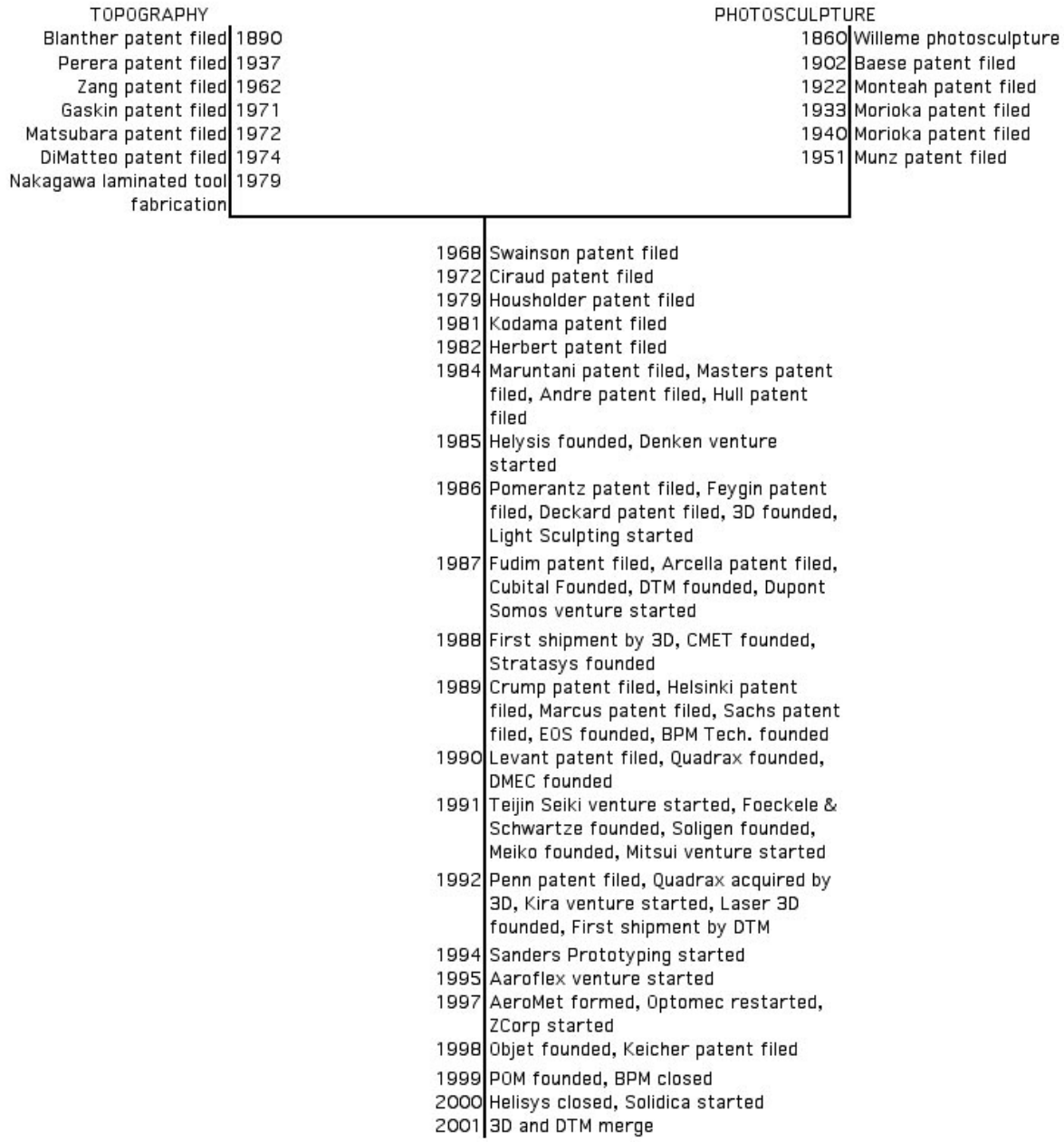

Figure 1.15: Early Chronology of Additive Processes [37].

Due to the large variety of processes that emerged due to the expansion of AM, it became difficult to talk about the topic once an extensive list of commercial variations of every process emerged. So ASTM divided AM in 7 categories [33]:

- **Binder Jetting (BJ):** a process which deposits a liquid bonding agent to selectively join powder materials;
- **Directed Energy Deposition (DED):** a process which uses a focused thermal energy to fuse material as this is deposited;
- **Material Extrusion (ME):** a process which dispenses material through a nozzle or orifice;
- **Material Jetting (MJ):** a process which selectively deposits droplets of build material;

- **Powder Bed Fusion (PBF):** a process which selectivily fuses regions of a material powder bed with a focused thermal energy;
- **Sheet Lamination (SL):** a process which bonds sheets of material to form the final part;
- **Vat Photopolymerization (VP):** a process which selectively cures a liquid photopolymer by light-activated polymerization.

Due to the large variety of processes, its important to know the characteristics of each and every one in order to properly choose the one that fits the needs of a part to be built. This is done in Table 1.3:

Table 1.3: Characteristics of ASTM categories [47]

Category	Advantages	Disadvantages	Materials
BJ	• Free of support/substrate • Design freedom • Large build volume • High print speed • Relatively low cost	• Fragile parts with limited mechanical properties • May require post processing	• Polymers • Ceramics • Composites • Metals • Hybrid
DED	• High degree control of grain structure • High quality parts • Excellent for repair applications	• Surface quality and speed requires a balance • Limited to metals/metal based hybrids	• Metals • Hybrid
ME	• Widespread use • Inexpensive • Scalable • Can build fully functional parts	• Vertical anisotropy • Step-structured surface • Not amenable to fine details	• Polymers • Composites
MJ	• High accuracy of droplet deposition • Low waste • Multiple material parts • Multicolour	• Support material is often required • Mainly photopolymers and thermoset resins can be used	• Polymers • Ceramics • Composites • Hybrid • Biologicals
PBF	• Relatively inexpensive • Small footprint • Powder bed acts as an integrated support structure • Large range of material	• Relatively slow • Lack of structural integrity • Size limitations • High power required • Finish depends on precursor powder size	• Metals • Ceramics • Polymers • Composites • Hybrid
SL	• High speed • Low cost • Ease of material handling	• Strength and integrity of parts depend on adhesive used • Finishes may require post processing • Limited material use	• Polymers • Metals • Ceramics • Hybrids

VP	• Large parts • Excellent accuracy • Excellent surface finish and details	• Limited to photopolymers only • Low shelf-life, poor mechanical properties of photopolymers • Expensive precursor/Slow build process	• Polymers • Ceramics

In CEiiA there are several Additive Manufacturing available processes [48]. The one chosen to manufacture the MECSE's Mechanical Subsystem is the Selective Laser Sintering (SLS). This is a Powder Bed Fusion (PBF) process which is detailed in the next section.

1.2.2.2 Powder Bed Fusion

All PBF processes are characterized by including thermal source(s) to induce fusion between the powder particles, a method for controlling powder fusion in a specific region of each layer and a mechanism to add and smooth the added powder layers [34].

SLS was the first commercialized PBF process. It was originally developed for producing plastic prototypes using a point-wise laser scanning technique but its application has been extended to metal and ceramic powders [34] and according to the survey made by reference [35], nowadays SLS is the second most used AM process.

The process starts by spreading a layer of powder over the building platform. This layer is fused forming the first cross section of the model. The building platform is then lowered the height equal to the thickness of the powder layer. A new layer of powder is spread across the building platform and the process is repeated until the final model is finished. The non melted powder remains loose, providing support to the part during building process, eliminating the need for supports, and cleaned during the post processing and recycled [34, 49].

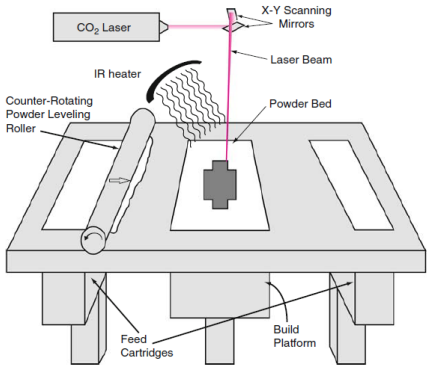

Figure 1.16: Schematic of SLS process [34].

During the building process, the temperature inside the building chamber is maintained below the powder's melting point in order to reduce the laser energy required to fuse it. Some machines vary the temperature layer by layer and adjust laser power to improve output quality. However this implies that models must have a cool down period so high tolerance and quality of fusion is ensured as well as handling. The chamber is normally filled with nitrogen in order to minimize oxidation and degradation of the powder [34, 49].

The materials used in SLS processes have limited shelf-life (interval of time for which the material remains in condition to be used). Exposure to moisture, excess light, and other contaminants must be avoided in order to prevent unwanted chemical reactions. Materials must also be checked periodically once its properties can degrade depending on how many times the powder has been recycled. This means that it is important to check on the building process to ensure that material is behaving as expected. A procedure for maintaining consistent material quality through recycling should also be observed [34].

SLS machines are made up of three components: a heat source to induce fusion of the powder (typically a laser beam), a method to control the heat source and a mechanism to add new layers of material powder over the previous layers (typically 0.1mm thick). Although they are designed to operate unattended, careful maintenance must be performed frequently due to the fragility of the components such as the laser pointer [34].

In order to produce satisfatory parts, the optimum process parameters must be tuned. This can be divided in four categories [34]:

- **Laser parameters:** such as laser power, spot size, pulse duration or pulse frequency;
- **Scan parameters:** such as scan speed, scan spacing or scan pattern;
- **Powder parameters:** such as particle shape, size and distribution, powder bed density, layer thickness or material properties;
- **Temperature parameters:** such as powder bed temperature, powder feeder temperature, temperature uniformity.

However, it must not be disregarded that some of this parameters are interdependent. For example, the required laser power increases with melting point of the material and lower powder bed temperature, and also varies depending on materials absorptivity which is influenced by the material and powder shape, size and packing density [34]. All this parameters influence the mechanical properties of the finished parts. Therefore, some literature review about Mechanical Properties of AM produced components must be done.

1.2.2.3 Mechanical Properties

For aerospace applications, good strength paired with good ductility is mostly required [39]. Hence, titanium and its alloys are the major pick due to their high strength to weight ratio as well as excellent corrosion resistance. However, titanium usage is limited by its higher cost of acquisition and machining leading to a carefull balance between mechanical beneficts and added cost [50]. This restrictions imposed on titanium aerospace components can be greatly impacted by AM once the buy-to-fly ratio and the lead time for production are hugely reduced, dropping the costs down [51].

Ti-6Al-4V is one of the most widely used titanium alloys either in aerospace and AM [39, 52, 51, 53]. Although common CubeSat structures and the current MECSE's structure are made of Aluminium [15], all fundamental bibliography about AM Mechanical Properties use Ti-6Al-4V as a case study, so all the references presented in this section refer to this alloy. This discrepancy presents no problem because the most important informations for this work are related with

the building process and its implications in the mechanical properties rather than the material being used in the literature.

In reference [39], a static and dynamic tensile tests were performed to powder-bed samples in parallel and perpendicular direction relative to the layers. The parallel samples (labeled as XY-direction) present no distinction between X and Y as there are no differences in mechanical properties. The perpendicular samples (labeled as z-direction) are parallel to the building direction, perpendicular to the layers.

For the *static tensile tests*, the samples were tested in as-built and annealed (843ºC/2h/furnace cooling) conditions. On the other hand, for the dynamic *high cycle fatigue tests*, the samples were tested in as-built condition and Hot Isostatically Pressed (HIP) condition at 1000 bar at 843ºC for 2h by furnace cooling (FC).

The static tests resulted in an average yield strength of 811-897 MPa, an ultimate strength of 859-971 MPa, an elongation of 12.1-17.1% and a reduction of area of 34.5-46.0%. This values show that the as-built and annealed samples tested in XY-direction met properties of wrought material. In the Z-direction, however, the samples do not met properties of cast material. On the other hand, the dynamic tests showed a fatigue limit of around 600 MPa at 2×10^7 cycles, meeting properties of wrought material.

An binary comparasion of the influence of tests direction in tensile properties was then done and is depicted in Table 1.4.

Table 1.4: Influence of single parameters on strength (yield, ultimate) and ductility (elongation, reduction of area). Adapted from [39].

	Comparison of	with	*Condition / test direction*	Strength $R_{p,0.2}$	Strength R_m	Ductility A	Ductility Z
Powder-bed samples	xy-direction	z-direction	*as-built*	102%	102%	88%	75%
	xy-direction	z-direction	*843°C/2h/FC*	103%	107%	115%	89%
	843°C/2h/FC	as-built	*xy-direction*	93%	95%	146%	105%
	843°C/2h/FC	as-built	*z-direction*	92%	90%	111%	89%

From the data in Table 1.4, the following conclusions may be drawn:

- The samples tested in the XY-direction have higher strength than the samples in the Z-direction;
- The annealing treatment decreased strength and increased ductility of the samples.

With the data collected in this study, the authors stated that for aerospace applications the as-built condition is the most balanced due to the baseline process temperature. Regarding the tests direction they stated that the maximum loads in operation that a part must withstand shall be alligned parallel to the layers [39].

Another similar work is [51] in which they intent to establish the effects of process parameters and input materials on mechanical properties (yield and ultimate stress, total elongation and elastic modulus) using LENS™, a process very similar to SLS, by analyzing stress relieved and HIP'ed samples of Ti-6Al-4V in both Static and Fatigue Tests. The first ones were relieved

in vacuum for 2h at 700-730ºC while the second for 2h at 900ºC at a pressure of 100 MPa. The results are depicted in Table 1.5.

Table 1.5: Average Tensile Properties of Bulk Ti-6Al-4V Produced via the LENS™ Process [51].

Condition	Test Direction	Yield Strength (MPa)	Ultimate Strength (MPa)	Total Elongation (%)	Elastic Modulus (GPa)
Stress Relieved	X	1065	1109	4.9	116
Stress Relieved	Y	1066	1112	5.5	116
Stress Relieved	Z	832	832	0.8	112
HIP'ed	X	946	1005	13.1	118
HIP'ed	Y	952	1007	13.0	118
HIP'ed	Z	899	1002	11.8	114

As expected, the Static Tests results show an anisotropy in both stress relieved and HIP'ed condition (the X and Y direction strengths were much higher than those in the Z direction) but with more relevance in stress relieved condition. This larger anisotropy is result of lack of fusion in the material. In the HIP'ed condition, the raise of temperature and pressure reduces the porosity in the samples by consolidating the material. Consequently, an significant ductility is shown in all three directions. Another consequent result is the higher strength but lower ductility in stress relieved condition compared to HIP'ed. This result is consistent with the previous in which the annealed samples had lower strength but higher ductility [39].

Because the Z direction is the critical once, a comparation of the results obtained in both conditions with wrought Ti-6Al-4V was done and is depicted in Table 1.6.

Table 1.6: Measured Z direction Tension Properties produced via LENS™ Process versus Properties of wrought Ti-6Al-4V [51].

Condition	Yield Strength (MPa)	Ultimate Strength (MPa)	Total Elongation (%)	Elastic Modulus (GPa)
Stress Relieved	832	832	0.8	112
HIP'ed	899	1002	11.8	114
Wrought	827	896	10	110

The results in Table 1.6 show that the samples in both conditions have strengths comparable (stress-relieved) or even better (HIP'ed) than wrought material but with a significant loss of ductility in the stress-relieved condition and a slight improvement in HIP 'ed condition. Taking into account that the results in the other two directions are better than the ones in the Z direction, it is clearly shown that the PBF process can improve material's performace [51].

A Fatigue Test was also performed to the samples in both conditions (Figure 1.17). The results showed that the stress-relieved samples have much lower fatigue strengths than the HIP'ed and also displayed anisotropy (the Z direction fatigue strengths were significantly lower than those in the X and Y direction). The results even showed that the samples in HIP condition have a fatigue strength similar or even better than wrougth material and on the other hand, the stress-relieved samples have a fatigue strength similar to cast material in the X and Y direction but the Z direction not meeting any of the previous (cast or wrougth) fatigue strengths.

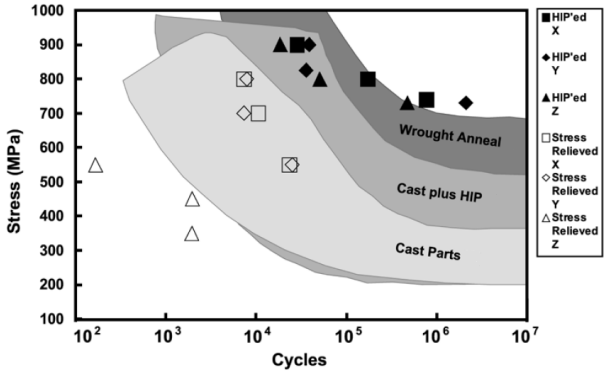

Figure 1.17: Comparison of measured fatigue in both the stress relieved and HIP'ed conditions [51].

Independently of the AM process or the material used, all the AM products go through a set sequence of tasks. This process may have some differents according to the machine used or the product geometry but a Generic AM Process may be defined for the metal systems [34].

1.2.2.4 Generic AM Process

This Generic AM Process involves a number of steps that move from the virtual Computer-Aided Design (CAD) description to the physical resultant part [34]. This steps are listed below and illustrated in Figure 1.18.

- **Step 1: CAD:** All AM parts must start from a software model that fully describes the external geometry. This can involve the use of any CAD software but the output must be a 3D solid or surface representation.
- **Step 2: Conversion to Stereolithography Tessellation Language (STL):** Nearly every AM machine accepts the STL file format, which has become a *de facto* standard, and nearly every CAD system can output such a file format. This file describes the external closed surfaces of the original CAD model and forms the basis for calculation of the slices.
- **Step 3: Transfer to AM Machine and STL File Manipulation:** The STL file describing the part must be transferred to the AM machine. Here, there may be some general manipulation of the file so that it is the correct size, position, and orientation for building.
- **Step 4: Machine Setup:** The AM machine must be properly set up prior to the build process. Such settings would relate to the build parameters like the material constraints, energy source, layer thickness, timings, etc.
- **Step 5: Build:** Building the part is mainly an automated process and the machine can largely carry on without supervision. Only superficial monitoring of the machine needs to take place at this time to ensure no errors have taken place like running out of material, power or software glitches, etc.
- **Step 6: Removal:** Once the AM machine has completed the build, the parts must be removed. This may require interaction with the machine, which may have safety interlocks to ensure for example that the operating temperatures are sufficiently low or that there are no actively moving parts.
- **Step 7: Postprocessing:** Once removed from the machine, parts may require an amount of additional cleaning up before they are ready for use. Parts may be weak at this stage or

they may have supporting features that must be removed. Therefore, this often requires time and careful, experienced manual manipulation.

- **Step 8: Application:** Parts may now be ready to be used. However, they may also require additional treatment before they are acceptable for use. For example, they may require priming and painting to give an acceptable surface texture and finish. Treatments may be laborious and lengthy if the finishing requirements are very demanding. They may also be required to be assembled together with other mechanical or electronic components to form a final model or product.

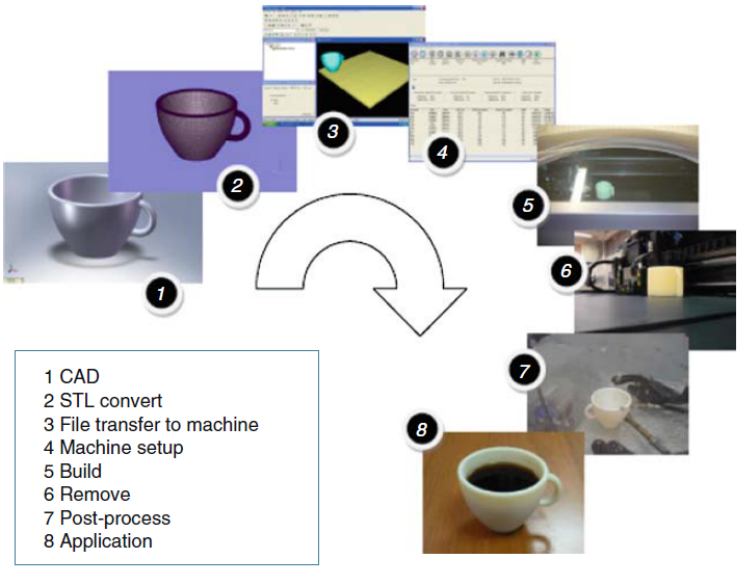

Figure 1.18: The eight stages of the AM process [34].

A key simulation technology being leveraged to shorten the design cycle for AM is Topology Optimization, a nonparametric optimization technique that identifies and removes areas of a design space not contributing to the stiffness of the part or to the part load path [28]

1.2.3 Structural Optimization

Structural Optimization (SO) plays a high role in the design of structures. Engineers are always seeking new ways to improve quality and so, in the early stages of the design process, questions towards finding the best design in terms of load bearing capacity, reliability, accuaracy and costs had to be answered [51]. SO, by means of mathematical algorithms, allows to extract the best performance of a structure, reducing the material used while optimizing its stiffness. Since the cost of the project plays such an important role in its feasible or not, engineers have turned their attention towards SO in order to become more technological competitive and environmental friendly, with high-performance at lower costs [54]. In Figure 1.19 is presented an example of an optimization where material is removed, reducing a part's weight and optimizing its stiffness.

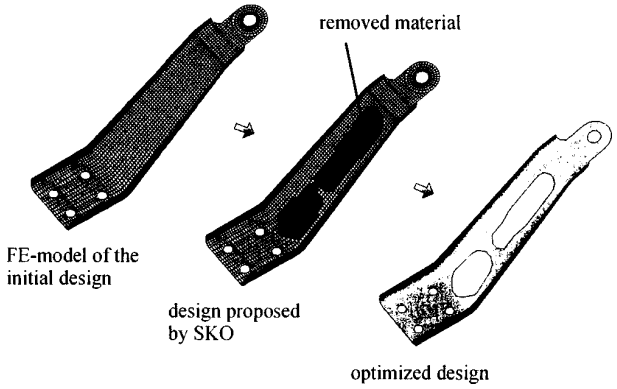

Figure 1.19: Structural Optimization of a bracket for a gearshift guide control [55].

There are mainly three types of SO – sizing, shape and topology [56]. Each of them addresses a different aspect of the structural design process [6] and all three are depicted in Figure 1.20.

In a sizing SO problem, the design variables are the section properties (thickness or cross section) while the layout of the structure is fixed, the state variables (deflection, stress, etc.) are known *a priori* and fixed as well [6, 56]. An example of this procedure is finding the optimal member areas in a truss structure. On the other hand, a shape SO problem deals with finding the optimum shape for the domain satisfying all the connectivities [6, 56]. An example of this procedure is finding the optimal shape for the holes in a beam. Finally, in Topology Optimization (TO), the goal is to determine the connectivity, the shape and the location of voids in the design domain [57]. In these problems, only the applied loads, the constraints and the volume to be removed are known [6].

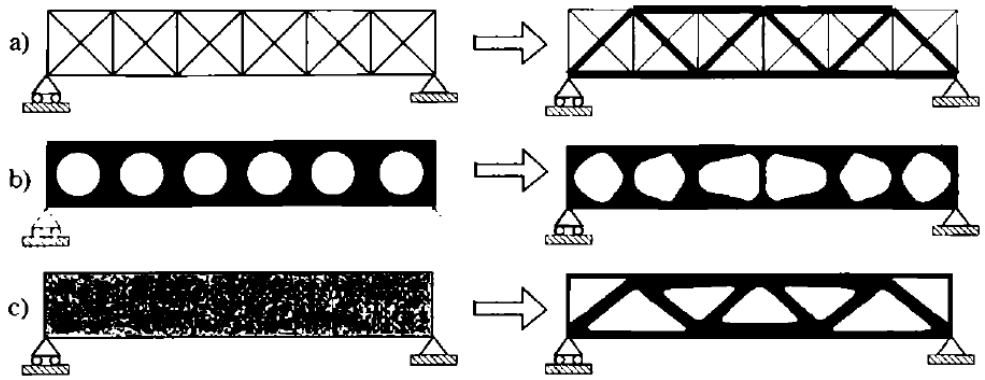

Figure 1.20: Three categories of structural optimization. a) Sizing optimization of a truss structure, b) shape optimization and c) topology optimization [6].

Due to its characteristics, TO allows a greater design freedom than size or shape optimization [57]. As such, TO has extended implication in conceptual and preliminary phases of design, where changes in the design of the final structure have great impact in its performance, being used to find efficient design concepts whereas size and shape optimization are used for detail design with resource to TO design proposals [56, 57].

Once the main goal of this master dissertation is to propose a new structure for the MECSE, TO will be used thereunto, being detailed in the next section.

1.2.3.1 Topology Optimization

Topology Optimization of structures is a rapidly growing field of particular interest to the automotive and aerospace industries [7] since it allows to reduce the total structure volume, weight and cost [58], allowing to design more sustainable products once the environmental, economic and sustainability areas are maximized [44].

TO has its roots in Mitchells' work [59], who developed a theory for the topology of thin-bar structures, optimized with regard to weigth. He acheived a structure where the bars are all perpendicular to each other and form an optimal arrangement in terms of either maximum tensile or compressive stress [55]. 70 years after, his work was extended and the first general theory of topology optimization was formulated, applied primarily to exact analytical optimization of grid-type structures.

The first numerical method were later developed. These could dealt with different materials that could be isotropic, anisotropic and/or porous [60]. One of the pioneers in these numerical methods was Bendsoe [61]. In his work he developed a method that would be later called SIMP (**S**olid **I**sotropic **M**icrostructure (or **M**aterial) with **P**enalization or Power Law method [60]. It is based on the Finite Element Method (FEM) (detailed in chapter 2), where the design domain is discretized into a mesh of elements. The material density of each element has to be rather 0 or 1, defining the element to be a void or a solid, altering the stiffness of the structure once it is linearly dependent on the density. However the optimization of large number of discrete variables is computationally infeasible and therefore the density of each element varies continuously between 0 and 1. Intermediate values of density represent fictitious material and are not meaningful for the solution. Consequently, they need to be penalized. This is achieved by introducing a penalization factor which forces the final design to be 0 or 1 [62].

SIMP however presents some complications such as the checkboard problem and mesh-dependency of results [6]. The first is verified when alternating solid and void elements order in checkboard fashion and is related with the features of the FEM, specifically due to bad modelling by overestimating the stiffness of checkboards. The second one is intrinsic to the existence of solutions to the continuous problem. On the other hand, this method has the advantage of requiring fewer design variables and starts from the original structure, without requiring previous structural analysis, reducing the computational time.

This method is the most commercially used and is implemented in the majority of CAE (Computer Aided Engineering) softwares (OptiStruct, Genesis, MSC/Nastran, Ansys, Tosca, etc.) being now used in a wide range of industries including automotive and aerospace [60].

Another numerical method is ESO (Evolutionary Structural Optimization) first proposed by Xie and Steven. This method is based on FEM as well and the optimization is achieved by removing inefficient material from the structure either based on stress, stifness or displacement. On stress based ESO for example, the engineer starts by defining a safe level. The stresses in all elements of the mesh are calculated and divided by the maximum von Mises stress of the whole structure. The elements with a quoeficient lower than the safe level are deleted [54]. This method however has been demonstrated to result in highly non-optimal design [56].

Reference [4] presents an example of an TO done to an A320 nacelle hinge bracket with the purpose of manufacture it by AM Figure 1.21. The bracket is fixed to the main structure of the nacelle by 6 bolts and fatigue is the main design driver. The original part weighted 918 g and was made of HC101 steel. After the optimization process, the bracket's weight was reduced in 64% to 326 g, the material is now Ti-6Al-4V but the maximum stress dropped down more than 50%. This example clearly shows the benefits that TO brings to the design of structures. It is even highlighted the benefits of the combination of TO and AM. Of course it can be stated that the saving is not that big so the investment in time and software can be profitable. However, it must be remembered that each engine on a plane has 8 brackets and saving 600 g per hinge per engine per plane, represents a huge reduction in companies expenses in fuel in all flights and consequently a reduction on environmental impact.

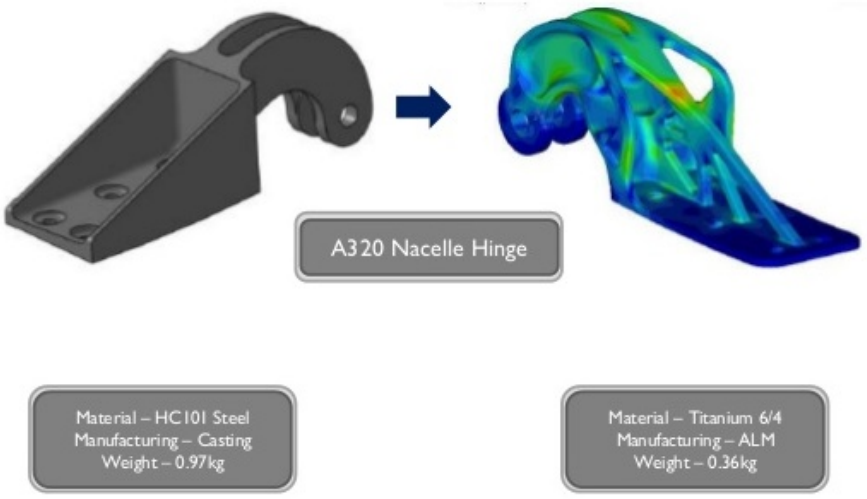

Figure 1.21: A320 nacelle hinge before and after Topology Optimization [4].

Reference [63] apllies TO to an 1U CubeSat structure with the intent to be produced by AM. Their work has two primarly objectives: the first, to obtain a new structure for the CubeSat and the second to study a new assembly procedure. Their workflow is depicted in Figure 1.22.

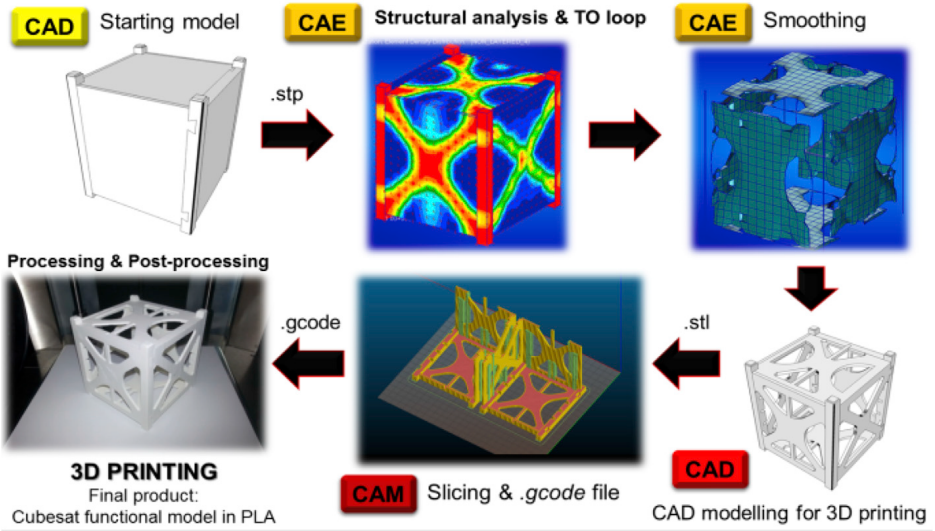

Figure 1.22: Steps followed in CubeSat Topology Optimization case-study [63].

Regarding the first objective, the TO was performed with the mass of the structure, max stress-strain relation and the first 5 modal frequencies as the responses, the maximum of 1.3 kg and the fixed dimensions of the rails as the constraints and the objective defined to maximize the specific stiffness. The proposed final optimized configuration is depicted in Figure 1.23.

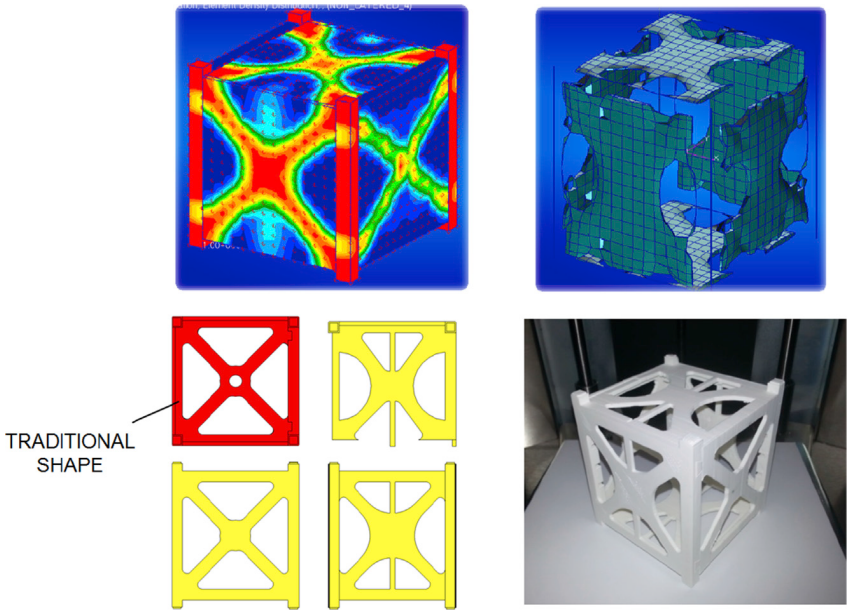

Figure 1.23: New optimized CubeSat's structure configuration [63].

The authors were able to conclude that the variation of the loads intensity and modes did not influence the panels topology but rather the objectives and the constraints play are major influences in the final result.

The second objective comes up due to the characteristics of AM production. Because it can be produced in one piece, but in that way they could not fit the systems inside, the objective was to minimize the number of parts composing the satellite structure. Their solution was a division of the structure in two parts, using an interlocking system between the two parts similar to a puzzle, with two males and two females for each of the two parts. Close to the junctions, a different material was used to avoid the need to bend the material in order to fit. This change made necessary the use of screw and bolts, increasing the number of parts. The final system is depicted in Figure 1.24.

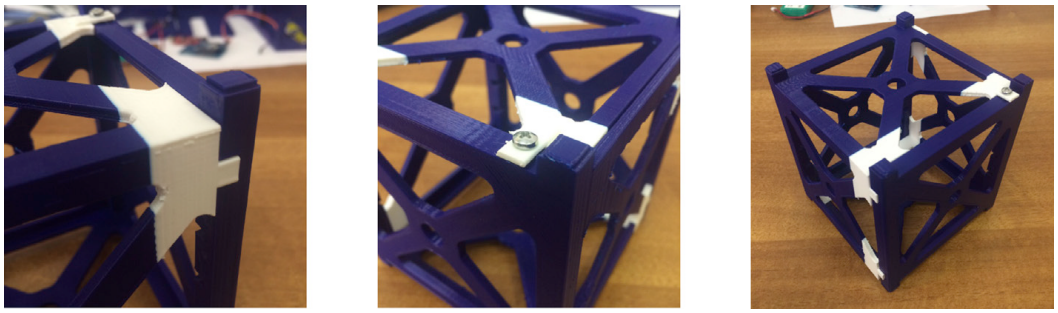

Figure 1.24: Final blocking system [63].

1.3 MECSE Project

Magnetohydrodynamics/Electrohydrodynamics CubeSat Experiment (MECSE) is an under development Small Satellite with scientific and educational purposes. It is the result of a collaborative effort between Centre for Mechanical and Aerospace Science and Technology (C-MAST) [64] and Centre of Engineering and Product Development (CEiiA) [48].

C-MAST was created in 1994 by a group of aerospace engineers that study from Astrodynamics to Technological Forecasting. C-MAST identifies its objectives as carrying-out high-level research in its activity areas; development of international collaboration and participation in international scientific and technological networks and project teams; contribution to national and regional capacity of industrial development and technology transfer; training and qualification of researchers on postgraduate and postdoctoral level and initiation of graduate students in scientific research in the activity areas; promotion of the scientific culture in academic environment and to general public.

CEiiA designs, implements and operates innovative products and systems for technology intensive markets and has recently started to explore space-related fields. CEiiA's mission is to promote a more competitive industry, and to achieve this, CEiiA connects companies, universities, and public entities in different countries. It aims to fast-forward the Portuguese space industry, therefore it accepted the challenge to support the development of MECSE due to its important and innovative mission objectives. A team of experienced engineers has been supporting the project technically and financially, which allows the materialization of MECSE concept [15].

MECSE is a 3U CubeSat (Figure 1.25) intended to be launch by 2020 at Guiana Space Centre (GSC) in French Guiana on VEGA LV [65] and placed in a LEO at an altitude of 350 km [66]. It will have an orbital period of 1.52 h, an orbital velocity of 7.7 km/s and a life time of 293 days [67].

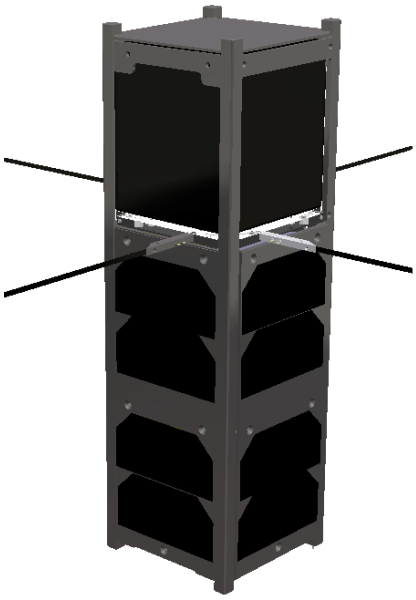

Figure 1.25: MECSE Preliminary Design [15].

MECSE's mission is to validate the theory that a magnetic field can reduce the plasma den-

sity surrounding the spacecraft during atmospheric re-entry. This phenomenon is known as RF blackout [2]. It is caused while a vehicle re-enters or flies through the Earth's atmosphere at hypersonic velocities creating a shock wave in front of the vehicle [68]. The created shock will significantly rise the temperature of the air surrounding the spacecraft ionizing the gas and creating a plasma layer around the vehicle. The communications with the vehicle will be cut-off whenever the plasma frequency exceeds the transmitting frequency of the communication signals [2]. The signal attenuation mainly depends on the plasma's density. The radio waves emitted from and to the vehicle cannot reach a ground station or a Global Positioning System (GPS) satellite and so the vehicle loses voice communication, data telemetry, GPS navigation, and electric countermeasures capability during RF blackout. RF blackout blocks communications of the vehicle for several minutes, depending on the angle of re-entry and the properties of the atmosphere. It is very obvious that the RF blackout problem is critical for flight safety of vehicles [68]. Figure 1.26 shows the Radio Frequency blackout phenomenon around a vehicle at hypersonic velocities with and without mitigation.

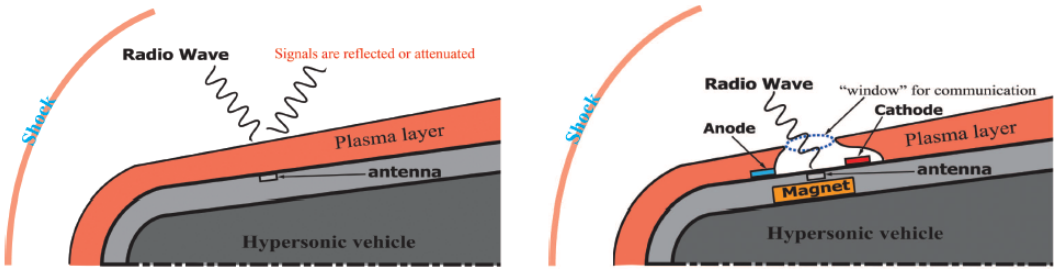

Figure 1.26: Hypersonic vehicle showing the plasma layer around the vehicle. In one case the waves are reflected and communication is lost and in the other case we see the mitigation scheme [69].

1.3.1 MECSE's Missions Objectives

The objectives for the MECSE's mission are:

- Study the formation of Plama in LEO by collecting data for different altitudes;
- Validate the theory that an electromagnetic field can manipulate the plasma layer.

1.3.2 VEGA

Vega is a four-stage LV (Figure 1.27) with a payload lift capability of 1500 kg on missions up to 700 km [65]. It was developed by Arianespace [70] and was first launched in February 2012 at the GSC launching 9 satellites onto LEO [66]. Vega was purpose-designed for the launch of small scientific or Earth observation satellites in response to the commercial market's requirements for a new-generation lightweight launch vehicle capable of orbiting small to medium-sized satellite payloads [71]. The Vega launch system was developed for a launch rate up to four launches per year [66].

The flight profile is optimized for each mission. It is based on the following flight phases and events (Figure 1.28):

- **1st stage:** flight with initial vertical ascent, programmed pitch manoeuvres and a zero-incidence flight;

- **2nd stage:** zero-incidence flight;

- **3rd stage:** flight, fairing separation and injection into sub-orbital trajectory.

Figure 1.27: VEGA's stages [71].

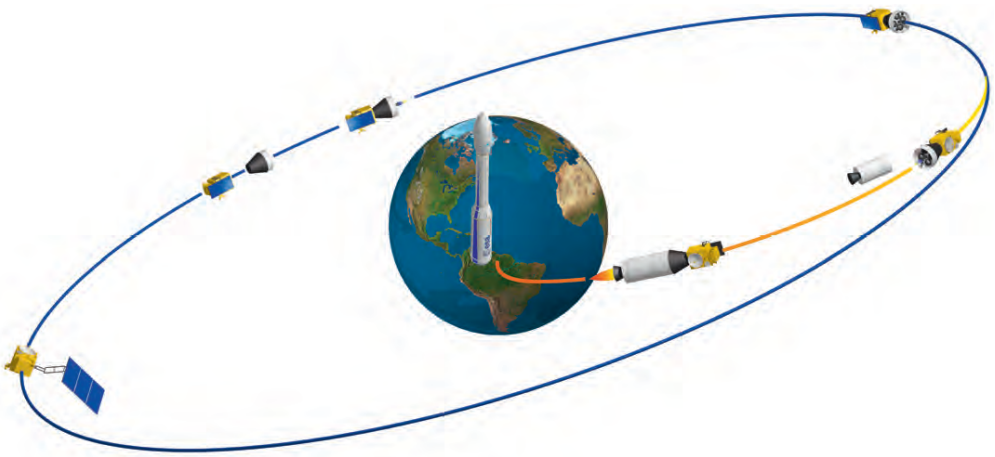

Figure 1.28: Standard Vega Mission Profile [71].

1.4 Dissertation Objectives

CEiiA challenged the author of this dissertation to optimize the structure of the MECSE that would allow a lighter and thus cheaper platform to access space.

The objectives established for this dissertation are:

- Investigate different Optimization methodologies;
- Investigate different AM processes and restrictions in the Mechanical System;
- Propose a new MECSE's Optimized Mechanical System;

1.5 Dissertation Outline

This master dissertation is divided in four chapters:

Chapter 1 presents the author's motivation to optimize the MECSE's Mechanical Subsystem, a State-of-the-Art, MECSE Project description and objectives of this master's dissertation.

Chapter 2 has the purpose of reviewing the Finite Element Analysis, by detailing how it must be conducted and explaining some key parameters. The mechanical environment to which the MECSE will be exposed is analysed and an insight of how Topology Optimization process and major influences is done.

Chapter 3 will all the work done from the geometry creation, going through the optimization results and FEA validation up to the assemblage methodology. A comparison between the proposed structure and the current one is also done.
describes the used methodology for the present work as well as all the results of this work.

Chapter 2

Background

This chapter contains a review of important theoretical and mathematical aspects for the objectives of this dissertation focusing on the structural subsystem as well as on topology optimization. These concepts are very important to aid in the decisions made in this dissertation.

2.1 Structural Analysis

In order to solve any engineering problem, there are three methods: the Analytical Method, the Numerical Method and the Experimental Method [72], depicted in Table 2.1.

Table 2.1: Methods to Solve Any Engineering Problem [72].

Analytical Method	Numerical Method	Experimental Method
• Classical approach • 100% accurate results • Closed form solution • Applicable only for simple problems like cantilever and simply supported beams, etc. • Complete in itself	• Mathematical representation • Approximate, assumptions made • Applicable even if a physical prototype is not available (initial design phase) • Real life complex problems • Results can not be believed blindly. Certain results must be validated by experiments and/or analytical method.	• Actual measurement • Time consuming and needs expensive set up • Applicable only if physical prototype is available • Results can not be believed blindly and a minimum of 3 to 5 prototypes must be tested
• Though analytical methods could also give approximate results if the solution is not closed form, in general analytical methods are considered as closed form solutions i.e. 100% accurate.	• Finite Element Method: Linear, nonlinear, buckling, thermal, dynamic, and fatigue analysis • Boundary Element Method: Acoustics, NVH • Finite Volume Method: CFD (Computational Fluid Dynamics) and Computational Electromagnetics • Finite Difference Method: Thermal and Fluid flow analysis (in combination with FVM)	• Strain gauge • Photo elasticity • Vibration measurements • Sensors for temperature and pressure, etc. • Fatigue test

In the CubeSat project, the validation through experimental methods is mandatory [13], but in early stages of the development they are not viable because its final structure is not yet defined. The analytical method is the only that gives exact solutions, but the MECSE's Mechanical Subsystem has a too complex geometry for this method [73]. Therefore, for this master dissertation the Finite Element Method is the numerical method chosen.

2.1.1 Finite Element Method

The Finite Element Method (FEM) is a numerical method that uses algebric equations to determine the approximated solution for the Partial Differential Equations (PDE) on a defined domain (ω). As all real life objects are continuous and have infinite degrees of freedom, solving any problem is not possible. FEM reduces the degrees of freedom from infinite to finite by dividing the domain into nodes and elements and the variables (such as displacement) are computed for all the nodes. In between the nodes, FEM uses and interpolation function ir order to compute the results [72, 74]. Common engineering applications of the method are structural analysis, heat transfer, fluid flow, mass transport, and electromagnetic potential [72, 73, 75].

The standard process involved in a Finite Element Analysis (FEA) is summed up in Figure 2.1.

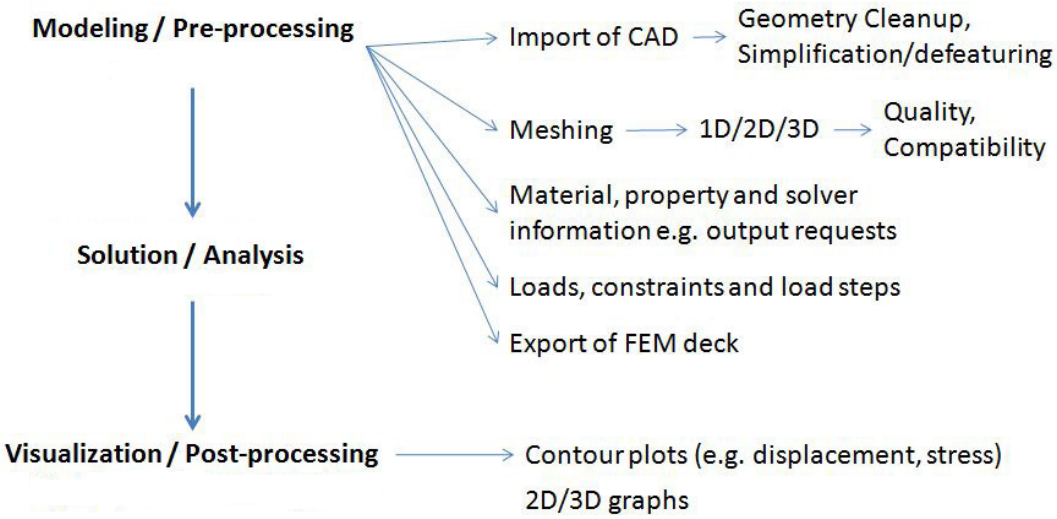

Figure 2.1: FEM standard process. Adapted from [72].

Each step of the FEA is seen in more detail below.

2.1.1.1 Pre-Processing

FEM process starts by the pre-processing of the problem. This step is prior to the analysis and is crutial to the results because directly reflects on the quality of the results taht will be generated.

Import CAD

The pre-processing starts with the import of the CAD geometry. However, the imported geometry is not often ready for the next steps of the process, needing to be cleaned up first, due to surfaces which are not stitched together, redundant (multiple) surfaces or/and the juncture between two surfaces containing gaps, overlaps or other misalignments [72].

After the clean up, some geometry simplifications may be appropriate or even required so better mesh quality can be achieved. As an example, fillets may be replaced by sharp edges and, consequently, must be kept in mind that the FEM model in a deviation from the original geometry. To account for this, the meshing process in this critical areas must be done with special care [72].

Meshing

Once the geometry is in an appropriate state, the mesh may be created. There are three types of elements that, according to the problem, may be used to model the structure of geometry: 1D, 2D and 3D (Figure 2.2). There are however other elements such as masses, springs and rigid connectors that are used in conjunction with structural elements to model, for example, shock absorvers, joint stiffness between linkages and isolation pads [74].

1D Elements: These elements are used when one of the dimensions of the geometry is much larger than the other two. They are represented by a line. When defining this type of elements, the software is aware of one of the dimensions. The other two and the cross section have to be defined by the user in addictional input. Some practical applications of this are long shafts and beams [72].

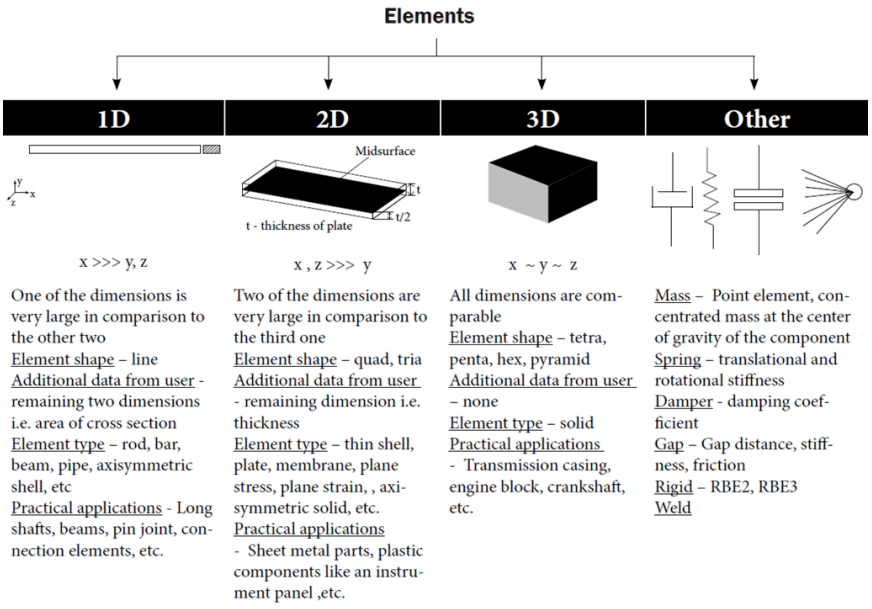

Figure 2.2: FEM types of elements [72].

2D Element: These elements are used when two of the dimensions are much larger then the third one. They are represented like a piece of paper and the software is aware of two of the dimensions. The third one, thickness, must be given by the user. One pratical application of this is sheet metal part [72].

3D Element: These elements are used when the three dimensions of the geomety have comparable size. When using this elements the software aware of all the dimensions and no addictional input is needded. Some pratical applications of this are gear box, engine block, crank shaft and clutch housing [72].

Some problems may be solved meshing the geometry with any of the elements. The only differences will be the number of nodes and elements, the accuracy and consequently, the time used to solve it. These consequences must be weighted against computational time. Reference [72] analysed a cantilever beam subjected to a vertical downward force and compared the stress obtained by meshes using the different types of elements. The results are depicted in Table 2.2.

Table 2.2: Analysis comparation between different types of elements [72].

	Nodes	Elements	Stress N/mm^2	Displacement mm
Analytical	–	–	105	4.23
1D	2	1	105	4.23
2D	909	800	103	4.21
3D	17,448	9,569	104	4.21

The meshing step is crucial to the FEM analysis as the mesh quality directly reflects the final result. The finer the mesh, the more accurate is the result and the computational time is increased. Even in one's geometry mesh, the density varies because in places where the results change rapidly, a finer mesh is desirable, while on the other hand, for places where the result is constant, larger elements may be used [76].

Material and Property information

After the mesh is built is completed, material and property information must be defined and assigned to the elements. Material information comprehends parameters such as elastic modulus (E), poisson's ratio (ν), shear modulus (G), mass density (ρ) and thermal expansion coefficient (α). Property information is typically thickness when 2D or 1D elements are implied [77].

Loads, Constraints and Solver Information

In structural analysis problems the purpose is to determine the response of the geometry to a set of loads and constraints that better represent the "real" physical model [72]. As mentioned in chapter 1, for this work the loads and constraints are provided by the LV operator at their User's Manual and detailed in subsection 2.1.3.

Additionally, not only the solver must be informed about what type of solution must perform but also which parameters must be outputed (such as displacement, element stresses, constraint forces, element forces, element strains amoung others) [77].

2.1.1.2 Solution

During the solution phase the software is responsible for computing the solutions requested by the user if no errors are encountered, in which case, the solution may be aborted. The user must then analyse the report given by the solver that details the error and fix them before re-running the analysis.

2.1.1.3 Visualization

The results obtained are written in a file that the user has to import to the post-process program in order for the results to be read and displayed. The requested output parameters are plotted and examined to see how the geometry responded to the various load cases. Based on the results, modifications may be made to the geometry and a new analysis may be run to understand how the modifications affected it.

2.1.2 Degrees of Freedom

Degree of freedom (DOF) is one of the core concepts in FEA since this method reduces any problem to a finite number of DOFs.

Observing points A and B depicted in Figure 2.3, if they are shifted out of plane and rotated arbitrarily in all axes, in order to define the position of point A completely we would need 6 DOF's i.e. 3 translations (U_x, U_y, U_z) and 3 rotations (θ_x, θ_y, θ_z). The total number of DOFs in any model is given by multiplying the number of nodes by the number of DOFs per node [72].

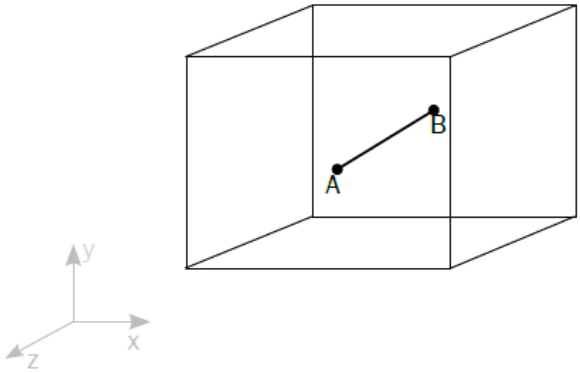

Figure 2.3: Degree of freedom [72].

However not all the elements have 6 DOFs per node. This number depends on the type of element, the family of element and the type of analysis. 1D and 2D elements have 6 DOFs but 3D only have the 3 translational DOFs per node. This can be understood by observing Figure 2.4.

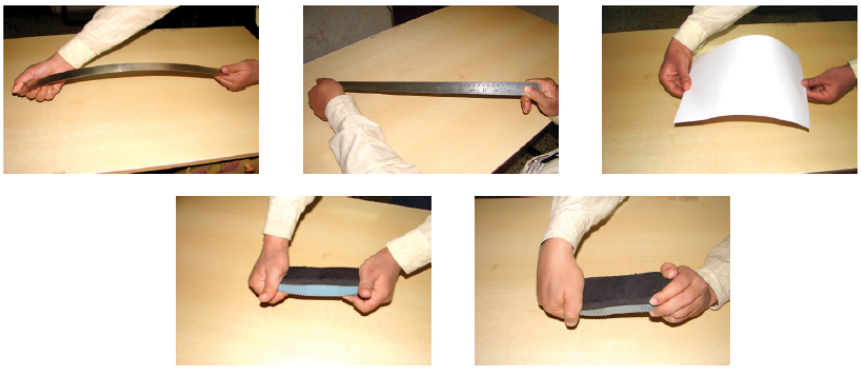

Figure 2.4: 1D and 2D DOFs vs 3D DOFs [72].

As depicted in Figure 2.4, the piece of paper (2D geometry) and the long steel scale (1D geometry) can easily be bent and twisted (rotational DOFs) while the paper weight (3D geometry) can not. Therefore 3D elements are formulated with 3 DOFs per node as opposed to 1D and 2D that are formulated with all the 6 DOF's per node [72].

2.1.3 Mechanical Loading

Satellites are launched using multistages LV whose purpose is to lift the satellite off the ground and accelerate it to orbital velocity. During launch, the rocket engines produce very harsh vibrations which propagate throughout the structure of the LV and are transmitted to the satellite

through its attachment interface. The engines also produce a high level of acoustic noise which generate high acoustic loads and broadband vibration on the LV. Significant acoustic and broadband random vibrations are produced by the LV's interaction with the atmosphere during the transonic phase of the flight. In addition, the satellite is also subjected to shock loads produced by the pyrotechnic devices used for the ignition and separation of the various stages of the LV [78].

At any point during the flight the spacecraft can simultaneously be subjected to a combination of high frequency, low frequency, quasi-static, acoustic, and shock loads in all axes, depicted in Figure 2.5. This phenomena shows the need to split these well-defined loads in order to allow the structure to be analysed, ensuring it is capable to withstand the launch environment [78].

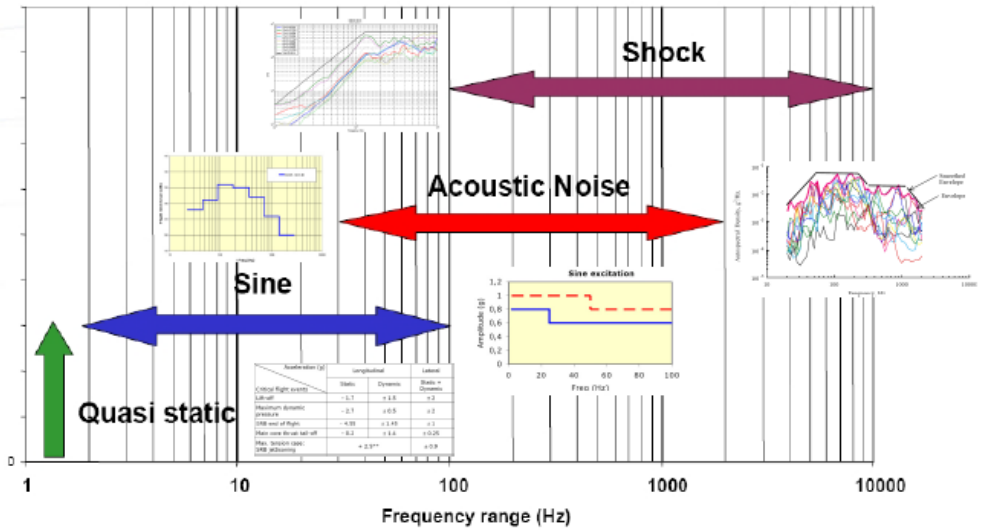

Figure 2.5: Static and Dynamic Environment Specifications (Typical Range) [79].

2.1.3.1 Quasi Static Loads

The Quasi Static Loads (QSL) are low frequency dynamic loads produced by phenomenas such as wind loading, asymmetric vortex shedding, asymmetric ignition, and pressure oscillations during the early stages of launch. These loads are derived by the launch agency on the basis of their experience, calculations, and considering appropriate statistical safety factors. They may be presented in the form of an envelope diagram which gives vertical versus lateral loads.

The QSL are applied at the satellite in a static analysis and are used for the preliminary sizing of the structure. The capability of the structure to withstand these loads without failure is usually demonstrated via structural analysis and tests [78].

2.1.3.2 Sine Loading

During launch the satellite will experience significant low frequency dynamic loads that can be well-approximated by sinusoidal functions. The frequency range depends on the LV characteristics because if a satellite fundamental frequency was in this range it would be in a condition of structural resonance and this would cause amplification of the loads on the satellite due to the resonance phenomenon and could result in structural failure.

For the VEGA LV specific case, there are lateral modes and longitudinal modes of vibration so two different lower limits are set, one for the lateral modes and the other for the axial ones. The satellite must be designed to withstand sinusoidal loads over the range specified by the launch agency [78].

2.1.3.3 Acoustic and Random Loading

Some of the phenomena occurring during launch produce a broadband excitation. The characteristics of the oscillations lose the typical sinusoidal behaviour associated to low frequency excitation to become much more random in nature.

The spacecraft has to be able to withstand without failures these vibrations. This type of loads are transmitted to the spacecraft in two ways, either as vibrations through the satellite to LV interface or as acoustic energy absorbed by the external surfaces of the satellite. These two forms of random loading are specified separately by the launch agency.

For small satellites the random vibration loading is more significant than the acoustic loading. The random vibration experienced by the spacecraft during launch is dependant on the launch configuration and varies considerably from launch to launch. These are defined as a power spectral density profile [78].

2.1.3.4 Shock Loading

The shock loading during flight is produced by the mechanisms used to separate the various stages of the LV or fairing jettisoning. These systems use explosive charges with the purpose of breaking some connection and the explosion of the pyrotechnic and the strain energy suddenly released produce a very rapid transient load (shock) that is characterised by a very high acceleration and very high frequency oscillations rapidly damped.

The shock environments are specified using Shock Response Spectra (SRS), which is a method to capture the severity or damaging potential of a shock. The SRS produces a curve that gives acceleration as a function of frequency, and each point of the curve represents the maximum acceleration response of a single degree of freedom system. Shocks are not a great concern for the primary structure of the satellite, unless there are some brittle materials (such as ceramics) where it can produce cracks and fractures [78].

Every loading phenomena requires a different analysis method to be applied. As the purpose of this dissertation is the development of a new CubeSat structure, only the QSL will be applied in the FEA in order to compute the displacement, stress, strain and the first natural frequency of the structure. As so, a Linear Static Analysis will be applied to compute the first three and a Modal Analysis will be used to extract the natural frequency.

2.1.4 Linear Static Analysis

In a linear static analysis the effects of steady loading on a structure are calculated with Equation 2.1.

$$K\ u = F \quad (2.1)$$

where K is the stiffness matrix of the structure (process seen in detail in subsubsection 2.1.4.1), u is the displacement vector and F is the loads vector applied to the structure. This equation is the equilibrium of external (rigth hand side) and internal (left hand side) forces [72].

After the calculation of the displacements, the stress and the strain of the structure can be computed. The strain (ε) is defined as the quotient between elongation δ and the original element length (l):

$$\varepsilon\ =\ \frac{\delta}{l} \quad (2.2)$$

where $\delta\ =\ u_2 - u_1$ is the difference between the length of the element after the load is apllied and the original length of the element. The strain is now used to compute the stress, σ, assumed to be a linear function of the strain in the linear elastic range, by the constitutive relation of the material, or Hooke's law, stated as:

$$\sigma = C\ \varepsilon \quad (2.3)$$

where C is the constitutive matrix given, in the case of a 3D element, by

$$\Big[C\Big] = \frac{E}{(1+\nu)(1-2\nu)} \begin{bmatrix} 1-\nu & \nu & \nu & 0 & 0 & 0 \\ & 1-\nu & \nu & 0 & 0 & 0 \\ & & 1-\nu & 0 & 0 & 0 \\ & & & \frac{1-2\nu}{2} & 0 & 0 \\ & & & & \frac{1-2\nu}{2} & 0 \\ Symmetry & & & & & \frac{1-2\nu}{2} \end{bmatrix} \quad (2.4)$$

where E and ν are the modulus of elasticity and the Poisson's ratio of the material, respectively.

In Figure 2.6 a flowchart of a FEM problem in a linear static analysis is detailed.

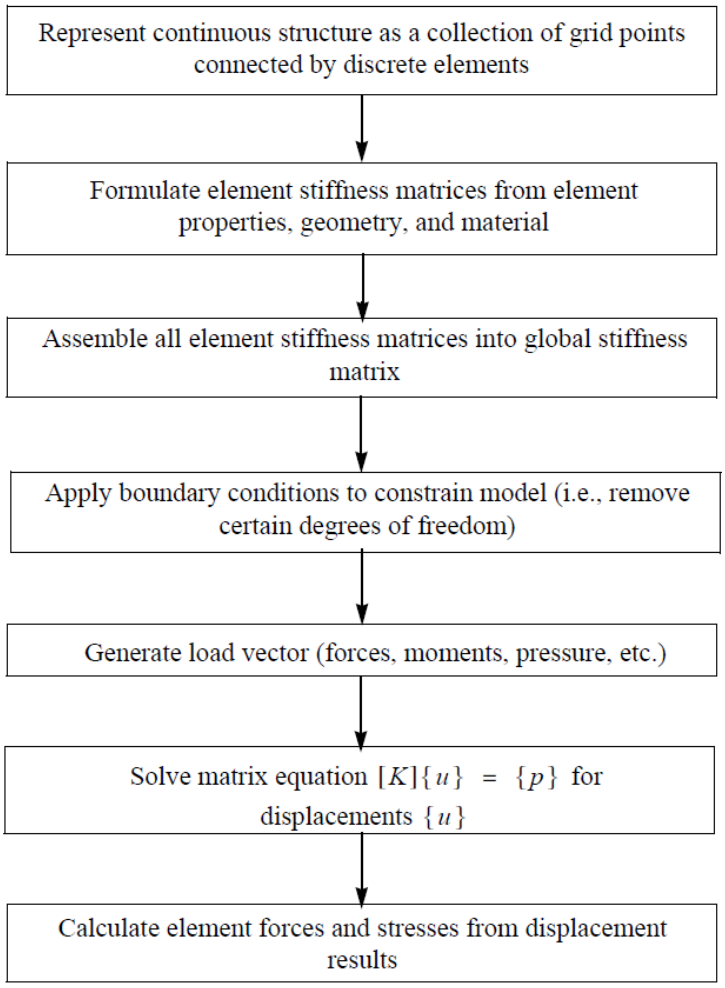

Figure 2.6: Linear Static Analysis Flow [74].

2.1.4.1 Assemblage of the Stiffness Matrix

This section is presented in order to better understand the process of assemblage of the stifness matrix, as it is a critical step in the optimization process, detailed in section 4.2, the major objective of this dissertation.

As mentioned in the previous section, the stiffness matrix K of the structure is an assemblage of individual striffness matrices of each element of the mesh. In order to understand this process an example is developed in this section.

In Figure 2.7 a series of springs and its representation in FEM (where each spring is represented by one element and its end by nodes) is depicted. One of the extremities is fixed to the wall and the other is pulled with a constant force. The objective is to find the displacement of the springs.

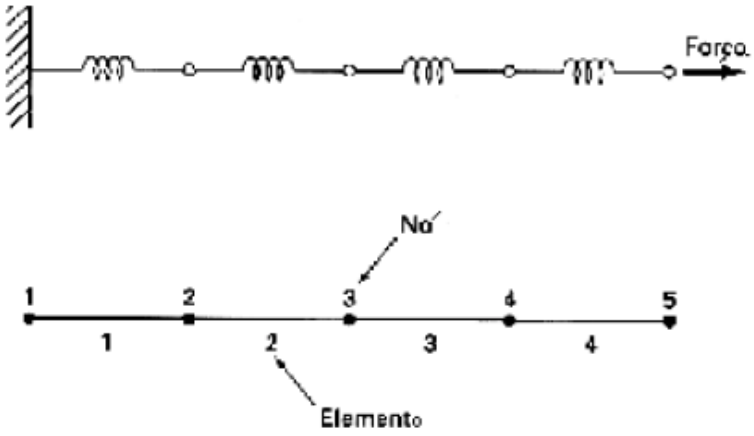

Figure 2.7: Problem description and discretization [80].

In Figure 2.8 one individual element is ilustrated as well as the forces that its nodes are subjected to.

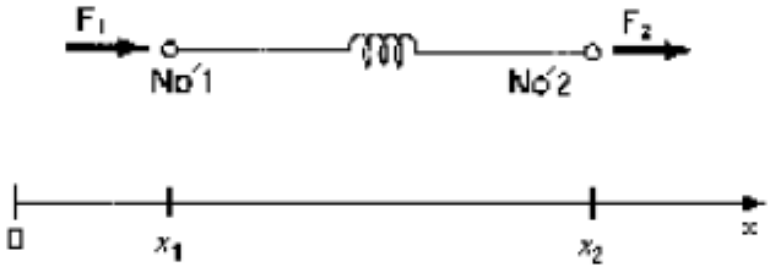

Figure 2.8: Individual element [80].

The relationship between the force F and the displacement x may be represented as:

$$F = kx \quad (2.5)$$

where k represents the constant of the spring. If the force F_1 is apllied to node 1, the following exists:

$$F_1 = k(x_1 - x_2) \quad (2.6)$$

where x_1 is the displacement of node 1 and x_2 is the displacement of node 2. Developing the equation above:

$$F_1 = kx_1 - kx_2 \quad (2.7)$$

The same also apllies to node 2, but in a symetrical way since a balance must exist.

$$F_2 = -kx_1 + kx_2 \quad (2.8)$$

Rewriting this equations in a matrix form:

$$\begin{bmatrix} k_{11}^e & -k_{12}^e \\ -k_{21}^e & k_{22}^e \end{bmatrix} \begin{Bmatrix} x_1 \\ x_2 \end{Bmatrix} = \begin{Bmatrix} F_1^e \\ F_2^e \end{Bmatrix} \quad (2.9)$$

where the exponential e denotes the elements that each entry corresponds to and the numbers associated to the k denotes their location in the element matrix. Proceding in this way for all the elements, the structure K matriz is assembled as depicted in Equation 2.10.

$$\Big[K\Big] = \begin{bmatrix} k_{11}^1 & -k_{12}^1 & 0 & 0 & 0 \\ -k_{21}^1 & k_{22}^1 + k_{11}^2 & -k_{12}^2 & 0 & 0 \\ 0 & -k_{21}^2 & k_{22}^2 + k_{11}^3 & k_{12}^3 & 0 \\ 0 & 0 & -k_{21}^3 & k_{22}^3 + k_{11}^4 & -k_{12}^4 \\ 0 & 0 & 0 & -k_{21}^4 & -k_{22}^4 \end{bmatrix} \quad (2.10)$$

2.1.5 Modal Analysis

Modal analysis, also called eigenvalue analysis, is an analysis method used to calculate the vibration shapes and associated frequencies that a structure will present. These are fundamental to know because if cyclic loads are applied at these frequencies, the structure may experience resonance that will lead to catastrophic failure. It is also crucial to know the shapes to make sure that the loads are not applied at points that will cause the resonance condition [72].

Natural frequencies and mode shapes are functions of the structural properties and boundary conditions. If the structural properties change, the natural frequencies change, but the mode shapes may not necessarily change. If the boundary conditions change, then the natural frequencies and mode shapes both change [81].

For this dissertation, only the natural frequencies will be taken into account in the optimization process and so only the mathematical process to compute them will be detailed.

Considering no damping and no applied load, the equation of motion in matrix form is:

$$\Big[M\Big] \Big\{\ddot{u}\Big\} + \Big[K\Big] \Big[u\Big] = 0 \quad (2.11)$$

where $\Big[M\Big]$ is the mass matrix, $\Big\{\ddot{u}\Big\}$ the acceleration, $\Big[K\Big]$ the stiffness matrix and $\Big[u\Big]$ the displacement. This is the equation of motion for undamped free vibration [81]. To solve it we assume a harmonic solution of the form:

$$\Big\{u\Big\} = \Big\{\phi\Big\} sin(\omega t) \quad (2.12)$$

where $\Big\{\phi\Big\}$ is the eigenvector and ω is the circular natural frequency. This harmonic form of the solution means that all DOFs of the vibrating structure move in a synchronous manner. The configuration does not change its basic shape during motion, only its amplitude changes [81].

Performing the differentiation and replacing into Equation 2.11, the following is obtained:

$$-\omega^2 \left[M\right] \left\{\phi\right\} sin(\omega t) + \left[K\right] \left\{\phi\right\} sin(\omega t) = 0 \quad \textbf{(2.13)}$$

which after simplifying becomes

$$(\left[K\right] - \omega^2 \left[M\right]) \left\{\phi\right\} = 0 \quad \textbf{(2.14)}$$

This equation is called the eigenequation and forms the basis for the eigenvalue problem. This has two possible solutions:

- If $det(\left[K\right] - \omega^2 \left[M\right]) \neq 0$, the only possible solution is $\left\{\phi\right\} = 0$. This is the trivial solution and has no valueable information since it represents the case of no motion (det denotes the determinant of a matrix).
- If $det(\left[K\right] - \omega^2 \left[M\right]) = 0$. The determinant is zero only at a set of discrete eigenvalues ω_i^2. There is an eigenvector $\left\{\phi_i\right\}$ which satisfies and corresponds to each eigenvalue.

Each eigenvalue and eigenvector define a vibration mode of the structure. The i-th eigenvalue is related to the i-th natural frequency (f_i) as follows:

$$f_i = \frac{\omega_i}{2\pi} \quad \textbf{(2.15)}$$

The number of possible eigenvalues and eigenvector is equal to the number of dynamic DOFs [81].

2.2 Topology Optimization

A general optimization problem is mathematically stated as:

$$\begin{aligned} &Minimize\ f(x) = f(x_1, x_2, x_3, ..., x_n) \\ &Subjected\ to\ g_j(x) \leq 0, \quad j = 1, ..., m \\ &x_i^L \leq x_i \leq x_i^U \end{aligned} \quad \textbf{(2.16)}$$

where $f(x)$ is the objective function, $g(x)$ are the constraint functions, and x is a vector of design variables.

There are four different types of TO: density-based methods, hard-kill methods, boundary variation methods and biologically inspired methods [57]. The approach used by *Optistruct* is a density-based method called SIMP (Solid Isotropic Material with Penalization) [62].

The basic goal of SIMP is minimizing an objective function, on a fixed domain of FE, identifying whether each element consists of solid material or void. This is done by imposing a penalty

factor (p) to every element's stiffness forcing the solution to be 0 or 1 [57].

Mathematically this may be written as

$$x_e = \rho_e / \rho_0 \quad (2.17)$$

where x_e is the relative density of the element, ρ_e is the density of the element and ρ_0 is the material density. This changes the stiffness of the elements according to Equation 2.18.

$$K_e = x_e^p K_0 \quad (2.18)$$

where K_e is the stiffness of the element, p the penalty factor and K_0 is the stifness of the material. The penalty factor for a 3D analysis is given by Equation 2.19.

$$p \geq \max \left\{ 15 \frac{1-\upsilon^0}{7-5\upsilon^0} \quad , \quad \frac{3}{2} \frac{1-\upsilon^0}{1-2\upsilon^0} \right\} \quad (2.19)$$

where υ^0 is the Poisson ratio of the material. According to [6], in a 3D problem, the smallest allowable p is 3. In Figure 2.9 the density penalization according to penalty factor value is depicted. As seen, the bigger the p, the bigger will be the penalization and more forced is the solution to whether be 0 or 1.

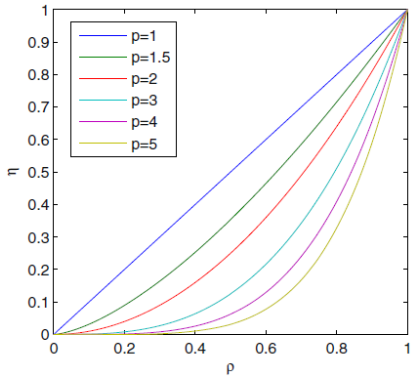

Figure 2.9: Intermediate density penalization [57].

2.2.1 Member Size Control

The member size controls the dimension to be retained by the elements in topology optimization. It can be splited in Minimum Member Size and Maximum Member Size [62].

2.2.1.1 Minimum Member Size

The minimum member size (MINDIM) control limits the formation of small members, minimizing the checker board effect. Avoiding thin members enhances the simplicity of the design and consequently its manufacturability. Minimum member size is then considerated to function as a quality control rather than quantity control [62, 82].

It is recommended that the MINDIM to be at least 3, and no more than 12 times the average

element size. The average element size, in a 2D domain, is given by the average of the square root of the area of the elements, and in a 3D domain by the average of the cubic root of the volume of the elements.

Illustrated in Figure 2.10 is a cantilivered beam optimized in 3 different cases. In the first case at the left, no MINDIM control was applied and the occurance of the check board effect is noted. At the center a minimum member size of 60 and at the left of 90 were applied and its effects are clearly seen as the members thickness increase, thus eliminating the checkboard effect.

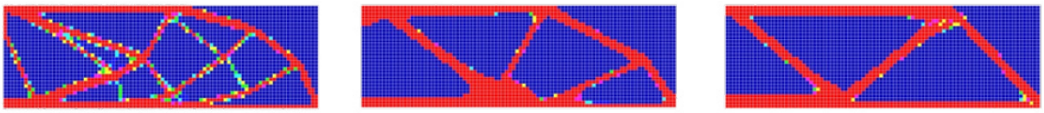

Figure 2.10: Member size control of a cantilivered beam [62].

2.2.1.2 Maximum Member Size

Opposingly to the minimum member size, the maximum member size (MAXDIM) limits the formation of large members. This control is not directional which means that if the thickness of a member is less than the MAXDIM, the constraint is satisfied.

The MAXDIM must be at least twice the MINDIM, and so the minimum mesh requirement is that MAXDIM has to be 6 times the average element size. In addition, the MAXDIM shall be less than half the width of the thinnest part of the design region, which implies that a fine mesh is required to achieve good results with this constraint. Figure 2.11 depicts the impact of the MAXDIM control in a design domain. On the left hand side the design without MAXDIM control and in the rigth hand side the design with MAXDIM.

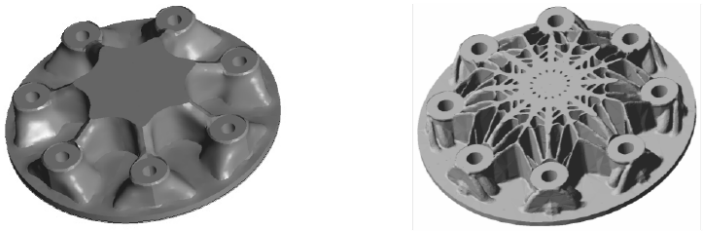

Figure 2.11: Maximum member control size of the design domain [62].

2.2.2 Pattern Grouping

Pattern grouping links the optimization variables together in a way that the desired reinforcement is formed. One-plane, two-plane, three-plane and cyclical symmetry pattern grouping are the available options to ensure the symmetry of the solution is created. The symmetry design can be obtained regardless of the boundary conditions or loads and can also be used for irregular element meshes [62, 82].

Figure 2.12 ilustrates the results obtained for different symmetry conditions. The top left images demonstrate the situation of no pattern grouping apllied and the solution presents no symmetry. The top rigth and the bottom left present symmetry with respect to one plane. The bottom

right presents symmetry with respect to the two planes used separately in the previous cases. The enforcement of the symmetry conditions in the different situations result in significantly different designs.

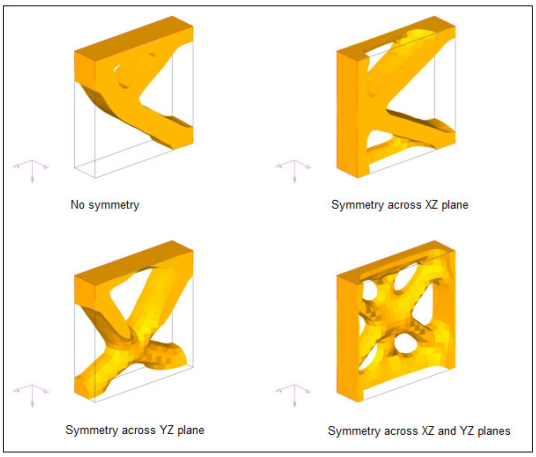

Figure 2.12: Pattern grouping of a block of material [62].

2.2.3 Optimization Loop

The computational optimization process can be outlined as in Figure 2.13. As shown, the model goes through a first analysis and evaluation as basis for the first optimization evaluation. Then, by altering the design variables the loop is gone through repeatedly until the optimization is achieved [62, 82].

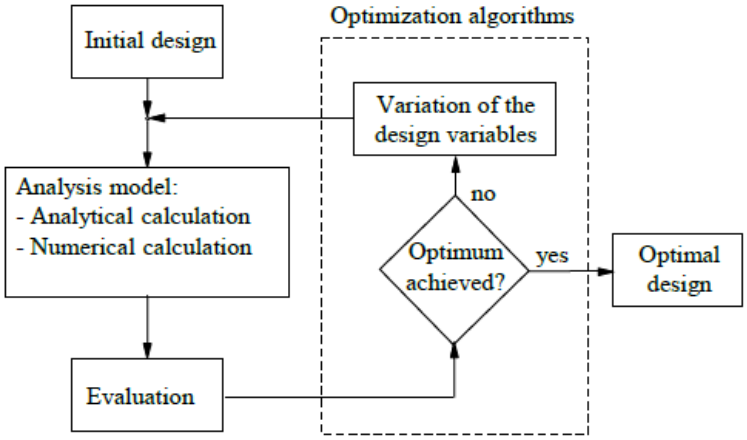

Figure 2.13: Optimization loop [62].

Chapter 3

Structural Optimization

There are several considerations that must be taken into account when designing a new satellite's structure. These considerations ensure that the final design fulfil all the design objectives. For the MECSE's project, a complete investigation of all the CubeSat Design Requirements has already been done [15] and a list of the high level requirements that shall be considered in the design of the mechanical is compiled in Table 3.1.

Table 3.1: CubeSat Design Requirements [15].

#ID	Design Requirements	Rationale
DR-01	The Structural Subsystem shall integrate all the spacecraft equipment	Subsystem Requirement
DR-02	The Structural Subsystem shall connect mechanically and electrically the spacecraft equipment	Subsystem Requirement
DR-03	The Structural Subsystem shall protect mechanically the spacecraft equipment during launch	Subsystem Requirement
DR-04	The Structural Subsystem shall ensure the integration within the P-POD and the test pod	Subsystem Requirement
DR-05	When inside the P-POD the CubeSat's power system shall be at a power off state, to prevent the CubeSat from activating any powered functions	CDS
DR-06	The Structural Subsystem's mass shall not exceed 600g	Systems Engineering
DR-07	The CubeSat shall have an access port area on a side face	CDS
DR-08	No external components other than the rails shall touch the inside of the P-POD	CDS
DR-09	Rails shall have a minimum width of 8.5mm	CDS
DR-10	The edges of the rails will be rounded to a radius of at least 1mm	CDS
DR-11	No components shall exceed 6.5mm normal to the surface	CDS
DR-12	The ends of the rails on the +/-Z face shall have a minimum surface area of 6.5mm x 6.5mm contact area for neighboring CubeSat rails	CDS
DR-13	Aluminum 7075, 6061, 5005 and/or 5052 will be used for both the main CubeSat Structure and the rails. If other materials are used the developer will submit a DAR and adhere to the waiver process	CDS
DR-14	The CubeSat rails and standoff, which are in contact with the P-POD rails and adjacent CubeSat standoffs, shall be hard anodized aluminum to prevent any cold welding within the P-POD	CDS
DR-15	Separation springs are not required for 3U CubeSats	CDS
DR-16	The CubeSat center of gravity shall be located within 20mm from its geometric center in the X and Y directions	CDS
DR-17	The 3U CubeSat center of gravity shall be located within 70mm from its geometrical center in Z direction	CDS
DR-18	The Subsystems shall be distant from each other 15.24mm	PC/104Plus
DR-19	The Batteries shall be distant from each other 23:5mm	COT Requirement
DR-20	The Structural Subsystem shall be able to resist the lateral and longitudinal loads imposed by the launcher during all the phases of ascension	VEGA Requirement

As detailed in chapter 2, the FEM is the numerical method chosen for the structural optimizations and analysis presented in this work. Following the workflow involved in FEA depicted in Figure 2.1, the work is described step by step.

The softwares used for the realization of this masters dissertation were CATIA® [83], Altair HyperMesh™ [84], Optistruct™ [85] and Altair HyperView™ [86].

3.1 Pre-processing

3.1.1 Geometry Creation

The approach defined for this dissertation was the creation of a fully dense shell of material, representing the outer contour of the structure, with the size of a standard 3U CubeSat, detailed in Appendix A, which is the form factor defined for the MECSE.

The created geometry was imported from CATIA® [83] into the Altair HyperMesh™ [84] in order to start the FEM process. Due to the simplicity of the geometry, no cleanup, simplification or defeaturing was necessary prior to meshing.

3.1.2 Meshing

The initial intention for this work was to perform the optimization for a 3D mesh. This was created and prepared for analysis but when intended to run it required too much of computational capacity, altering the initial proposal from a 3D mesh to a 2D mesh which reduces the computational capacity required for the optimizations because they have a reduced stiffness matrix and therefore reduced solution time with no loss in accuracy [72].

In order to simplify the meshing process, only one quarter of the geometry was meshed and afterwards this was mirrored so the mesh of the full strcuture was obtained. This was possible because the MECSE structure has 2 symmetry planes, ZY and ZX.

The mesh was all created with square elements with a side of 1 mm. The reason for the use of this element dimension without any mesh convergence study is explained in subsection 3.2.1.

The symmetry of the mesh was performed and an equivalence of nodes was done (in order to eliminate the duplicate nodes that appear were the symmetry meshes join). The fully done mesh is depicted in Figure 3.1.

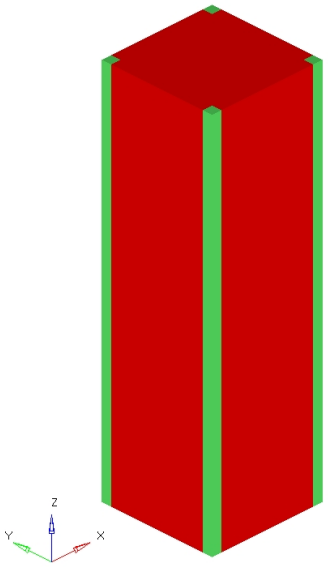

Figure 3.1: 2D mesh.

With the structure of the CubeSat finished, the electronic components and its attatchments to structues were to be defined. Firstly, the systems were modulated with concentrated mass points in their center of gravity (CG). The CONM2 card was used in order to account for the inertia of the systems inside the structure. The placement of the CONM2 and their mass was done according to the current placement and mass of the systems, detailed in Table 3.2 and depicted in Figure 3.2.

Table 3.2: Electronics mass and center of gravity [15]

System	Mass [kg]	CGx [mm]	CGy [mm]	CGz [mm]
Payload	1.200	3.00	2.00	69.75
Antenna	0.100	-1.03	0.00	52.30
Battery 1	0.270	-1.64	4.02	-19.61
Battery 2	0.270	-1.64	4.02	-44.96
PMB	0.200	-2.82	6.180	-91.57
Transceiver	0.075	-2.94	0.57	-108.34
MagneTorquer	0.206	31.73	0.94	-125.28
OBC	0.077	0.67	8.00	-141.70

The reference point for the CG's is the geometrical center of the CubeSat, highlighted with a yellow node in Figure 3.2.

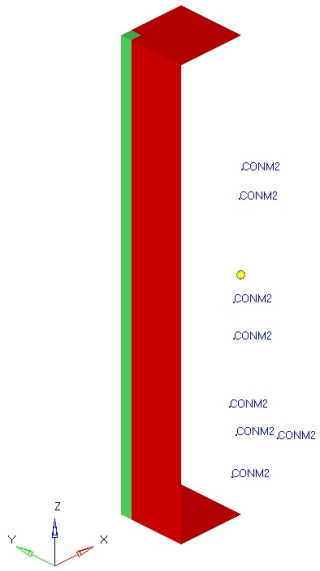

Figure 3.2: CONM2.

The concentrated mass points are now required to be attached to the structure of the CubeSat by rigid connections in order to represent the presence of a physical body inside the structure. This was done by RBE3 rigid connector. This RBE3 element allows forces and moments applied to reference points to be distributed to a set of independent DOFs based on the RBE3 geometry and local weight factors. Unlike others elements such as the RBE2, the RBE3 does not add additional stiffness to the structure [74].

The RBE3 were created attaching all the nodes in the interior of the voids to the CONM2 elements in the CG of the electronic conmponents. This allows to obtain the ideal placement of where the attachement shall be done. This is depicted in Figure 3.3.

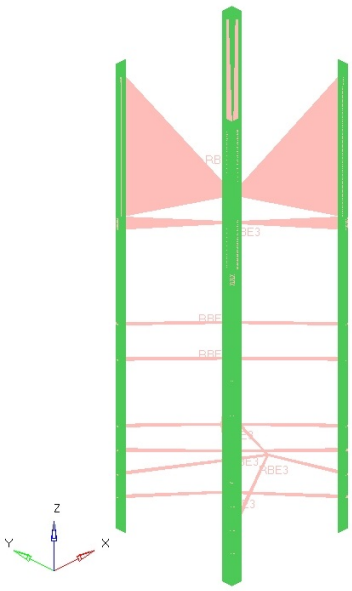

Figure 3.3: RBE3.

The geometry was then divided in Design Domain and a Non-Design Domain. The CDS state that the CubeSats must have 4 rails, one at which corner, and that "*no external component other than the rails shall touch the inside of the P-POD*" [13]. The minimum dimensions the rails must have are depicted in Appendix A. This division will allow to inform the software that in the Non-Design Domain the geometry can not be optimized.

3.1.3 Loads, Constraints and Load Steps

As previous stated, the loads that the MECSE must withstand are defined by the LV provider. The constraints are also defined by them given that they define the position of the CubeSat inside the LV. The load steps used in the analysis are created according to load case (LC) and its corresponding constraints.

3.1.3.1 Loads

Vega User's Manual [66] and Announcement of Opportunity for the Launch of Multiple Light Satellites on a Vega Flight [87] define that the CubeSat will lay down horizontally at the time of the launch. The maximum quasi-static acceleration in the longitudinal axis (Y) is 14.5G in compression and 10.5G in tension and the maximum lateral loads are 3G along X and Z axis (Figure 3.4). Both longitudinal and lateral main frequencies must be bigger than 90 Hz. Reference [88] defines that a CubeSat must survive to temperatures from -20ºC to +50ºC.

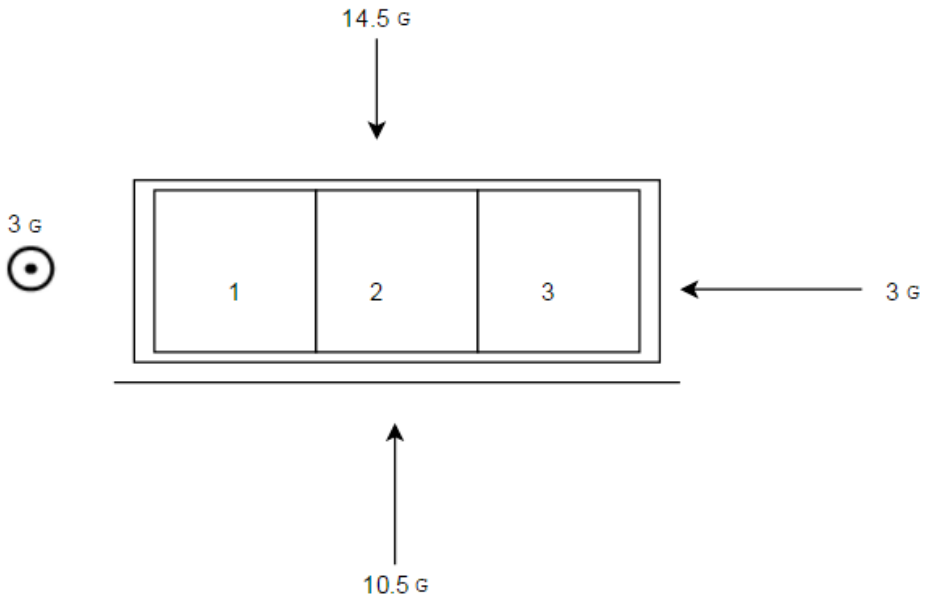

Figure 3.4: Loads acting on MECSE within VEGA LV [15].

The loads were defined as gravity loads (GRAV) which defines acceleration vectors for gravity. The acceleration felt by the MECSE were calculated considering a gravitational acceleration of $g = 9806,4\ mm/s^2$ and are depicted in Table 3.3.

Table 3.3: Grav loads by load case where a is the acceleration module and X, Y, Z are the components of the acceleration vector.

LC	G's	a [mm/s^2]	X	Y	Z
LC 1	14.5	142192.80	0	+1	0
LC 2	10.5	102967.20	0	-1	0
LC 3	3	29419.20	+1	0	0
LC 4	3	29419.20	-1	0	0
LC 5	3	29419.20	0	0	+1
LC 6	3	29419.20	0	0	-1

The thermal loads are not considered in the optimization process because they are not supported [82].

3.1.3.2 Boundary Conditions

As previously stated, the MECSE will be layed down horizontally during launch, with only its rails touching the P-POD. This means that the CubeSat will only be simply supported and not fixed inside the container.

Given that, the constraints were applied differently for all the LC. They were applied in the nodes of the edges that will oppose the movement, restricting it in the direction of the load. However, this is not enough for the software to compute the results because all three directions must be constrained at least at one node to prevent rigid body motion (infinite displacement). Therefore the corner nodes are constrained in the other two directions as control condition. In other words, taking first load case as an example, the acceleration is in the Y direction so the nodes are all constrainted in the Y direction and the corner nodes in the X and Z directions, as depicted in Figure 3.5.

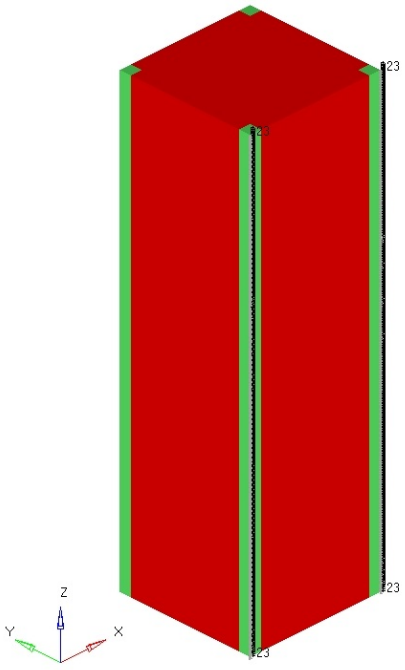

Figure 3.5: Constraints in LC 1.

This logic was apllied to the rest of the load cases, with exception of the fifth and sixth cases. These are different only because they are apllied to the edges of the supports instead of the edges of the body of the CubeSat, but following the same logic: as the load is in the Z direction, all the nodes are constrained in this direction, with the corner nodes being in the X and Y direction as well.

3.1.3.3 Load Steps

The Load Steps (LS) were created joining the LC and the constraints of each case together. For example, the LC 1 is joined with the constraints for the first case to form the LS 1. This was done for all the quasi-static loads informing the software that it should consider a Liner Static analysis in those LS.

An additional LS was created to extract the natural frequencies of the structure using an EIGRL card. This command allows the software to perform real eigenvalue analysis with the Lanczos method, extracting the requested number of natural frequencies.

A summary of the LS can be consulted in Table 3.4.

Table 3.4: Load Steps summary.

Load Step	Analysis Type	Load Case	Constraint	Nº Nat. Freq
LS 1	Linear Static	LC 1	Const_1	-
LS 2	Linear Static	LC 2	Const_2	-
LS 3	Linear Static	LC 3	Const_3	-
LS 4	Linear Static	LC 4	Const_4	-
LS 5	Linear Static	LC 5	Const_5	-
LS 6	Linear Static	LC 6	Const_6	-
LS 7	Normal Modes	-	-	5

In the optimization process all the LS are considered simultaneously and the software computes a solution that fulfils all the constraints and mets the objective. If any constraint is violated, the software outputs the solution as *infeasible*.

3.1.4 Material and Properties

The current MECSE structure is made of Alluminium 7075-T6 [15]. This alluminium has a high percentage of Zinc (indicated by the first digit 7xxx) and has not suffered modifications about the original alloy (indicated by the second digit x0xx). The third and fourth digits indicate the aluminium purity of the specific aluminium alloy. The Tx refers to the temper suffered by the material, and in this case, T6 means the material was solution heat treated and then artificially aged [89].

This alloy is prone to corrosion, it pusesses a high mechanical resistance and a high fatigue resistance making it ideal for aerospace applications, among others heavy loading applications [90].

The mechanical properties of the alloy were investigated and the apllied in FEA are the depicted in Table 3.5. Eventhough this properties do not consider the AM characteristics, as seen

in subsubsection 1.2.2.3, depending on the building process and post process actions the material's performance can be improved. As this parameters are yet to be defined, the standard properties were used.

Table 3.5: Mechanical properties of Aluminium 7075-T6 [91].

Density [t/mm^3]	2.81e-9
Young's Modulus [MPa]	71700
Shear Modulus [MPa]	26900
Poisson Ratio	0.33
Tensile Yield Strength [MPa]	503

3.2 Analyses

In the latest section, all the actions taken in order to bring the stucture from a CAD geometry into a FEM mesh were detailed. At this point, in order to perform any optimization, the optimization parameters used are the only missing information. These were not detailed in the last section because in all the optimizations run there were differences and therefore they are detailed before each result is depicted and discussed.

Some similarities can also be observed through every optimization run: the two symmetry planes, ZY and ZX; the first natural frequency having to be bigger than 90 Hz; and the optimization objective which was to minimize the mass of the structure.

3.2.1 Optimization Results

The first optimization was performed by usign as a constraint the yield strength of the material, considering a Margin of Safety (MS) of 0.2 and all the above mentioned constraints and objective. A thickness of 2 mm was given to the structure with the exception of the CubeSat's supports that are required to have a minimum height of 6.5 mm [13]. The 2 millimeters thickness was chosen as the minimum thickness because when dealing with aluminium, thicknesses smaller than that, despite beign able to resist the mechanical loading, will not form a handy structure.

As a result of the first optimization run, all the Design Domain was eliminated. This means that for the MECSE structure, with the chosen configuration and systems, the rails would be enough to withstand all mechanical loading which it is subjected to. It is also related with the modeling method used, due to the lack of properties of the systems (modelled only with concentrated mass points), and their attachment to the structure. Consequently, this would not form a viable structure and further strudy maust be conducted.

Due to this result, it was decided to study the influence of the MINDIM on the optimization of the structure. The MAXDIM control was not used because, if the goal is to minimize the mass achieving a structure as small as possible, it has no sense to aplly this control. The values used for the MINDIM control were 2, 4, 6, 8 and 10 millimeters.

To study these effects, the optimization parameter related to strenght was deleted and was replaced by a displacement constraint lower than the maximum displacement of the original MECSE's structure. This decison was made with the intent of creating a structure that would

be more rigid than the original because, afterwards the structure will have to be cut as it will be built in one piece (subsection 3.2.3). So, a value of 0.5 mm was apllied as a displacement constraint for the optimization.

After the analyses were completed, it was found that another major parameter would influence the mass of the optimized structure, the threshold. This parameter is related to the lower limit of the density of the elements that are not eliminated, due to the continuity of the density variable in TO (see section 4.2). In other words, if a threshold of 0.2 is used, the elements eliminated are the ones with a density lower than this value and the ones with a density equal or higher are retained.

In 3.6(a), 3.6(b) and 3.6(c), the same geometry at different threshold is depicted. It can be observed that the elemens with intermidate densities are eliminated if they are below the threshold value. This implies that the higher the threshold the lower the mass of the geometry. However, as it can be seen in 3.6(c), too high values of threshold may result in non connected elements and so the maximum allowable threshold must be determined for each particular case under analysis.

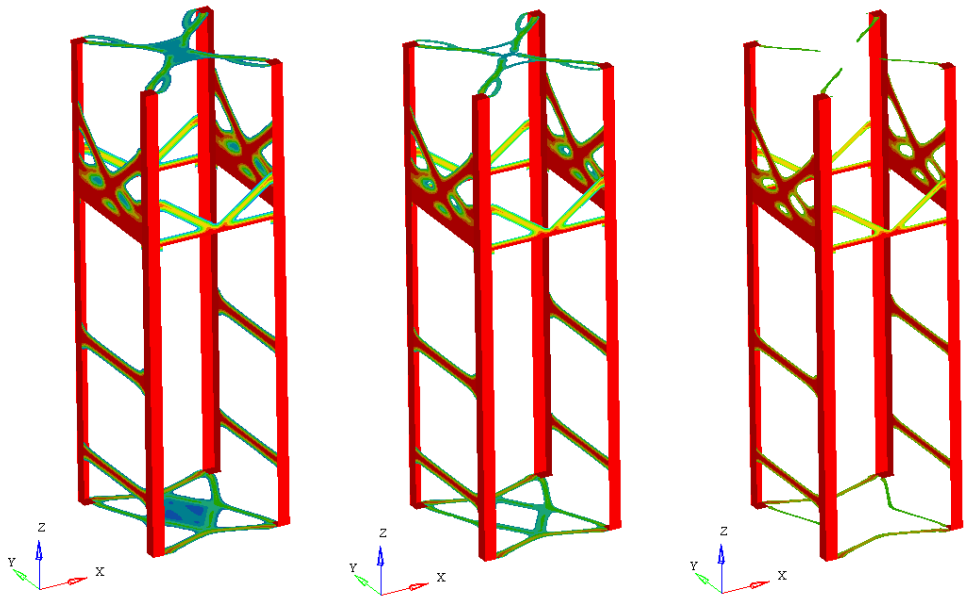

(a) Threshold of 0.2. (b) Threshold of 0.3. (c) Threshold of 0.5.

Figure 3.6: Threshold influence on the geometry.

The optimizations were run for a structure with a thickness of 2 and 3 mm and the mass variation with all the parameters is depicted in Figure 3.7 and Figure 3.8. The tables with each of the graphics were built can be found in Appendix C.

By analysing both graphs it was concluded that the higher the threshold, the lower the mass. It was also possible to conclude that, in both cases, the MINDIM of 2 and 6 mm had a greater mass reduction of all the cases and the MINDIM 4 was the case less affected by the threshold variation. This shows that the use of these parameters is not trivial, and for each optimization it is crutial to study them.

In the 2 mm geometry, for a threshold of 0.5, the MINDIM 2 has a mass of 229g, which represents a mass reduction of almost 55%, when comparing with the original MECSE's structure, and MINDIM 6 has a mass of 235g, which reduced close to 50% of the mass value.

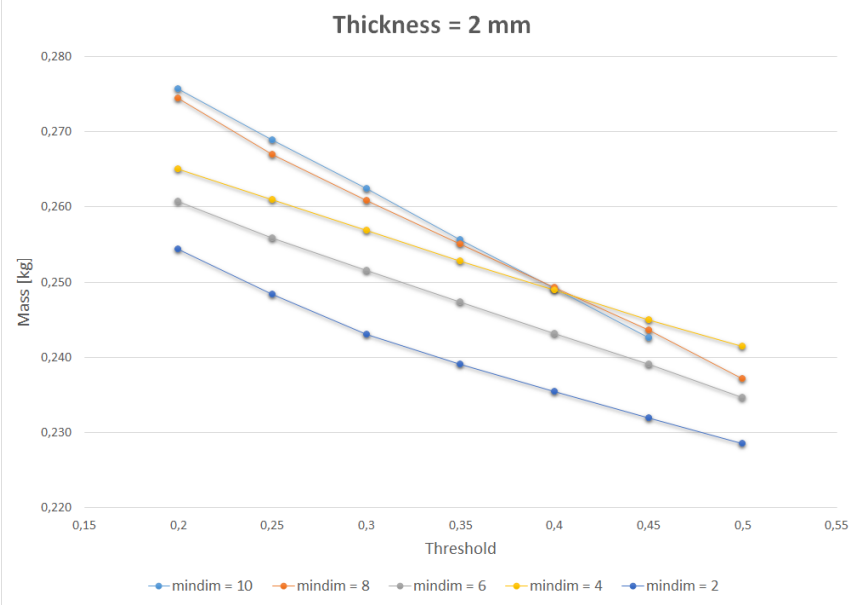

Figure 3.7: Mass variation with optimization parameters for t=2 mm.

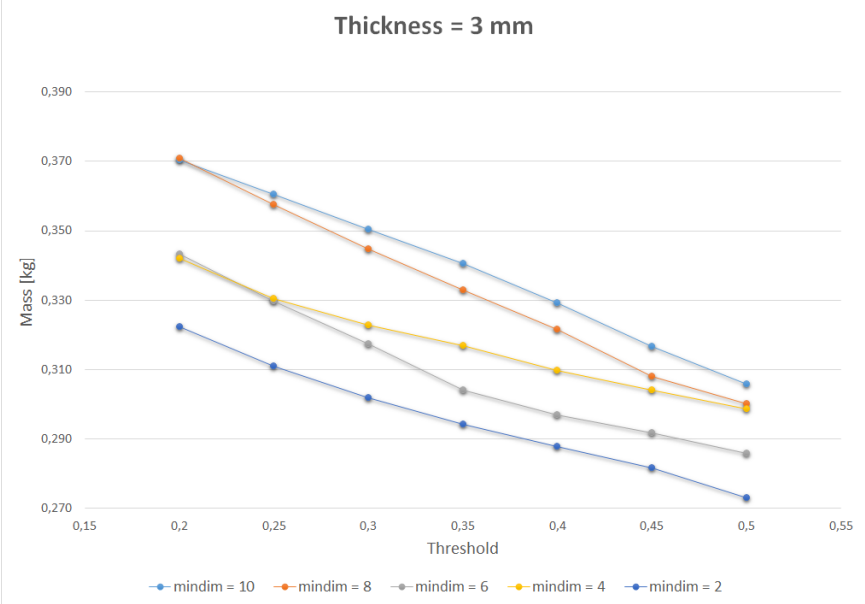

Figure 3.8: Mass variation with optimization parameters for t=3 mm.

Furthermore, it was concluded that the 3 mm geometry had not, in any case, a greater mass reduction than the 2 mm geometry. Given so, the 3 mm structure was not considered the best geometry.

Detailing the analysis in the 2 mm geometry, it may be observed that the three greater mass reductions occur for a MINDIM of 2, 6 and 10 at a threshold of 0.5. The geometries achieved in

this cases are depicted in 3.9(a), 3.9(b) and 3.9(c), respectively. These three geometries will be subjected to a FEA.

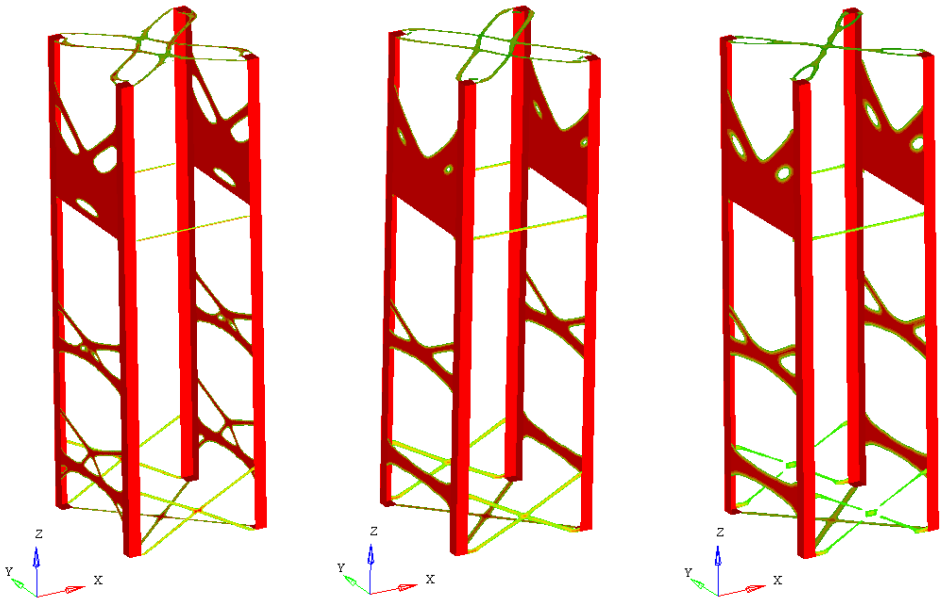

(a) MINDIM 2. (b) MINDIM 6. (c) MINDIM 10.

Figure 3.9: MINDIM influence on the geometry.

Comparing the three structures depicted above it can be noticed that the material in the side faces is maintained is the same areas, which correspond to the areas where the RBE3 are fixed to the rails, for the batteries and the electronics. These areas differ from each other in layout because of the minimum dimension that all members must have. The same is applied for the differences verified in the top faces of the geometry.

The side faces close to the payload section have retained more material than other parts of the geometry due to the modelation method. As the payload is not yet defined, RBE3 were defined along the rails for the heigth defined for the payload, and by doing this all the load is distributed for a large number of nodes which leads to a non-optimized zone. However, without the definition of the systems, no other aproximations may be done. When defined, the RBE3 of the payload must be updated in order to optimize this zone.

3.2.2 FEA Validation

A FEA was then required in order to understand the impact of the threshold variation in the stuctural integrity of the generated geometries. These analyses will allow the selection the best geometry for the MECSE's structure.

The FEA analysis results are depicted in Table 3.6 and Table 3.7. At the lowest value of threshold, 0.5, the MINDIM 10 drops its natural frequency for lower than the defined 90 Hz and its consequently rejected. All the MINDIM 10 were not further considered because only at this value of threshold, its mass was lower than other MINDIM geometries.

It was observed that, in a similar way to mass, the natural frequency drops with the increase of the threshold. Also, the increase in the MINDIM increases the natural frequency of the structure for the same threshold.

Comparing the results between the MINDIM 2 and 6, it can be noticed that both structures have displacement values lower than the limit imposed in the optimization, and stress values much lower than the tensile strength meaning both structures withstand the loads apllied.

Table 3.6: Displacement, stress and first natural frequency for MINDIM 2 geometry.

mindim=2								
	threshold=0.2		threshold=0.3		threshold=0.4		threshold=0.5	
Subcase	disp [mm]	stress [MPa]	disp [mm]	stress [MPa]	disp [mm]	stress [MPa]	disp [mm]	stress [MPa]
LC 1	0.017	4.556	0.017	4.642	0.018	5.660	0.020	5.036
LC 2	0.012	3.299	0.013	3.315	0.013	4.081	0.015	3.849
LC 3	0.017	4.333	0.017	5.513	0.018	6.992	0.085	15.640
LC 4	0.017	4.365	0.017	5.539	0.018	6.977	0.085	15.700
LC 5	0.004	1.325	0.004	1.247	0.004	1.061	0.004	1.274
LC 6	0.011	1.044	0.012	0.970	0.014	0.943	0.014	0.983
1st Nat. Freq. [Hz]	108.788		103.706		100.284		97.993	

Table 3.7: Displacement, stress and first natural frequency for MINDIM 6 geometry.

mindim=6								
	threshold=0.2		threshold=0.3		threshold=0.4		threshold=0.5	
Subcase	disp [mm]	stress [MPa]	disp [mm]	stress [MPa]	disp [mm]	stress [MPa]	disp [mm]	stress [MPa]
LC 1	0.016	4.826	0.017	4.779	0.017	5.149	0.018	4.835
LC 2	0.012	3.496	0.012	3.436	0.012	3.473	0.013	3.501
LC 3	0.016	3.592	0.016	3.624	0.017	4.084	0.019	4.818
LC 4	0.016	3.815	0.016	3.625	0.017	4.113	0.019	4.819
LC 5	0.004	1.224	0.004	1.195	0.004	1.200	0.004	1.178
LC 6	0.010	0.857	0.011	0.857	0.012	0.862	0.013	0.865
1st Nat. Freq. [Hz]	117.801		112.726		106.724		101.270	

The MINDIM 2 for a threshold of 0.5 as the structure chosen for the the MECSE's structure because is the ligthest while withstanding all the loads and with a natural frequency over 90 Hz. In 3.10(a) the displacement plot for the worst LC and the shape of the structure when the first natural frequency is reached are depicted. For this geometry the worst case is the LC4.

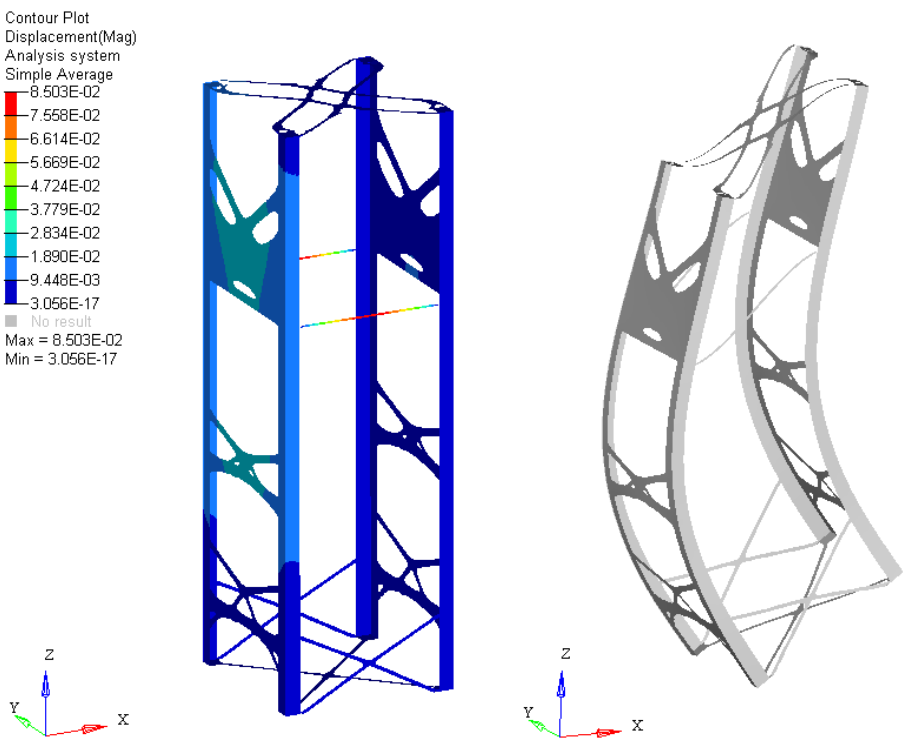

(a) Displacement. (b) First eigenvalue (f=97.993 Hz).

Figure 3.10: FEA validation for MINDIM 2 at threshold 0.5.

3.2.3 Construction of the final geometry

After the optimization process, it was required to design a geometry based on the results. This was done by exporting the results back to CATIA® [83] and using the optimization results as a guide line, the final geometry was created. It was ensured that no member has less than 2 mm, not violating the requirements previously established. In 3.11(a) and 3.11(b) both the created geometry and the optimization results are, respectively, depicted and can be compared.

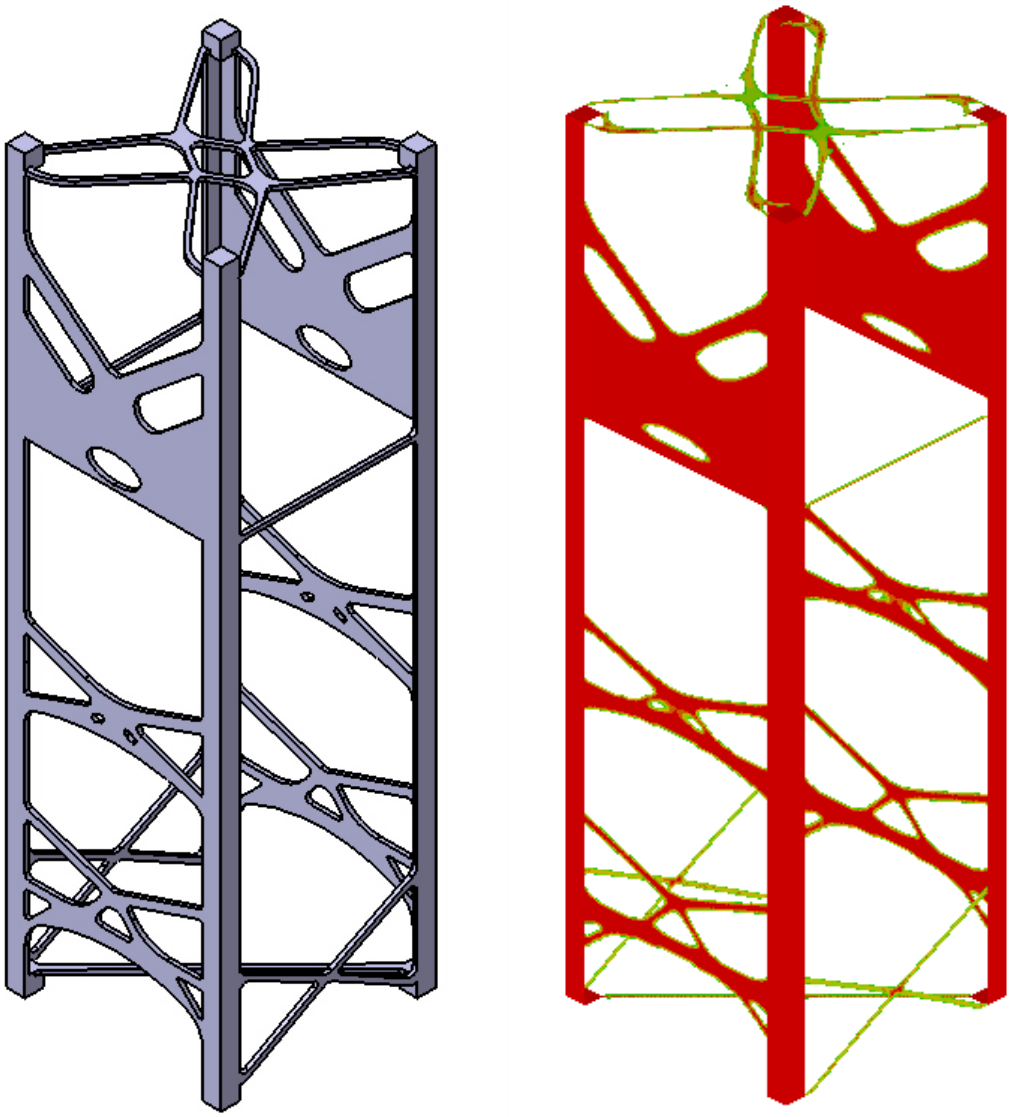

(a) Created geometry. (b) Optimization result.

Figure 3.11: Comparison between the created geometry and the optimization result.

Observing both figures it can be seen that only small changes are made: on the top face of the CubeSat the optimized result was smoothed in order to eliminate the irregularities presented; on the payload, batteries and systems faces the holes were rounded in the inner side and flatted in the outer side and all fillets were added in all the corners. This geometry has a mass of 211g.

In order to be a fully functional geometry, it is required to define supports for all the systems that integrate the MECSE and a method for its assemblage and disassemblage inside de structure.

Firstly, the supports for the antenna, batteries and boards were defined. For the antenna, these supports were designed using four of its own screw holes, allowing to reduce the mass of the support. However the thickness used has less than 2 millimeters. This is the only part of the all geometry that does not follow the restriction imposed before due to lack of space. The antena width is 98 mm and as the CubeSat's is 100 mm wide, leaving only 1 mm in each side. This supports are depicted in Figure 3.12.

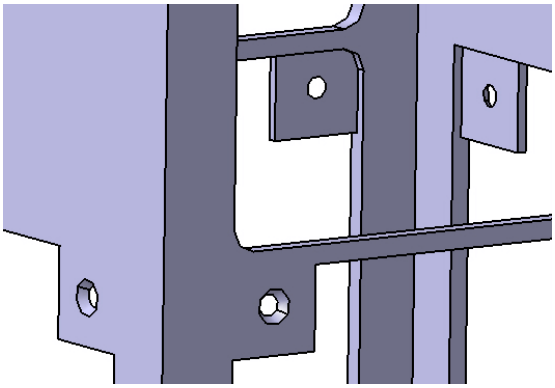

Figure 3.12: Antenna supports.

The batteries and the boards support (D.1(a) and D.1(b) in Appendix D) were designed to make the structure as modular as possible, in such a way that a block (Figure D.2 and Figure D.3 in Appendix D) may be formed outside the CubeSat, using a rod, spacers (in the boards case), washers and nuts to join them together (D.4(a) and D.4(b) in Appendix D), and when assembled in the CubeSat, it is only required to screw the block to the structure rails with flat head countersunk M2 screws.

The use of this type of M2 screw is related to the restriction that,no member except for the rail, can touche the inside of the P-POD. With them, the head face of the screw is at the same level as the rails outer face, complying with the restriction.

The rods, spacers, washers and nuts were M3 size because all the systems have M3 holes.

For the payload no supports were built because its geometry is not yet defined. When defined, supports must be designed.

This solution for the supports required a modification of the geometry. As the supports are design to be screwed to the rails, and there are design standards [48] that dictate the distance between the center of the screw holes and the end of the rail as well as the distance between the screw holes and the perpendicular face of the support, some material was added in this critical regions as shown in Figure 3.13. The standard dictate that the distance between the center of the screw holes and the end of the rail have to be $2D + 1$, where D is the diameter of the hole and that the distance between the screw holes and the perpendicular face of the support have to be $1D + 2$.

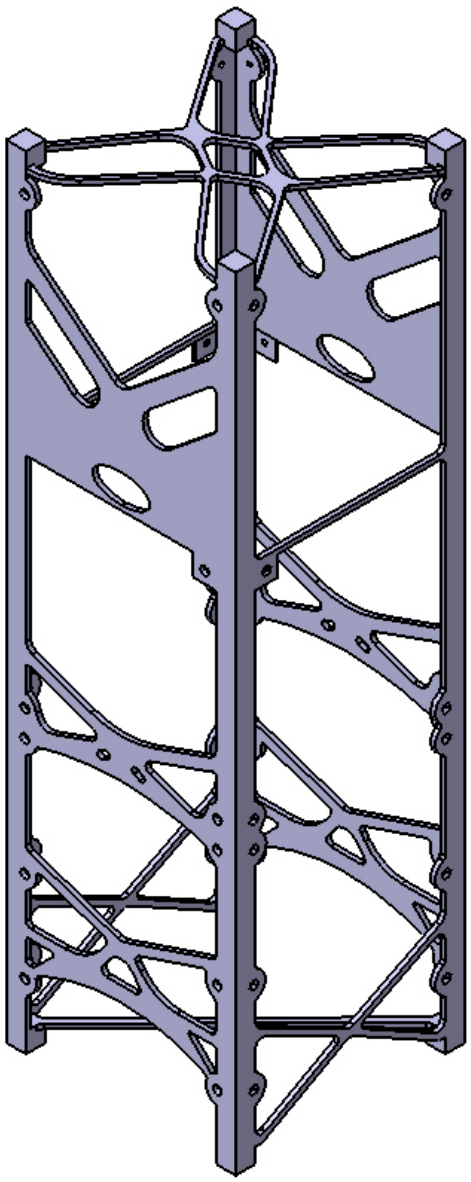

Figure 3.13: Optimized geometry with fixation points.

Due to the addition of material in the screw areas the mass of the CubeSat had an increase of 8g, increasing its total mass from 211g to 219g.

Then, it was necessary to define a solution for the assemblage and disassemblage of the systems inside the CubeSat. As the structure is to be additive manufactured, it is possible to build it in one piece. However, it would be imposible to install the systems inside the structure because some of them are larger than the distance open between the rails. Consequently, the structure must open, in one or more places, and then closed for CubeSat's normal operation.

The solution to this problem was to use the systems supports both as supports for the systems and as fixing points for the removable faces of the structure, allowing no more parts to be added, thus no more weight. The faces selected to be removable were the two with more material so the removable parts are stronger on its own.

This methodology required, however, additional fixers and excesses of material to be created on the top of the geometry, in the payload area, otherwise it would be a too large distance with no screw which, when the CubeSat is under loading, it could open, bending the face and break it in an extreme case. In Figure 3.14 this section is detailed as well as the screws that will be used to attatch both parts together.

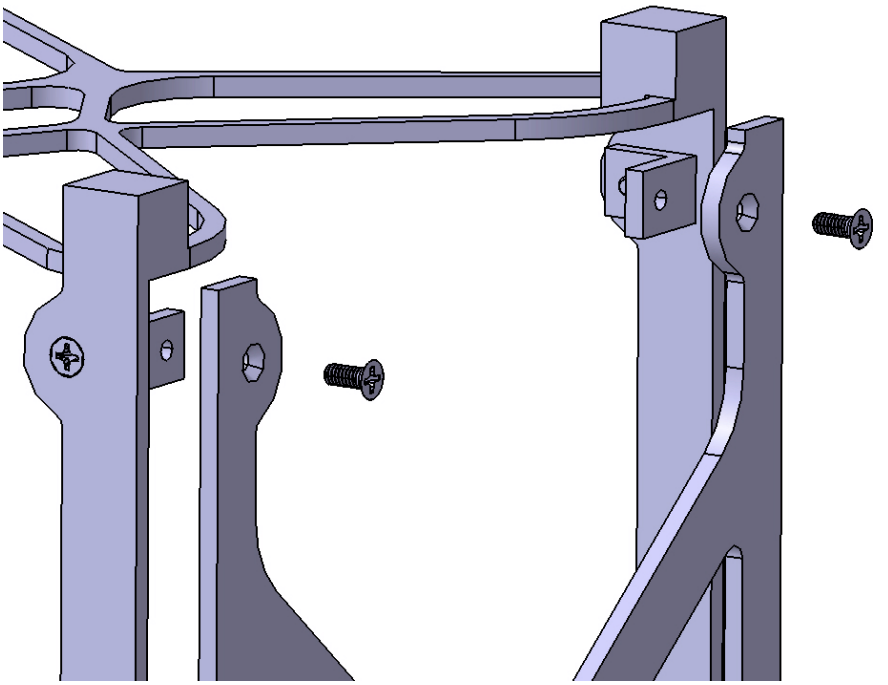

Figure 3.14: Detailed assembly.

3.2.4 Final Geometry FEA

Due to the changes made to the structure, namely the faces separation and the material addition in the screw areas, the mechanical behaviour is altered and must be analyzed in order to find if the structure still withstands the loading.

The FEA process was repeated. A special attention was now given to the holes because triangular elements shall not be encountered in its outer edges and an even number of elements around the hole is recomended [72].

The screws, rods and spacers where modelled with 1D CBAR elements. This type of elements was used because the cross-section of all these components is constant and because they are subjected to bending, besides tension and compresion [72]. The cross section of each element was defined with its dimensions.

The supports and the fixers were modelled with 2D elements. In order to connect the 1D CBAR elements to the structure, RBE2 elements were used. These were defined by attaching the CBAR elements to all the nodes in the edge of the corresponding hole with infinite stiffness in the 3 translational DOFs and no stiffness in the 3 rotacional DOFs.

The RBE3 elemenst were also modified with exception of the payload's. While on the optimization the systems supports were not defined and was pretended to find the best place to

put them and so the RBE3 were apllied in all the area were the system is placed, now as the supports have been defined an accurate representation is demanded. Consequently, the RBE3 are now only fixed to the CBAR elements, which represent the rods at its extremities.

The payload's RBE3 were not changed as this system is not yet defined, having been modelled in the same way as they were for the optimizations. The final mesh for analysis is depicted in Figure 3.15.

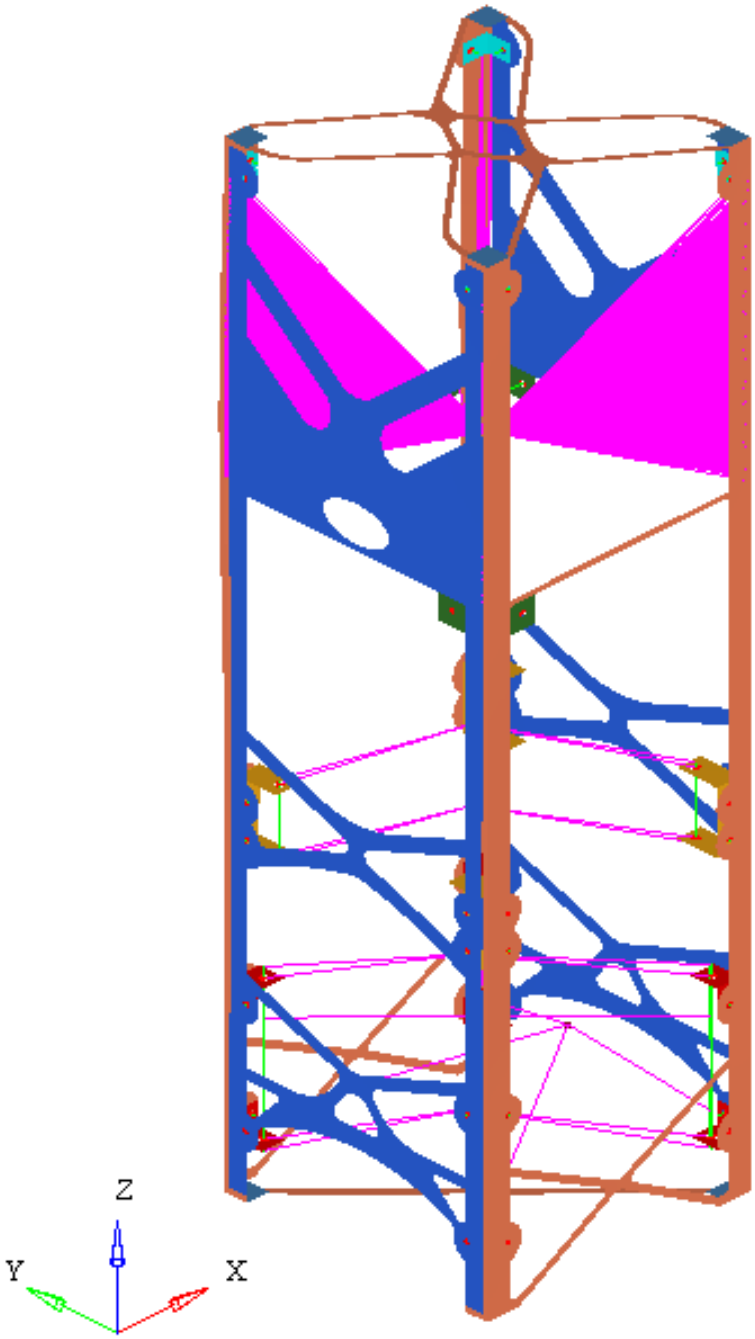

Figure 3.15: Discretization of the final geometry.

The results of the analysis are shown in Table 3.8 and in Table 3.9. The results for the worst case, LC 1, are depicted below in 3.16(a), 3.16(b) and 3.16(c) and for the rest of the LC, the plots may be found in Appendix E.

Table 3.8: FEA of the final geometry.

	LC 1	LC 2	LC 3	LC 4	LC 5	LC 6
disp [mm]	2.30	1.54	0.15	0.15	0.03	0.03
SPC Force [N]	19.18	11.80	8.21	8.34	3.04	3.39
stress 1D [MPa]	485.20	325.10	31.95	30.10	10.50	12.53
stress 2D [MPa]	113.70	73.39	11.82	10.57	2.43	2.46

Table 3.9: Natural frequencies of the final geometry.

	1st	2nd	3rd	4th	5th
Eigenvalue [Hz]	76.13	93.23	116.77	122.92	141.95

By analysing the results, it is clear that this solution for assemblage and disassemblage of the structure is not optimal. The first natural frequency drops below the limit of 90Hz and the stress in the 1D elements is higher than the allowable. The stress in the 2D elements has increased but it is not critical.

It is also observed that the LC 1 is the worst case for the structure, which is logical as it is the case with the higher acceleration applied.

The displacement of the structure increases more than four times the maximum imposed for the optimization process. This occurs due to the large distance from the baterries support to the fixers on top of the structure.

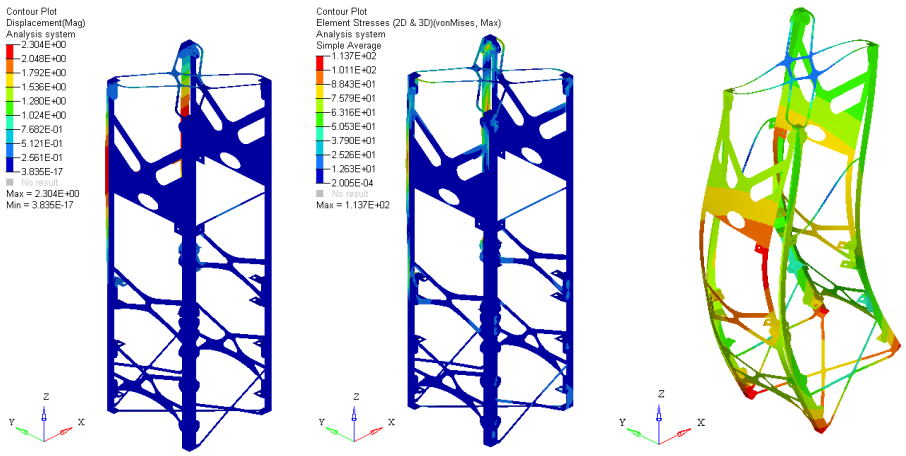

(a) Displacement. (b) Stress. (c) Eigenvalue.

Figure 3.16: Results plots for LC 1.

Althoug with this assemblage method the CubeSat does not yet fulfill all the requirements, when the payload is defined and its supports designed and put in place, the requirements will be fulfilled because not only the natural frequency of the sturcture will raise but also the displacement will diminish, validating this structure in order to be launched.

The validation of this structure is not only a good achievement for the MECSE project as the mass of the structure is reduced allowing for an increase of the payload mass, but also validates a design process that may be implemented all around the world in all CubeSat projects. By doing so, the potential of every mission increases as the useful mass increases. Alternatively, it may be used in order to drop off the costs of the projects as the LV will be able to rather increase the number of CubeSats per flight or rather diminish the operation's costs as less fuel is required to reach orbit.

3.3 Comparison between current and proposed MECSE's Mechanical System

As the main objective of this work is to propose a new structure for the MECSE, it is necessary to understand the differences between both structures. So, the diagrams depicted in 3.17(a) and 3.17(b) were drawn.

This comparasion was done by dividing all the components in the structure into three categories: systems, structure and hardware. In the systems category are considerer the payload, the antenna, the batteries and all the boards. In the structure category only the structural elements are considered and in the hardware category all the non structural elements are considered (such as supports, rods, spacers,etc.).

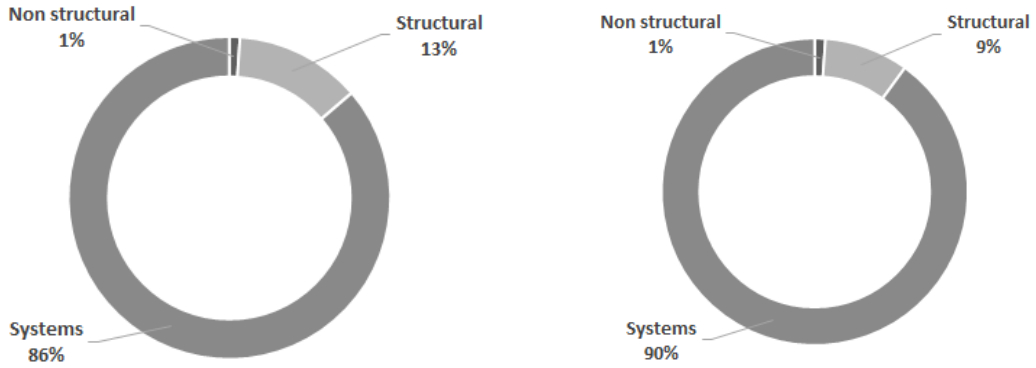

(a) Current structure (b) Proposed structure

Figure 3.17: Mass balance of the MECSE

The current structure has a total mass of 2.78 kg and the proposed a final mass of 2.66 kg which represents a reduction of 115g. This difference is all due to the reduction of mass of the structural elements because the systems and the non structural elements have the same mass in both structures.

Consequently, weigthing the mass, the percentage of payload increases and the structure reduces although there is not any reduction in the systems mass. The 115g saving may be used to increase the payload mass if necessary.

Chapter 4

Conclusions

With the realization of this dissertation, a ligther structure is proposed. This geometry was obtained by Topology Optimization and is intended to be built by additive manufacturing.

The CubeSats are small satellites which use is increasing exponentialy and are used in a variaty of missions with a variaty of different objectives from science to communications.

In order to reduce the costs of space exploration, TO and AM are beign paired up to do so, creating new geometries with reduced mass and increased striffness. Their use is growing in all sectors so different as medicine and aerospacial applications.

All the CubeSat must be designed and tested in accordance with the CDS [13], defined by the creators of the CubeSat project. However, the LV providers also issues specific rules trough the LV User's Manual which, for the MECSE, will be the Vega User's Manual [66], and its content supersedes all the rest.

TO was performed in order to find an optimized geometry for the MECSE. So the optimization's objective was defined in order to find a structure that woulb be more rigid than it currently is.

The influence of the minimum member size and the optimization threshold were studied and it was concluded that the mass reduces with the increase in the threshold and that the MINDIM 2, 6 and 10 presented the lower mass. It was verified that the use of MINDIM is not trivial.

This three geometries were sujected to a FEA at a threshold of 0.5 (the maximum value considered) and the MINDIM 10 was rejected due to its natural frequency being lower than the defined for the LV User's Manual. Between the MINDIM 6 and MINDIM 2, the second was chosen because it was ligther than the MINDIM 6.

This structure was built in CATIA® [83] as well as all the supports required for the assembalge of the systems inside. The design of the supports imposed modifications to be made in the screw areas with the addition of material.

In order to assemble all the systems inside, the geometry was trimmed so the two faces of higher mass could come out, the systems inserted, and then the faces woulb be screwed back into place leaving the supports with a double mission of supporting the systems and closing the CubeSat.

The systems supports were designed so they can be assembled separately of the structure and then, as a block, to be screwed in place.

As significant changes were done to the geometry, it was necessary to reanalyse the struc-

ture. A new FEA was performed and the resuls showed that the structure did not meet the requirements anymore, with the first natural frequency of the structure dropping well below the minimum 90Hz.

Once the payload and its supports are defined, reanalyses must be conducted because their presence will diminish the displacement and increase the natural frequency of the structure. This will allow the MECSE to meet all requirements in order to be deployed.

The optimized structure was then compared with the current and a reduction in 115g was achieved due to the reduction of mass in the structural elements.

4.1 Accomplishments

The first accomplishment of this work was the investigation about small satellites, their aplli-cations and their design requirements.

The second objectives of this dissertation was to investigate different optimization method-ologies and different AM processes and its restrictions in the building process. Investigation was conducted and the state-of-the-art was elaborated where all the most relevant works are detailed.

A new optimized structure of the MECSE was achieved while reducing the mass when compared to current MECSE's structure.

4.2 Difficulties

One of the major difficulties encountered was meshing. As it was detailed, meshing is the crutial step in any FEM related work as its quality determines the accuracy, or the lack of it, of the results. Due to the lack of experience in doing so, substantial amount of time has to be put into this task, in a constant learning process, and with several setbacks and new beginings.

4.3 Future Work

The first step in the future work must be the definition of the Payload. Without the definition of this core system, a final optimization must be run in order to further optimize the payload face and define the final supports systems.

The strcuture shall be analysed with models of the real systems inside the CubeSat as their presence increases the stiffness of the structure.

The building process must be carefully studied and a material's characterization performed in order to be aware of the full capacity of the building process as well as its limitations.

References

[1] W. Larson, J. Wertz, and J. J. Puschell, *Space Mission Engineering: The New SMAD*. Hawthorne, CA: Space Technology Library, 2015. 1, 2, 3, 4, 5, 6

[2] F. Dias, J. Páscoa, and C. Xisto, "Numerical Computations of MHD Flow on Hypersonic and Re-Entry Vehicles," in *ASME 2016 International Mechanical Engineering Congress and Exposition*, 2016. 1, 25

[3] O. Diegel, S. Singamneni, S. Reay, and A. Withell, "Tools for sustainable product design: Additive manufacturing," vol. 3, 08 2010. 1

[4] M. Tomlin and J. Meyer, "Topology optimization of an additive layer manufactured (alm) aerospace part," pp. 1–9, 01 2011. 1, 22

[5] R.-J. Yang and A. I. Chahande, "Automotive applications of topology optimization," vol. 9, pp. 245–249, 07 1995. 1

[6] M. P. Bendsoe and O. Sigmund, *Topology Optimization: Theory, Methods and Applications*. Springer, Feb. 2004. 1, 20, 21, 41

[7] O. Sigmund, "Design of material strucutres using topology optimization," Ph.D. dissertation, Technical University of Denmark, Lyngby, 1994. 1, 21

[8] H. Helvajian and S. W. Janson, *Small Satellites : Past , Present , and Future*. Virginia: American Institute of Aeronautics, Inc, 2009. 2

[9] José Manuel Rebordão. Posat-1. [Accessed: 11-Apr-2018]. [Online]. Available: http://www.fernandocarvalhorodrigues.eu/posat/posat1ph.html 2

[10] G. Mantzouris, P. Papadopoulos, N. Nikitakos, M. Manso, A. Bordetsky, Z. Sarris, G. Markarian, and K. Kourousis, "Picosatellites for maritime security applications - the lambdasat case," 12 2015. 3

[11] M. Rycroft and N. Crosby, *Smaller Satellites: Bigger Business?* Strasbourg, France: Springer, 2002. 3

[12] NASA, "Small Spacecraft Technology State of the Art," California, Tech. Rep., 2014. 3, 4

[13] Cal Poly, "CubeSat Design Dpecification," Tech. Rep., 2014. 3, 4, 5, 6, 7, 29, 49, 52, 65, 74, 75, 76

[14] A. K. Kennedy, "Resource Optimization Algorithms for an Automated Coordinated CubeSat Constellation," Ph.D. dissertation, Massachusetts Institute of Technology, 2015. 3, 4

[15] A. R. M. Azevedo, "Design of MECSE Nanosatellite Mechanical Subsystem," Master's thesis, Universidade da Beira Interior, 2017. 3, 5, 15, 24, 45, 47, 49, 51

[16] Elizabeth Mabrouk. (2015) What are smallsats and cubesats? [Accessed: 11-Apr-2018]. [Online]. Available: https://www.nasa.gov/content/what-are-smallsats-and-cubesats 4

[17] M. Swartwout, "The first one hundred cubesats: A statistical look," vol. 2, pp. 213–233, 01 2013. 4, 5

[18] Planet Labs Inc. (2018) [Accessed: 24-Apr-2018]. [Online]. Available: https://www.planet.com/ 4

[19] C. L. Gustafson and S. W. Janson, "Think Big, Fly Small," Tech. Rep., 2014. 4

[20] C. Williams, B. Doncaster, and J. Shulman, "Nano / Microsatellite: market forecast 2018," SpaceWorks, Tech. Rep., 2018. 4

[21] J. Bouwmeester and J. Guo, "Survey of worldwide pico- and nanosatellite missions, distributions and subsystem technology," *Acta Astronautica*, vol. 67, no. 7, pp. 854 – 862, 2010. [Online]. Available: http://www.sciencedirect.com/science/article/pii/S0094576510001955 4

[22] M. Swartwout, "Twenty (plus) years of university-class spacecraft: A review of what was, an understanding of what is, and a look at what should be next," 10 2018. 4, 5

[23] I. Nason, J. Puig-Suari, and R. Twiggs, "Development of a family of picosatellite deployers based on the cubesat standard," in *Proceedings, IEEE Aerospace Conference*, vol. 1, March 2002, pp. 1–1. 5, 6

[24] E. Blundell, A. Toorian, J. Puig-Suari, and R. Twiggs, "CubeSats as Responsive Satellites," in *3rd Responsive Space Conference*, 2005. 5

[25] A. Chin, R. Coelho, R. Nugent, R. Munakata, and J. Puig-Suari, "CubeSat: The Pico-Satellite Standard for Research and Education," in *AIAA SPACE 2008 Conference & Exposition*, San Diego, California, 2008. 5

[26] Cal Poly, "Poly Picosatellite Orbital Deployer Mk III Rev. E User Guide," Tech. Rep., 2014. 5, 6

[27] J. Puig-Suari, C. Turner, and W. Ahlgren, "Development of the standard cubesat deployer and a cubesat class picosatellite," in *2001 IEEE Aerospace Conference Proceedings (Cat. No.01TH8542)*, vol. 1, March 2001, pp. 1/347–1/353 vol.1. 5, 6

[28] F. Calignano, D. Manfredi, E. Ambrosio, S. Biamino, M. Lombardi, E. Atzeni, A. Salmi, P. Minetola, L. Iuliano, and P. Fino, "Overview on additive manufacturing technologies," vol. PP, pp. 1–20, 01 2017. 7, 19

[29] Clare Scott. (2017) 18-year-old 3d prints lightest satellite to ever be launched into space. [Accessed: 11-Apr-2018]. [Online]. Available: https://3dprint.com/174397/cubes-in-space-satellite-launch/ 7

[30] Herbert J. Kramer. Tomsk-tpu-120, the first 3d printed cubesat mission. [Accessed: 11-Apr-2018]. [Online]. Available: https://directory.eoportal.org/web/eoportal/satellite-missions/t/tomsk-tpu-120 7

[31] Sarah Saunders. (2017) 3d printed russian cubesat will be placed into orbit from the iss this july. [Accessed: 11-Apr-2018]. [Online]. Available: https://3dprint.com/160325/3d-printed-cubesat-in-orbit-july/ 7

[32] ASTM International. [Accessed: 11-Apr-2018]. [Online]. Available: https://www.astm.org/ 7

[33] ASTM F2792-12a, "Standard Terminology for Additive Manufacturing Technologies (Withdrawn 2015)," West Conshohocken, PA, Tech. Rep., 2012. 7, 12

[34] I. Gibson;, D. W. Rosen, and B. Stucker, *Additive Manufacturing Technologies*. Springer, 2010. 7, 8, 14, 15, 18, 19

[35] M. Coré-Baillais, H. Bensoussan, A. Richardot, and H. Kusnadi, "The State of 3D Printing," Sculpteo, Tech. Rep., 2017. 7, 8, 14

[36] B. Vayre, F. Vignat, and F. Villeneuve, "Metallic additive manufacturing: State-of-the-art review and prospects," vol. 13, pp. 89–96, 01 2012. 7

[37] D. Bourell, J. Beaman, M. Leu, and D. Rosen, "A brief history of additive manufacturing and the 2009 roadmap for additive manufacturing: Looking back and looking ahead," pp. 24–25, 01 2009. 7, 8, 9, 10, 11, 12

[38] T. T. Wohler, "Wohlers Report," WOHLERS ASSOCIATES, INC, Tech. Rep., 2017. 7, 8

[39] E. Brandl, C. Leyens, and F. Palm, "Mechanical properties of additive manufactured ti-6al-4v using wire and powder based processes," vol. 26, p. 012004, 12 2011. 8, 15, 16, 17

[40] J. E. Blanther, "Manufacture of Countor Relief-Maps," 1892. 8

[41] O. J. Munz, "Photo-Glyph Recording," 1956. 8, 9

[42] Y. Zhai, D. A. Lados, and J. L. LaGoy, "Additive manufacturing: Making imagination the major limitation," *JOM*, vol. 66, no. 5, pp. 808–816, May 2014. [Online]. Available: https://doi.org/10.1007/s11837-014-0886-2 9, 10, 11

[43] W. K. Swainson, "Method, Medium and Apparatus for Producing Three-Dimensional Figure Product," 1971. 9

[44] R. F. Housholder, "Molding Process," 1979. 10, 21

[45] H. Kodama, "Automatic method for fabricating a three-dimensional plastic model with photo-hardening polymer," *Review of Scientific Instruments*, vol. 52, no. 11, pp. 1770–1773, 1981. 10, 11

[46] A. J. Herbert, "Solid object generation," vol. 8, pp. 185–188, 08 1982. 11

[47] S. A. Tofail, E. P. Koumoulos, A. Bandyopadhyay, S. Bose, L. O'Donoghue, and C. Charitidis, "Additive manufacturing: scientific and technological challenges, market uptake and opportunities," *Materials Today*, vol. 21, no. 1, pp. 22 – 37, 2018. [Online]. Available: http://www.sciencedirect.com/science/article/pii/S1369702117301773 13

[48] CEiiA. (2016) [Accessed: 11-Apr-2018]. [Online]. Available: https://www.ceiia.com/ 14, 24, 59

[49] Loughborough University. (2018) About additive manufacturing: Powder bed fusion. [Accessed: 3-May-2018]. [Online]. Available: http://www.lboro.ac.uk/research/amrg/about/the7categoriesofadditivemanufacturing/powderbedfusion/ 14

[50] R. Boyer, "An overview on the use of titanium in the aerospace industry," *Materials Science and Engineering: A*, vol. 213, no. 1, pp. 103 – 114, 1996, international Symposium on Metallurgy and Technology of Titanium Alloys. [Online]. Available: http://www.sciencedirect.com/science/article/pii/0921509396102331 15

[51] P. A Kobryn and S. Semiatin, "Mechanical properties of laser-deposited ti-6al-4v," 01 2001. 15, 16, 17, 18, 19

[52] B. Baufeld, E. Brandl, and O. van der Biest, "Wire based additive layer manufacturing: Comparison of microstructure and mechanical properties of ti–6al–4v components fabricated by laser-beam deposition and shaped metal deposition," *Journal of Materials Processing Technology*, vol. 211, no. 6, pp. 1146 – 1158, 2011. [Online]. Available: http://www.sciencedirect.com/science/article/pii/S0924013611000306 15

[53] A. M. Beese and B. E. Carroll, "Review of mechanical properties of ti-6al-4v made by laser-based additive manufacturing using powder feedstock," *JOM*, vol. 68, no. 3, pp. 724–734, Mar 2016. [Online]. Available: https://doi.org/10.1007/s11837-015-1759-z 15

[54] X. Huang and Y. M. Xie, *Evolutionary Topology Optimization of Continuum Structures: Methods and Applications*, 1st ed., L. John Wiley & Sons, Ed. West Sussex, United Kingdom: Wiley, 2010. 19, 21

[55] H. A. Eschenauer and N. Olhoff, "Topology optimization of continuum structures: A review," vol. 54, 07 2001. 20, 21

[56] MSC Software Corporation, "MSC Nastran User's Guide for Topology Optimization," MSC.Software Corporation, Santa Ana, CA, Tech. Rep., 2007. 20, 21

[57] J. Deaton and R. V. Grandhi, "A survey of structural and multidisciplinary continuum topology optimization: Post 2000," vol. 49, 01 2014. 20, 40, 41

[58] G. I. N. Rozvany and T. Lewiński, *Topology Optimization in Structural and Continuum Mechanics*, 01 2014, vol. 549. 21

[59] "A limit of economy of material in shell structures," *Proceedings of IASS Annual Symposia*, vol. 2014, no. 3, 2014. 21

[60] G. I. N. Rozvany, "Rozvany, g.i.n.: A critical review of established methods of structural topology optimization. structural and multidisciplinary optimization 37, 217-237," vol. 37, pp. 217–237, 02 2009. 21

[61] M. P. Bendsøe, "Optimal shape design as a material distribution problem," *Structural optimization*, vol. 1, no. 4, pp. 193–202, Dec 1989. [Online]. Available: https://doi.org/10.1007/BF01650949 21

[62] I. Altair Engineering, *Practical Aspects of Structural Optimization: A Study Guide*, 2nd ed., Michigan, 2015. 21, 40, 41, 42, 43

[63] P. Gaudenzi, S. Atek, V. Cardini, M. Eugeni, G. Graterol Nisi, L. Lampani, M. Pasquali, and L. Pollice, "Revisiting the configuration of small satellites structures in the framework of 3D Additive Manufacturing," *Acta Astronautica*, vol. 146, no. February 2017, pp. 249–258, 2018. 22, 23

[64] C-MAST. (2007) [Accessed: 11-Apr-2018]. [Online]. Available: http://www.aerospace.ubi.pt/new/html/ccta.html 24

[65] Arianespace. (2010) Vega: The light launcher. [Accessed: 11-Apr-2018]. [Online]. Available: https://www.arianespace.com/vehicle/vega/ 24, 25

[66] Arianespace, "Vega User's Manual," Arianespace, Tech. Rep., 2014. 24, 25, 49, 65

[67] J. E. T. B. Monteiro, "Mission Analysis and Design of MECSE Nanosatellite," Master's thesis, Universidade da Beira Interior, 2017. 24

[68] M. Kim, M. Keidar, and I. D. Boyd, "Analysis of an Electromagnetic Mitigation Scheme for Reentry Telemetry Through Plasma," *Journal of Spacecraft and Rockets*, vol. 45, no. 6, pp. 1223–1229, 2008. 25

[69] M. K. Kim, "Electromagnetic manipulation of plasma layer for re-entry blackout mitigation," Ph.D. dissertation, University of Michigan, 2009. 25

[70] Arianespace. (2010) [Accessed: 11-Apr-2018]. [Online]. Available: http://www.arianespace.com/ 25

[71] Arianespace, "The World's Spaceport," Tech. Rep., 2015. 25, 26

[72] I. Altair Engineering, *Practical Aspects of Finite Element Simulation: A Study Guide*, 3rd ed., Michigan, 2015. 29, 30, 31, 32, 33, 36, 39, 46, 61

[73] D. L. Logan, *A First Course in the Finite Element Method*, 2nd ed. Pacific Grove, CA, USA: Brooks/Cole Publishing Co., 2000. 29, 30

[74] MSC Software Corporation, "MSC Nastran Linear Static Analysis User ' s Guide," Tech. Rep., 2014. 30, 31, 37, 48

[75] J. Fish and T. Belytschko, *A First Course in Finite Elements*. USA: John Wiley & Sons, Inc., 2007. 30

[76] Y. Liu and G. Glass, "Effects of Mesh Density on Finite Element Analysis," in *SAE world congress*, 2013. 32

[77] MSC Software Corporation, "Patran 2016 User 's Guide," Tech. Rep., 201. 32

[78] G. S. Aglietti, G. Richardson, and P. Quill, "Launch Environment," *Encyclopaedia of Aerospace Engineering*, 2010. 34, 35

[79] A. Calvi, "Spacecraft Loads Analysis: An Overview," Noordwik, The Netherlands, 2011. 34

[80] P. V. Gamboa, "Conceitos Fundamentais do Método dos Elementos Finitos," Covilhã, 2011. 38

[81] MSC Software Corporation, "MSC Nastran Dynamic Analysis User's Guide," Tech. Rep., 2012. 39, 40

[82] M. S. Corporation, "MSC Nastran 2007: User's Guide for Topology Optimization," Tech. Rep., 2007. 41, 42, 43, 50

[83] Distrim Sistemas. (2016) Catia. [Accessed: 8-May-2018]. [Online]. Available: http://www.distrim.pt/catia/ 46, 58, 65

[84] Altair. (2018) Altair hypermesh. [Accessed: 14-Aug-2018]. [Online]. Available: https://altairhyperworks.com/product/hypermesh 46

[85] Altair. (2018) Altair optistruct. [Accessed: 2-Oct-2018]. [Online]. Available: https://altairhyperworks.com/product/OptiStruct 46

[86] Altair . (2018) Altair hyperview. [Accessed: 2-Oct-2018]. [Online]. Available: https://altairhyperworks.com/product/hyperview 46

[87] R. Lafranconi, "Announcement of Opportunity for the launch of Multiple Light Satellites on a Vega Flight," ESA, Tech. Rep., 2017. 49

[88] QB50, "System Requirements and Recommendations," Tech. Rep. 7, 2015. 49

[89] ASM Aerospace Specifications Metals, INC. (2018) Aluminum technical data sheets. [Accessed: 23-Sept-2018]. [Online]. Available: http://www.aerospacemetals.com/aluminum-distributor.html 51

[90] P. V. Gamboa, "Ligas de Alumínio," Covilhã, 2015. 51

[91] ASM Aerospace Specifications Metals, INC. (2018) Aluminum 7075-t6. [Accessed: 23-Sept-2018]. [Online]. Available: http://asm.matweb.com/search/SpecificMaterial.asp?bassnum=ma7075t6 52

Appendix A

CubeSat Design Requirements

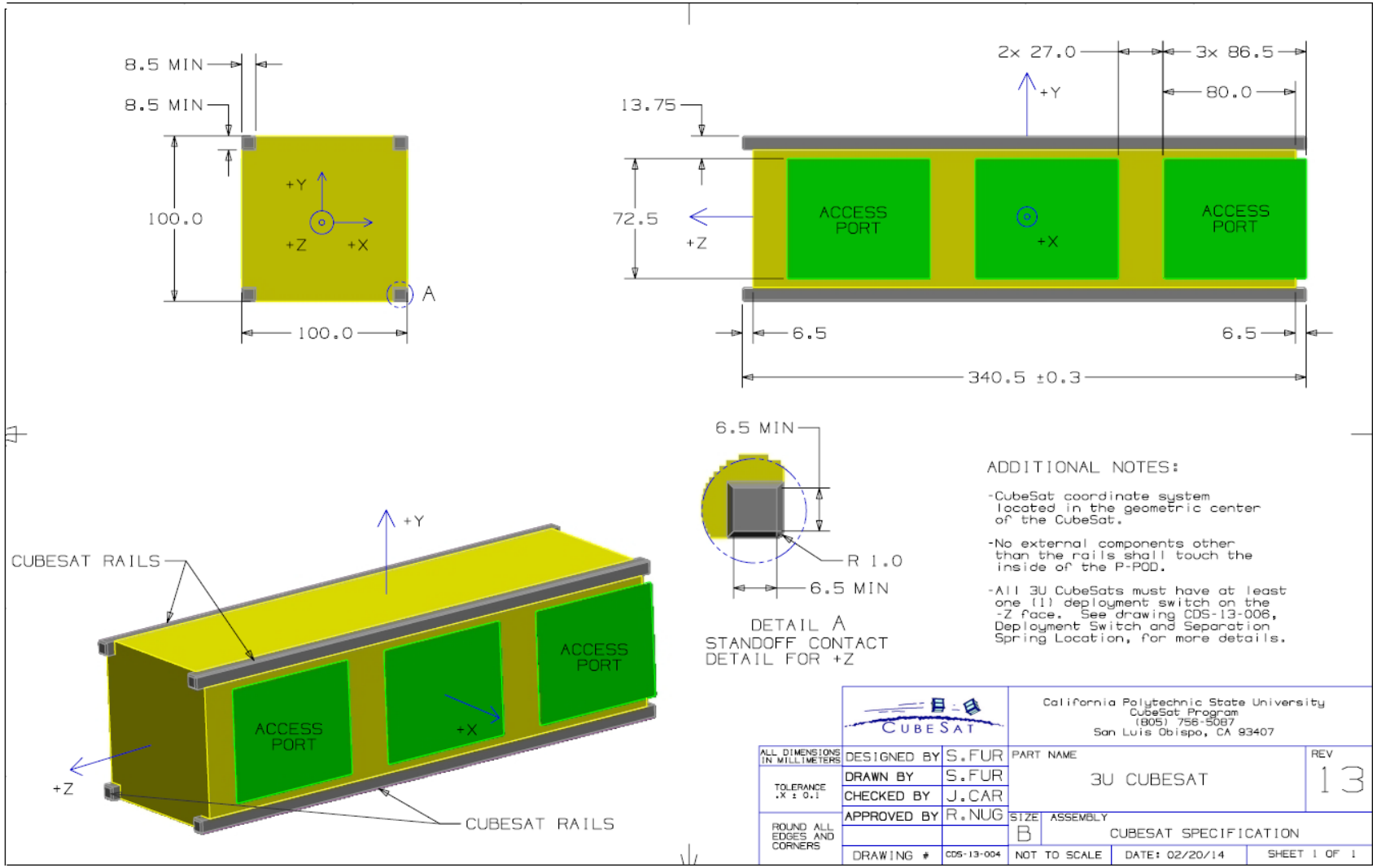

Figure A.1: 3U CDS [13].

Appendix B

Waiver Form

CubeSat Design Specification
Deviation Waiver Approval Request (DAR)

Date: August 1, 2009 Rev. 12

CubeSat Developers only fill out sections 1 through 9 and 15(optional). Email to: standards@cubesat.org

1. MISSION NAME:	**2. DAR NUMBER:**	**3. DATE:**
4. INITATOR	**5. INITIATING ORGANIZATION:**	
6. SPECIFIED REQUIREMENTS NUMBERS:	**7. JUSTIFICATION FOR DAR:**	**8. WAIVER TYPE** ☐ DIMENSIONS or MASS ☐ STRUCTURE ☐ ELECTRICAL ☐ OPERATIONS ☐ TESTING ☐ OTHER
9. DESCRIPTION OF DEPARTURE FROM REQUIREMENTS:		
10. CSEP DISPOSITION: ☐ ACCEPTED ☐ REJECTED ☐ CONDITIONALLY ACCEPTED	**11. ACCEPT/REJECT JUSTIFICATION:**	
CSEP AUTHORIZED REP.	**SIGNATURE**	**ORGANIZATION** / **DATE**
12. ACCEPTANCE CONDITIONS		
13. LAUNCH VEHICLE INTEGRATOR APPROVAL AUTHORITY: ☐ APPROVED ☐ DISAPPROVED ☐ CONDITIONALLY APPROVED	**14. LVI APPROVAL/DISAPPROVAL JUSTIFICATION:**	
LVI AUTHORIZED REP.	**SIGNATURE**	**ORGANIZATION** / **DATE**
15. APPROVAL CONDITIONS		

Figure B.1: DAR (page 1) [13].

1. MISSION NAME:	DEVIATION WAIVER APPROVAL REQUEST CONTINUATION PAGE	2. DAR NO.	3. DATE:
16. CONTINUATION (indicate item or block number):			

Figure B.2: DAR (page 2) [13].

Appendix C

Optimization Results

Table C.1: Mass of the geometry for t=2 mm according to the variables.

	mindim=2		mindim=4		mindim=6		mindim=8		mindim=10	
threshold	mass [kg]	% reduction	mass [kg]	% reduction	mass [kg]	% reduction	mass [kg]	% reduction	mass [kg]	% reduction
0.2	0.254	38.36	0.265	32.83	0.261	35.02	0.274	28.28	0.276	27.68
0.25	0.248	41.71	0.261	34.87	0.256	37.55	0.267	31.84	0.269	30.90
0.30	0.243	44.86	0.257	37.02	0.252	39.90	0.261	34.97	0.262	34.15
0.35	0.239	47.22	0.253	39.24	0.247	42.28	0.255	37.99	0.256	37.72
0.40	0.236	49.47	0.249	41.42	0.243	44.74	0.249	41.20	0.249	41.25
0.45	0.232	51.79	0.245	43.67	0.239	47.22	0.244	44.50	0.243	45.09
0.50	0.229	54.05	0.242	45.76	0.235	49.98	0.237	48.40	0.233	50.88

Table C.2: Mass of the geometry for t=3 mm according to the variables.

	mindim=2		mindim=4		mindim=6		mindim=8		mindim=10	
threshold	mass [kg]	% reduction	mass [kg]	% reduction	mass [kg]	% reduction	mass [kg]	% reduction	mass [kg]	% reduction
0.2	0.322	9.18	0.342	2.92	0.343	2.56	0.371	-5.07	0.370	-4.94
0.25	0.311	13.18	0.330	6.54	0.330	6.80	0.358	-1.54	0.360	-2.33
0.30	0.302	16.59	0.323	9.08	0.317	10.90	0.345	2.12	0.350	0.49
0.35	0.294	19.65	0.317	11.11	0.304	15.79	0.333	5.71	0.341	3.38
0.40	0.288	22.31	0.310	13.66	0.297	18.56	0.322	9.49	0.329	6.89
0.45	0.282	24.96	0.304	15.79	0.292	20.63	0.308	14.29	0.317	11.15
0.50	0.273	28.94	0.299	17.84	0.286	23.12	0.300	17.33	0.306	15.07

Appendix D

Systems Assemblage

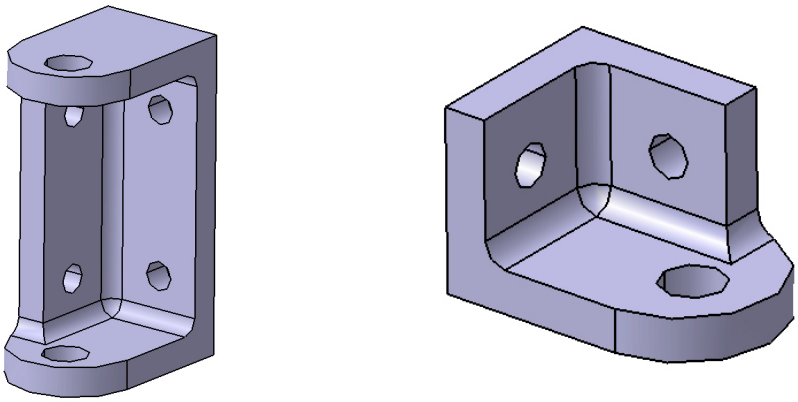

(a) Batteries support. (b) Boards support.

Figure D.1: Supports.

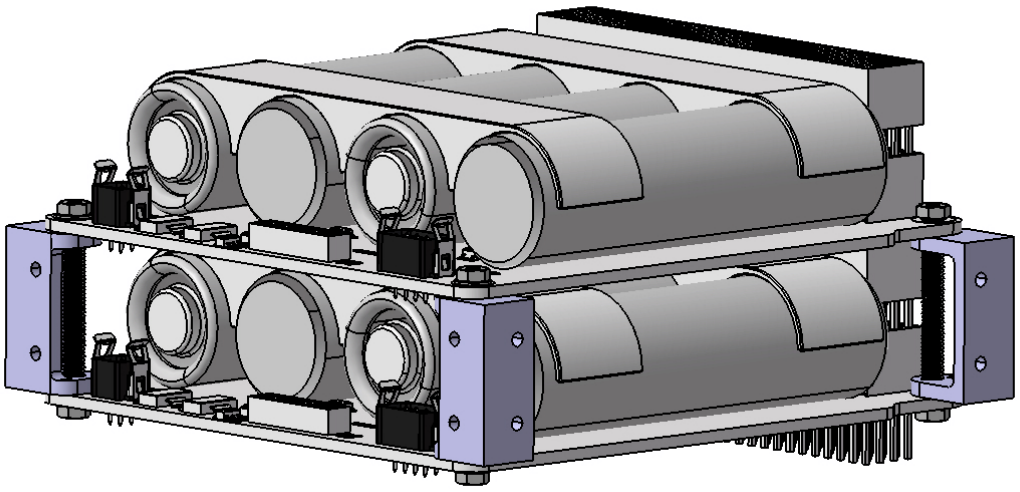

Figure D.2: Batteries support block.

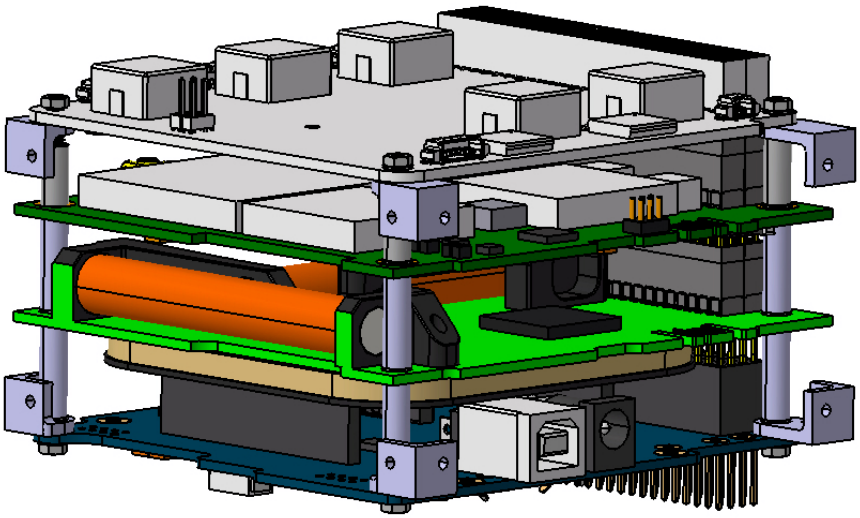

Figure D.3: Boards support block.

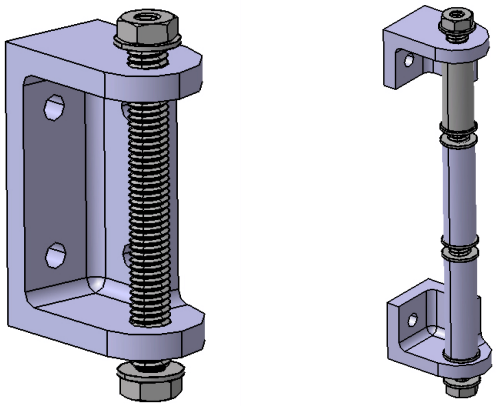

(a) Batteries support. (b) Boards support.

Figure D.4: Supports with rods, spacers, washers and nuts.

Appendix E

Final Geometry FEA

E.1 Displacement

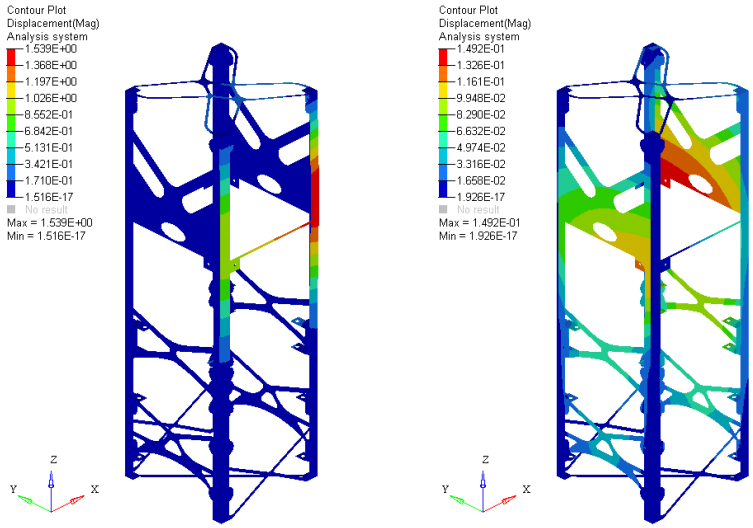

(a) LC 2. (b) LC 3.

Figure E.1: Displacement LC 2 and LC 3.

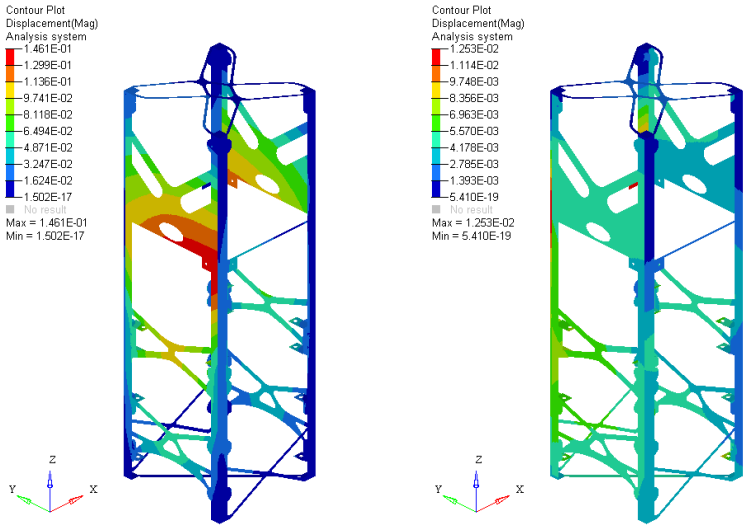

(a) LC 4. (b) LC 5.

Figure E.2: Displacement LC 4 and LC 5.

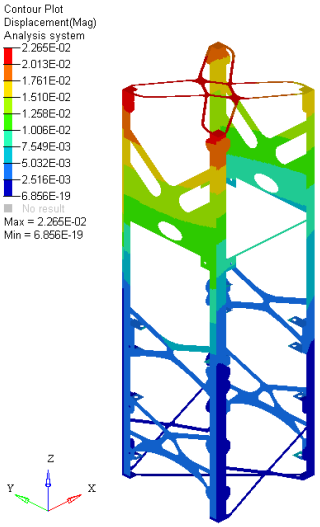

Figure E.3: Displacement LC 6.

E.2 2D elements Stress

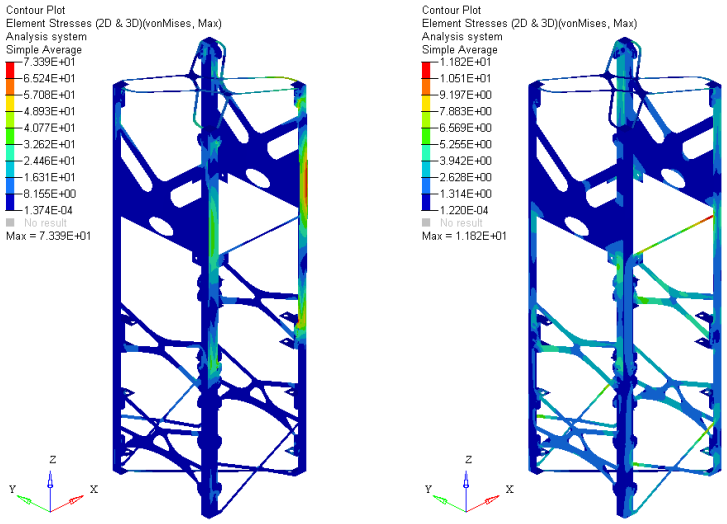

(a) LC 2. (b) LC 3.

Figure E.4: 2D Stress LC 2 and LC 3.

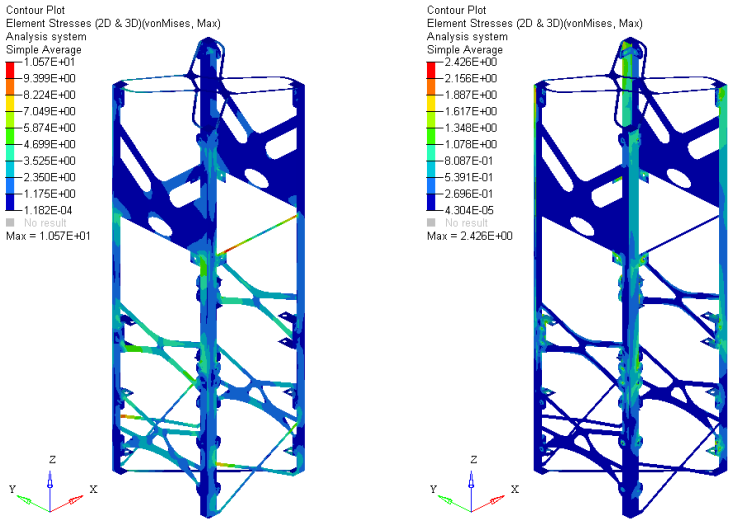

(a) LC 4. (b) LC 5.

Figure E.5: 2D Stress LC 4 and LC 5.

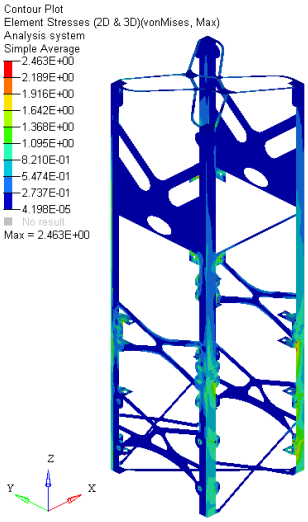

Figure E.6: 2D Stress LC 6.

E.3 Eigenvalue

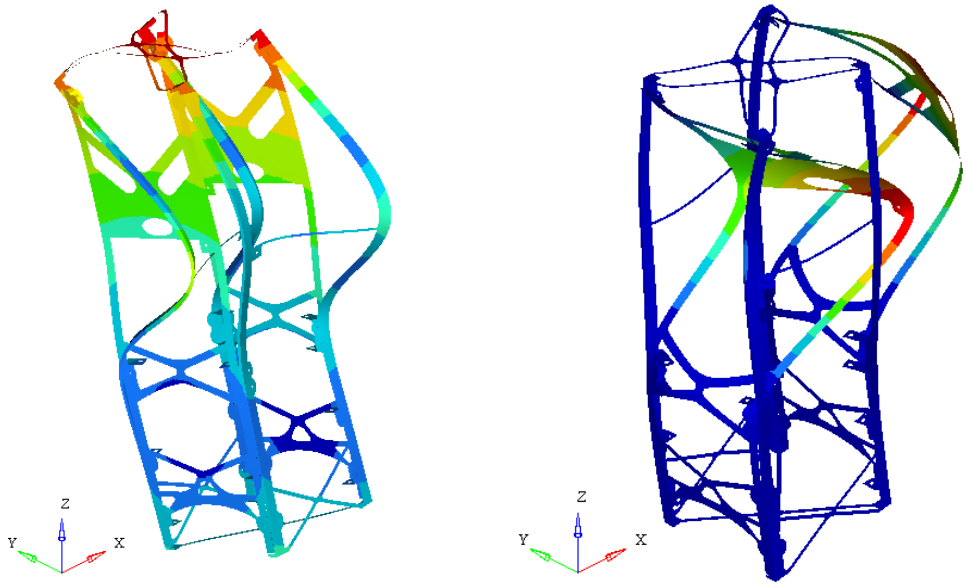

(a) f = 93.23 Hz. (b) f = 116.77 Hz.

Figure E.7: 1^{st} and 2^{nd} natural frequencies.

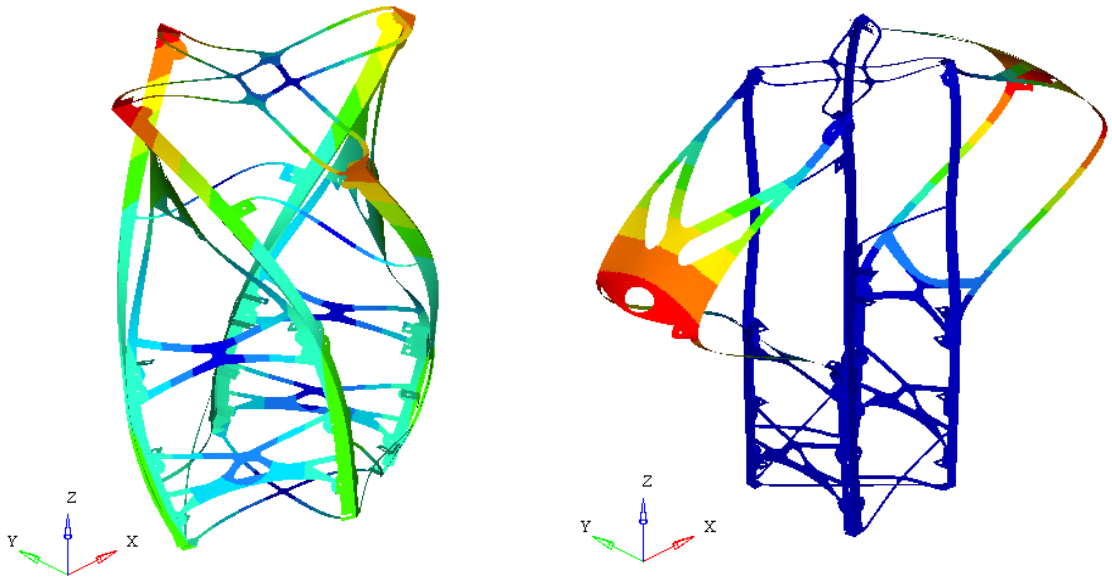

(a) f = 122.92 Hz. (b) f = 141.95 Hz.

Figure E.8: 3^{rd} and 4^{th} natural frequencies.